



NTNU – Trondheim
Norwegian University of
Science and Technology

Structural Analysis of Thin Concrete Shells

Hanibal Muruts
Ghebreselasie
Yuting Situ

Civil and Environmental Engineering (2 year)

Submission date: June 2015

Supervisor: Svein Ivar Sørensen, KT

Norwegian University of Science and Technology
Department of Structural Engineering

MASTEROPPGAVE 2015

for

Hanibal Muruts Ghebreselasie

og

Yuting Situ

Konstruksjonsanalyse av tynne betongskall

Structural Analysis of Thin Concrete Shells

Oppgaven går i korte trekk ut på følgende:

- Studere klassisk teori for aksesymmetriske skall, dvs. sylinder skall, kuleskall, kjegleskall, sirkulære plater og evt. ringbjelker.
- Beregningseksempler med sammensatte skall.
- Benytte FEM-programmet DIANA for analyse av de samme eksemplene som er beregnet med klassisk teori. Vurdering av krav til elementmodeller for å oppnå tilfredsstillende resultater for effekt av randforstyrrelser.
- Andre skallkonstruksjoner.
- Dimensjonering (nødvendig armering) av et av eksemplene beregnet lineært elastisk med de aktuelle metodene.
- Ikkelineær beregning av det siste eksempelet med DIANA.
- Lineær og ikkelineær analyse av beregningseksempler med sylindrisk skalltak med DIANA

Besvarelsen organiseres i henhold til gjeldende retningslinjer.

Veileder: Professor Svein Ivar Sørensen

Besvarelsen skal leveres til Institutt for konstruksjonsteknikk innen 10. juni 2015.

NTNU, 14. januar, 2015

Svein Ivar Sørensen
faglærer

Preface

This is the final report of our Master's thesis performed at the department of Structural engineering, part of the faculty of Engineering Science and Technology at the Norwegian University of Science and Technology (NTNU). This thesis is completed during a period of 20 weeks, and accounts for 30 credit points of the master's program. The subject of this thesis is "Structural analysis of thin concrete shells". The subject is chosen on the basis of personal interest and desire in venturing into an interesting area of structural analysis which is not broadly covered in the current curriculum of the structural engineering program at NTNU.

On this occasion we would like to thank our supervisor Professor Svein Ivar Sørensen for his guidance throughout the process. We would also like to forward our gratitude to Associate Professor Jan Arve Øverli for his support on working with the finite element software DIANA.

Trondheim, 10.06.2015

Hanibal Muruts Ghebreselasie
Yuting Situ

Abstract

From the perspective of structural engineering, shells due to their spatial curvature, possess a structurally efficient way of carrying loads acting perpendicular to their surfaces. However, the nature and geometry of shells makes them complicated to understand or predict their structural behaviour. The structural analysis of thin concrete shells can be conducted numerically using finite element analysis (FEA) or/and analytically on the basis of classical theory of thin shells. As finite element software are increasingly becoming primary tools for performing structural analysis, the knowledge of the analytical solution methods are becoming somehow less known among young structural engineers today. Hence, this paper aims to revisit the analytical analysis methods for concrete shell structures, and to investigate on how its results compare to that of the FEA. For a complete investigation of the structural analysis of thin concrete shells, the design and the accompanying verification by using nonlinear FEA is also briefly included. The study is limited to structural static analysis.

A combination of both a brief review of the theoretical background and a number of illustrative numerical examples are used as the basis for this study. Both the theory and the examples are focused on some of the most commonly build concrete shell structures, i.e axisymmetric shells and cylindrical shell roofs. Structural parts such as ring beams and circular plates, which are normally associated with concrete shell structures are also included. The finite element analysis of the structures in the numerical examples are performed in a finite element software called DIANA. Following the linear FEA, some of the structures in the numerical examples are designed accordingly, and analysed using nonlinear FEA. The nonlinear FEA are performed with the main focus on material utilization and verification of the load carrying capacity. Both the design and load calculations are done on the basis of the Eurocodes.

In most of the numerical examples considered in this study, a relatively good agreement between the solutions obtained from the FEA and the analytical method is found. In the last example, where a simply supported circular cylindrical shell roof is considered, the solutions from the FEA has shown some deviation of varying magnitude compared to the analytical solutions. Some of the possible sources of this deviation concerning assumptions and mesh density are discussed. The nonlinear FEA of the selected RC structures show that all the considered structures has the necessary capacity to carry the applied loading. Moreover the stress concentrations and crack patterns are relatively as one could expect on the basis of the linear FEA.

Following this study it can be concluded that the analytical solution method provides a relatively safe and independent way of verifying the results obtained from the FEA. Moreover it provides a valuable insight into the structural behaviour of shells, which is vital for objectively evaluating the accuracy of results obtained from FEA of any shell structure. The computations involved in the analytical solution procedure of concrete shell structures is however long and complicated thus it is highly exposed to calculation errors. To avoid this errors it is advisable for structural engineers to make a script, spreadsheet or a simple software that is based on the analytical method.

Sammendrag

Sett fra et konstruksjonsteknisk perspektiv har skall, grunnet dets romslige kurvatur, den egenskapen av å bære last som virker normalt på overflaten på en effektiv måte. Den naturlige egenskapen og geometrien til skall gjør at det er vanskelig å forutsi dets oppførsel ved belastning. Konstruksjonsanalyse av tynne betongskall kan gjennomføres numerisk ved bruk av elementmetoden og/eller analytisk på bakgrunn av den klassiske teorien for tynne betongskall. Elementprogrammer har stadig blitt mer brukt som hovedverktøy for konstruksjonsanalyse. Dette har medført at den analytiske beregningsmetoden har blitt mindre brukt og kjent blant dagens unge ingeniører. En del av formålet med denne masteroppgaven er derfor å rette blikket tilbake på den analytiske regnemetoden for tynne betongskall. Det ble lagt mye fokus på hvordan resultatene beregnet med denne metoden sammenligner seg med det som er beregnet ved bruk av elementmetoden. Denne oppgaven omfatter både lineær statisk og ikkelineær beregningsmetoder for tynne betongskall.

En grundig gjennomgang av den teoretiske bakgrunnen og flere regneksempeler er brukt for å få gjennomføre studie i den masteroppgaven. Både den teoretiske gjennomgangen og regneksempelene er gjennomført med hovedfokus på noen av de mest brukte tynne skall betongkonstruksjoner, som er aksesymmetrisk skall og sylindrisk skalltak. Konstruksjonsdeler som ringbjelker og sirkulære plater, som ofte er assosiert med betong skallkonstruksjoner, er også inkludert med i denne oppgaven. Alle elementanalyser i oppgaven er utført i elementprogrammet DIANA. Først ble lineære beregningene gjennomført, deretter ble noen av de konstruksjonene i regneksempelene dimensjonert. For å verifisere bæreevnen og materialutnyttelsen til disse armerte betongskall konstruksjonene, ble en ikkelineære analyse gjennomført. Både lastberegning og dimensjonering er utført i henhold til gjeldene norsk standarder.

I de fleste regneksempelene som er gjennomført i denne oppgaven, ble det funnet et relativt godt samsvar mellom begge beregningsmetodene. I det siste regneksemplet, hvor et fritt opplagt sylindrisk skalltak er beregnet, er det funnet noe avvik av varierende størrelse. Mulige årsaker for dette avviket kan ha noe å gjøre med element inndeling og antakelser, og dette er videre diskutert i oppgaven. Resultatene av ikkelineære beregningene har vist at alle konstruksjonene klarer å bære den dimensjonerende lasten som er påsatt. I tillegg, kan de spenningene og opprissingsmønstrene som er funnet sies å være som forventet basert på de lineære beregningene.

Fra dette arbeidet kan en konkludere med at den analytiske metoden er en relativ trygg og uavhengige metode å kontrollere resultater fra en elementanalyse. I tillegg bidrar den til mye verdifull kunnskap og forståelse av bæresystemet til skallkonstruksjoner. Dette er viktig når en vurderer gyldighet av resultater som er funnet fra en elementanalyse på ulike skallkonstruksjoner. Den analytiske regnemetoden er lang og komplisert slik at den er veldig utsatt for regnefeil. Derfor er det anbefalt for byggingeniører å ha en regneark eller brukervennlig program som er basert på den analytiske metoden.

Contents

Preface	i
Abstract	iii
Sammendrag	v
1 Introduction	1
1.1 Background	1
1.2 Aim and scope of the thesis	2
1.3 Structure of the report	2
2 Introduction to shells	5
2.1 Definition	5
2.2 Shells as structural elements	6
2.3 Thin shell concrete structures	7
3 Classical theory of thin shells	9
3.1 General	9
3.2 Background	9
3.3 Assumptions	10
3.4 Definition and notation	10
3.5 The governing equation of the general linear shell theory	12
3.5.1 Equilibrium	12
3.5.2 Strains	13
3.5.3 Stress-strain relations	13
3.5.4 Force-Displacement relations for shallow shells	14
Shallow shells	15
3.6 Membrane theory	16
4 Cylindrical shells	19
4.1 General	19
4.2 Governing differential equation	19
4.2.1 Damping length	21
4.2.2 Analysis of long cylindrical shells	22
4.2.3 Analysis of short cylindrical shells	22
4.3 Circular flat plates	24
4.4 Example 1: Cylindrical water reservoir enclosed by a circular flat plate	25
4.4.1 Circular plate	26
4.4.2 Cylindrical wall	27

4.4.3	Compatibility requirements	28
4.4.4	Distribution of the load effects	29
4.4.5	Remarks on the result from the analytical calculations	32
5	Shells of revolution	33
5.1	General	33
5.2	Membrane theory of shells of revolution	33
5.2.1	Displacements from the membrane theory	36
5.3	Bending theory in shells of revolution	37
5.3.1	Governing differential equation	37
5.4	Ring beams	41
5.5	Example 2: An idealized cylindrical concrete gas vessel enclosed by a spherical shell at the top	43
5.5.1	Cylindrical wall	45
5.5.2	Spherical shell	45
5.5.3	Ring beam	46
5.5.4	Compatibility requirements	47
5.5.5	Distribution of the load effects	48
5.5.6	Remarks on the result from the analytical calculations	53
6	Conical shells	55
6.1	General	55
6.1.1	Membrane theory of conical shells	56
6.2	Bending theory of conical shells	56
7	FEA	59
7.1	Analytical vs numerical solution	59
7.1.1	FEM	59
7.2	DIANA	63
7.2.1	Pre-processing phase and Discretization	63
7.2.2	Solution phase	64
7.2.3	Post-processing phase	64
7.3	Linear static analysis in DIANA	64
7.3.1	Axisymmetric elements in DIANA	65
7.3.2	Example 1 analysed in DIANA	66
7.3.3	Example 2 analysed in DIANA	68
7.4	Nonlinear finite element analysis	69
7.4.1	Reinforcement	70
7.4.2	Structural modelling	70
7.4.3	Material models	71
7.4.4	Solution procedure	72
7.4.5	Results from the Nonlinear FEA of the structure in example 1	73
7.5	Discussion	76
8	Cylindrical shell roofs	77
8.1	General	77
8.2	Background theory	77

8.2.1	Edge beams	79
8.3	Numerical examples analysed using linear and nonlinear FEA	80
8.3.1	Linear FEA	80
8.3.2	Reinforcement	81
8.3.3	Nonlinear FEA	81
8.3.4	Example 3: Circular cylindrical shell roof with fixed edges	81
	Linear FEA	81
	Analytical solution	81
	Nonlinear FEA	83
8.3.5	Example 4: A simply supported circular cylindrical shell roof	89
	Linear FEA	89
	Analytical solution	89
	Nonlinear FEA	92
8.4	Discussion	95
9	Conclusion	97
9.1	Recommendation for future study	99
A	RC design according to Eurocode 2	105
A.1	Design of the cylindrical water reservoir in example 1	105
A.1.1	Circular plate	106
A.1.2	Cylindrical wall	109
B	Reinforcement design according to the two layered approach	113
B.1	Design of the cylindrical roof shell in example 3	113
B.1.1	The two layered approach	114
C	Investigating the effect of the constraint along the curved edge in example 3	117
C.1	Additional constraint in Z direction	117
D	MatLab code	121

List of Figures

- 2.1 Classification according to the Gaussian curvature[8] 5
- 2.2 The Pantheon in Rome 8

- 3.1 Notations[1] 11
- 3.2 Forces on a shell element[1] 12
- 3.3 Deformed shell element[1] 14
- 3.4 Shallow shell illustration 16
- 3.5 Cylinder shell with membrane theory [10] 16

- 4.1 Forces on a cylindrical shell [20] 20
- 4.2 Definition of the coordinates 23
- 4.3 Illustration of the positive directions 23
- 4.4 Moments in a circular flat slab 24
- 4.5 Illustration of the structure in example 1 25
- 4.6 Slab moments 29
- 4.7 Shear force in the slab 30
- 4.8 Moment in the cylindrical wall 31
- 4.9 Shear force in the cylindrical wall 31
- 4.10 Circumferential force in the cylindrical wall 32

- 5.1 Differential element of axisymmetric shells of revolution[19] 34
- 5.2 Illustration of the equivalent vertical load [14] 35
- 5.3 Displacements from the membrane theory [14] 36
- 5.4 Forces on a shell element [19] 38
- 5.5 Vertical equilibrium [14] 39
- 5.6 Ring beam with distributed force the in radial direction 42
- 5.7 Ring beam with distributed moment in the radial direction 42
- 5.8 Illustration of the structure in example 2 43
- 5.9 Meridian moment 49
- 5.10 Shear force in the spherical shell 49
- 5.11 The in-plane forces 50
- 5.12 Moment in the cylindrical wall 51
- 5.13 Shear force in the cylindrical wall 52
- 5.14 Circumferential force in the cylindrical wall 52

- 6.1 Notations used in the description of conical shells [21] 55
- 6.2 Positive directions of the edge effects on a cone [21] 58
- 6.3 Illustration for the definition of x 58

7.1	Finite element analysis procedures [12]	61
7.2	A uniformly loaded cantilever beam	62
7.3	Discretized model	62
7.4	FEA options in DIANA	64
7.5	Axissymmetric elements in DIANA	66
7.6	Stress resultant diagrams from linear FEA of example 1	67
7.7	Stress resultant diagrams from linear FEA of example 2	69
7.8	Material models that are applied [5]	71
7.9	Load-deflection diagram at the center of the circular plate	74
7.10	Stresses in the concrete at load step 10	74
7.11	Crack patterns in example 1	75
7.12	Stresses in the reinforcement	75
7.13	Stresses in the reinforcement after including min. reinforcement	75
8.1	Notation and axis definition	78
8.2	CQ40S	80
8.3	Illustration of the structure in example 3	82
8.4	Comparison between analytical and FEA solutions	83
8.5	Shape of the deformed element model	84
8.6	Load-displacement curve at the midspan in example 3, $\frac{R}{t} = 100$	85
8.7	Load-displacement curve at the midspan in example 3, $\frac{R}{t} = 150$	86
8.8	Stresses in the concrete at the maximum capacity	86
8.9	Crack strain vectors at load step 14	87
8.10	Load-deflection curve at midspan without geometical nonlinearities, $\frac{R}{t} = 150$	88
8.11	Illustrations of the structure in example 4	90
8.12	Load-displacement curve at the midspan of the edge beams	93
8.13	Crack patterns in the concrete before and after the peak point	94
8.14	Stresses in the concrete before and after the peak point	94
8.15	Stresses in the reinforcement before and after the peak point	94
C.1	New translational constraint in z-direction	118
C.2	Variation of the stress resultants in φ direction	119
C.3	Variation of the stress resultants in x direction	120

List of Tables

- 4.1 Expressions for symmetrical bending of circular plates [1] 24
- 7.1 Results from the linear FEA using L6AXI 66
- 7.2 Results from the linear FEA using CL9AX 67
- 7.3 Results from the linear FEA using L6AXI 68
- 7.4 Results from the linear FEA using CL9AX 68
- 7.5 Structurally required amount of steel reinforcement in example 1 [$\frac{mm^2}{m}$] . . . 70
- 7.6 Final amount of reinforcement including minimum requirements according to the Eurocodes [$\frac{mm^2}{m}$] 70
- 7.7 Solution procedure for the nonlinear FEA 73
- 8.1 Geometric and material properties of the RC shell 82
- 8.2 Initial reinforcement input [$\frac{mm^2}{m}$] 84
- 8.3 Solution procedure for the nonlinear analysis 84
- 8.4 Geometric properties of the RC shell 89
- 8.5 Comparison between the FEA and analytical solutions of the structure in example 4 91
- 8.6 Comparison between the results with and without edge beams 91
- 8.7 Amount of steel reinforcement [$\frac{mm^2}{m}$] 92
- 8.8 Solution procedure for the nonlinear analysis 93
- A.1 Design values of the load effects in example 1 105
- B.1 Design values of the load effects in example 3 113

Chapter 1

Introduction

1.1 Background

Concrete shell structures, often referred to as 'thin shells' are suitable structural elements for building spacious infrastructures. They are often economical and suitable solution for different facility structures such as water tanks, large-span roofs, containment buildings, and silos. Loads acting on the surface of shell structures are mainly carried by the so called membrane action. This is a general state of stress consists of the in-plane normal and shear stress resultants only. In comparison, other structural forms such as beams and plates carry loads acting on their surfaces by bending action, which can be said is structurally less efficient. Usually the in-plane stresses in shells are low such that with a relatively small thickness it is possible to span over large distances. In addition, concrete shell structures can have various shapes and geometries and that has contributed to them often considered as visually attractive.

The structural analysis of thin concrete shells can be performed numerically using finite element analysis and/or analytically by using classical theory of thin shells. While FEA analysis is becoming increasingly prominent way of performing structural analysis, the analytical solution procedure is somehow becoming less relevant and known among young structures engineers today. This unfortunate development has the consequence of eliminating the advantages which are associated with the knowledge and understanding of the analytical method. Compared to structural elements such as beams, slab and walls, the structural behaviour of shells is not easy to predict. Hence evaluating the accuracy of the results obtained from FEA of shell structures is a challenging task. Having the knowledge and understanding of the analytical solution method can provide the basis for this verification and at the same time give a much needed insight into the structural behaviour of shells.

1.2 Aim and scope of the thesis

The aim of this paper is thus to revisit the analytical method for analysing thin concrete shell structures, and to investigate on how its results compare to what is obtained from the FEA. For a complete investigation of the structural analysis of thin concrete shells, the design and the accompanying nonlinear FEA of the selected shell structures is also briefly studied. The analytical solution procedure for shell structures of arbitrary geometry and loading is complicated. However, for some of the most commonly constructed concrete shell structures, a complete analytical solution procedure is available. The two types of concrete shell structures considered in this paper are axisymmetric shells and cylindrical shell roofs. Concrete structures that are made of axisymmetrical shells include structures such as containment buildings, tanks and silos. Similarly, cylindrical shell roofs are often preferred structural elements for large span concrete roof structures. The analysis in this study are mainly focused on static linear and nonlinear analysis, and ultimate limit design on the basis of the Eurocode.

1.3 Structure of the report

The structure of the report is as follows:

Chapter 2:

A basic definition and classification of shell surfaces is presented. A qualitative description of the structural features of shells together with some insight into the history of thin concrete shell structures is given.

Chapter 3:

The outline of the classical theory of thin shells which is the backbone behind the analytical solution procedure is briefly introduced. The governing differential equations of the general thin shell theory with its assumptions are presented. Furthermore the final equations under the assumptions of shallow shells are derived.

Chapter 4:

The necessary derivations leading to the final expressions for analysing cylindrical concrete shells is presented. The general outline of the theory behind circular slabs which are often associated with cylindrical shells is described. Example 1, a numerical example of an idealized cylindrical water tank connected with a circular slab is presented. This example is used to illustrate the practical application of the derived analytical solution procedures. The chapter rounds off with some concluding remarks on the results of the analytical calculations.

Chapter 5:

The necessary derivations leading to the final expressions for analysing shells of revolution especially spherical concrete shells is presented. The general outline of the theory behind

ring beams, which are often associated with spherical shells is included. Example 2, a numerical example of an idealized pressure vessel which demonstrates the connection between a cylindrical shell, ring beam and spherical shell is presented. The chapter rounds off with some concluding remarks on the results of the analytical calculations.

Chapter 6:

The necessary derivations leading to the final expressions for the analytical analysis of conical shells is presented.

Chapter 7:

An introduction into the finite element method (FEM) and the finite element software DIANA is presented. A linear FEA of both the structures in Example 1 and Example 2 with the emphasis on the choice of element type and mesh is performed. The results are then compared to those obtained from the analytical calculations. A nonlinear FEA of the structure in Example 1 with the main focus on design verification and material utilization is performed. Moreover, the necessary description and choices of the input parameters for the nonlinear FEA are presented. The chapter rounds off with some concluding remarks and discussion on the results of the FEA and the accuracy of the comparison with the corresponding analytical solutions.

Chapter 8:

The outline of the theory behind the analytical solution procedure and how it relates to the general theory of thin shells is presented. Example 3, a linear and nonlinear analysis of a numerical example of a fixed circular cylindrical shell is performed. Similarly in example 4, a linear and nonlinear analysis of a numerical example of a simply supported circular cylindrical shell with and without edge beams is performed. The chapter rounds off with some concluding remarks and discussion on the results of the FEA and accuracy of the comparison with the corresponding analytical solutions.

Chapter 9:

Main conclusion and some remarks about future works is presented.

Chapter 2

Introduction to shells

2.1 Definition

A shell can be defined as a body that is bounded by two surfaces parallel to its middle-surface, and is deformed in any arbitrary manner [11]. This is true for shells of a constant thickness, which will mainly be considered in this study. Generally any surface which is curved in one or more directions can be considered as a shell surface. This definition highlights the diversity of surfaces which can be characterized as shells. Hence, there are different ways of classifying shell surfaces. One particular way of classifying shell surfaces is according to their Gaussian curvature. The Gaussian curvature of a curved surface is a product of the two principal curvatures.

$$\kappa_g = \kappa_1 \cdot \kappa_2 = \frac{1}{r_1} \cdot \frac{1}{r_2}$$

where r_1 and r_2 are the corresponding radii of curvatures. The radius of curvature of a curve at a point is a measure of the radius of the circular arc that best approximates the curve at that point [6]. The principal radii of curvatures are thus the absolute maximum and minimum of the radius of curvatures. Based on the outcome of the above formula shell surfaces can be categorized into three types. A positive Gaussian curvature characterizes a clastic surface (a), a negative Gaussian curvature characterizes an anti-clastic surface (b), while as cylindrical or plane surfaces have a Gaussian curvature of zero(c).

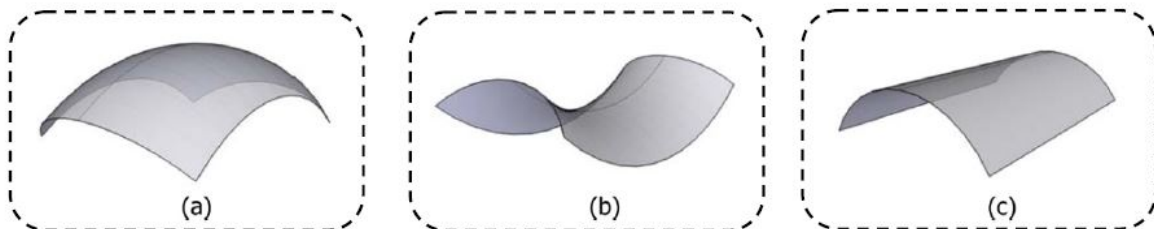


Figure 2.1: Classification according to the Gaussian curvature[8]

From the perspective of structural engineering, the main difference between these three types is the propagation of boundary effects in the shell. The effects tend to damp quickest for shells of positive Gaussian curvature and slowest for shells of negative Gaussian curvature.

Another way of describing shell surfaces is according to how the surfaces are generated. Using this method, in 1980 Heinz Isler classified shell surfaces into Geometric, Structural and Sculptural surfaces[8]. Geometric shells are well defined mathematically and which as a result can fairly be easily calculated analytically. These type of shells were quite significant in the development of shell structures at the times where computer aided calculation were not available. Structural shells which also are called experimental forms, are shapes that are developed by the observation of different 'natural' phenomena such as air pressure, gravity, and material flow. These observations together with small scale experiments were used in developing shell surfaces which behave accordingly. Structural shells obey the laws of nature under their own weight (pure tension or compression), unlike geometric shells which are based on approximations. The last type of shells are sculptural shells, which, as their name indicates, are formed artistically. This shapes er mostly modelled and calculated using computer programs.

In further discussions regarding the theory of thin shells, the classification method that will be used is the one according to geometry or curvature of the surface. Thus, geometrically shell surfaces can be classified as cylindrical shells, spherical shells, conical shells, paraboloidal shells etc.

2.2 Shells as structural elements

The use of shells as structural elements has contributed to the development of several different branches of engineering. Branches such as Architecture and Building, Power and chemical engineering, Structural engineering, Vehicle body structures etc. has been greatly influenced by the introduction of shell elements. The two essential features of shell structures that had made an impact on the above mentioned branches are continuity and curvature [2].

There are two ways of interpreting continuity, the first that might come to mind, is continuity in the sense that it is generated in one piece without any explicit connections or overlapping. This is among others important in the case with vessels containing fluid at pressure. However, structural continuity, is the feature that has had a great impact in structural engineering. This feature is better understood by the observation of an ancient masonry dome or vault. These constructions are often composed of separate stone sub-units which sometimes are not cemented to each other. However, they manage to hold the structure intact without falling out. This is because the vault is in a state of compression through out. Thus the sub-units are held in compression contact with each other. It is the fact that shells, due to their spacial curvature, can efficiently transmit forces in different directions in their surface that makes them structurally continuous.

The first shell structures were built long before the development of the shell theories. The early engineers could have understood the properties of shells by conducting small-scale

model tests. An important point that might have been clear for this engineers is that the difference between closed and open shells. It can easily be determined that closed surfaces are more rigid than open surfaces. This can for example be illustrated by the fact that eggs (or egg shells) become rather flexible when they are opened compared to their original state. In man made structures, openings are almost inevitable. Therefore to achieve more rigidity the openings needs to be some how compensated. In structures such as small boats this is done by adding stiffening ribs, large ships have decks and the shell formed roofs of buildings are often supplemented by some reinforced ring beams. Quantifying this difference in rigidity between closed and open shells, is one of the reasons for the development of the shell theory. In addition, the theory of shell structures is needed to insure precision, safety and economical design.

2.3 Thin shell concrete structures

From an architectural point of view, using concrete shells as roofing provides the possibility of constructing spacious columnless buildings which are attractive in many ways. The development of reinforced concrete has enhanced this possibility even further, and had a great impact in stimulating interest in using thin shell structures for various purposes.

The oldest known concrete shell is the Pantheon in Rome, which was completed about AD 125. It is a monolithic dome like structure with no reinforcement. However, modern thin shell structures which are reinforced with steel bars were first produced in beginning of the 1900s [7]. Concrete shells can be built by the assembly of several casted units or casted in one piece (monolithic). Monolithic concrete shells are structurally stronger than their counter parts. The two most well-defined systems of thin shell commonly used in concrete structures are the dome and the cylinder.



Figure 2.2: The Pantheon in Rome

Chapter 3

Classical theory of thin shells

3.1 General

In order to design any structure in detail, it is necessary to have some specific set of guidelines based on scientific methods. As for any other structural element, the guidelines for designing shell structures is provided by the branch of mechanics called structural mechanics. Engineers are mainly concerned with the man-made structures. In order to construct these structures, they are highly dependent on developing conceptual models that rationalizes the phenomena of nature. The development of these models largely depend on the understanding of mathematics, conducting experiments, assumptions and approximations.

3.2 Background

The theory of thin shells is first formulated by L.E.H. Love in 1888 in his paper on thin elastic shell theory. Love developed the shell theory on the basis of Kirchhoff hypothesis for thin plate structures proposed in in the mid 1800s [18]. Since then, there has been several shell theories developed with their own set of kinematic relations (strain - displacement relations). The central idea it that the deformation of shells due to loading is resisted by the membrane and bending effects, which can be separated.

The theory of structures often deals with idealized forms of the physical structures. A beam is for example often represented as a line that possesses a certain mechanical properties. Similarly, a shell is represented by a surface that possesses a certain mechanical properties like stiffness and strength. In this way load effects can be calculated easily, however one has to be aware that for the design of local problems this idealization might not be adequate. Further development of the theory employs Hooke's law (elastic material), equilibrium and compatibility. Hooke's law relates strains with stresses, equilibrium relates stress resultants with external loading and compatibility relates strains with deformation/displacements. These three sets of equations together with appropriate boundary

conditions make up the mathematical aspect of the problem. When dealing with dynamic loading the equilibrium equation is represented by the equation of motion.

Compared to flat plates, the shell theory is more complicated due to the geometry of the shell. It is possible to argue that the problem of shell structures is dominated by the geometry of the surface of the shell [2]

3.3 Assumptions

The classical theory of shells deals with shells that can be characterized as thin. A thin shell is a curved slab whose thickness h is small compared with its other dimensions and compared with its principal radii of curvature r_x and r_y [1]. This can be quantified by the ratio, radii of curvature to thickness of the shell, $\frac{R}{t}$. It can be said that shells with the ratio greater than 20 can be characterized as thin shells. In comparison, an egg shell has a ratio of around 55 and an aluminium bear can has a ratio of around 325 [10, ch.4.8]. In further development of the theory, we will mainly be dealing with uniform shells. The shells are uniform in the sense that the material properties do not vary through the thickness. Reinforced concrete (RC) is a composite material consisting of steel and concrete, nevertheless it is regarded as sufficiently uniform. This can be argued with the fact that the difference in Young's modulus between steel and concrete is not large enough [1].

Other assumptions include:

- Small deflections, the equilibrium equations refer to the original geometry
- Linear elastic behaviour
- Shear deformation is neglected
- Plane section remain plane after bending
- The transverse normal stress is negligible

3.4 Definition and notation

The geometry of a shell is fully defined by its thickness and the form of its middle surface. The middle surface is defined as the surface that bisects the thickness of the plate [19]. When analysing the shell, an infinitely small element which is defined by two pairs of adjacent planes perpendicular to the middle surface is considered, see Figure 3.1. These planes contain the principal radii of curvatures of the shell, r_x and r_y .

Further, the stresses and strains are denoted following their respective axes as $\sigma_x, \sigma_y, \tau_{xy} = \tau_{yx}$ and $\varepsilon_x, \varepsilon_y, \gamma_{xy}$. The resultant forces and moments per unit length of the middle surface are shown in Figure 3.1 and are defined as follows [1]:

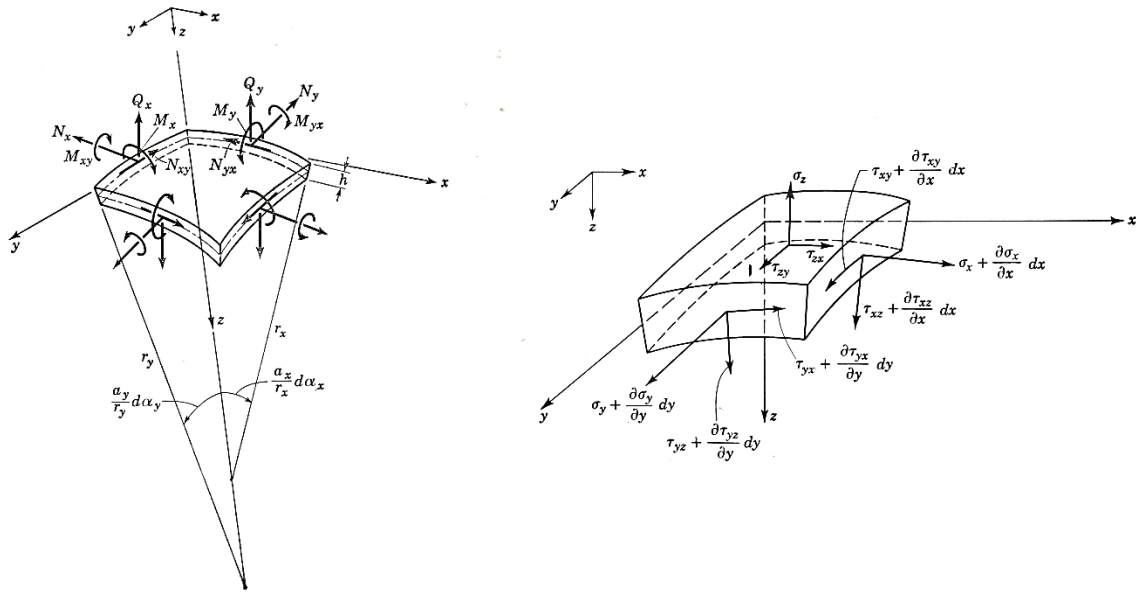


Figure 3.1: Notations[1]

$$\begin{aligned}
 N_x &= \int_{-h/2}^{h/2} \sigma_x \left(1 - \frac{z}{r_y}\right) dz & N_y &= \int_{-h/2}^{h/2} \sigma_y \left(1 - \frac{z}{r_x}\right) dz \\
 N_{xy} &= \int_{-h/2}^{h/2} \tau_{xy} \left(1 - \frac{z}{r_y}\right) dz & N_{yx} &= \int_{-h/2}^{h/2} \tau_{yx} \left(1 - \frac{z}{r_x}\right) dz \\
 Q_x &= \int_{-h/2}^{h/2} \tau_{xz} \left(1 - \frac{z}{r_y}\right) dz & Q_y &= \int_{-h/2}^{h/2} \tau_{yz} \left(1 - \frac{z}{r_x}\right) dz \\
 M_x &= \int_{-h/2}^{h/2} \sigma_x z \left(1 - \frac{z}{r_y}\right) dz & M_y &= \int_{-h/2}^{h/2} \sigma_y z \left(1 - \frac{z}{r_x}\right) dz \\
 M_{xy} &= - \int_{-h/2}^{h/2} \tau_{xy} z \left(1 - \frac{z}{r_y}\right) dz & M_{yx} &= \int_{-h/2}^{h/2} \tau_{yx} z \left(1 - \frac{z}{r_x}\right) dz
 \end{aligned} \tag{3.1}$$

The expressions $\frac{z}{r_x}$ and $\frac{z}{r_y}$ comes from the trapezoidal shapes of the sides along planes xz and yz . These expression will however be neglected due to the thin shell approximations. As a result:

$$N_{xy} = N_{yx} \quad \text{and} \quad M_{xy} = -M_{yx}$$

In addition σ_z, τ_{xz} and τ_{yz} are omitted due to the small thickness of the shell, and the same goes with the twisting moments about the z -axis. Thus, there will be a state of plane stress through out the shell. Derivation of the differential equations for the most used concrete shell elements will be presented in the proceeding chapters. However, the procedures for deriving the governing differential equation for a general shell element will be presented in the following sections.

3.5 The governing equation of the general linear shell theory

3.5.1 Equilibrium

As for any other structural systems, the equilibrium conditions for the differential shell element in Figure 3.2 must be met. The six equilibrium equations are:

$$\begin{aligned} \Sigma X &= 0 & \Sigma M_x &= 0 \\ \Sigma Y &= 0 & \Sigma M_y &= 0 \\ \Sigma Z &= 0 & \Sigma M_z &= 0 \end{aligned} \quad (3.2)$$

Due to the simplification of thin shell element mentioned before, the equation $\Sigma M_z = 0$ is omitted, thus five equations are remained. When setting up the equilibrium equations, the external loads on the shell element must also be included in the form of pressure components p_x, p_y, p_z . The equilibrium equations are derived in Ref. [1], and are given

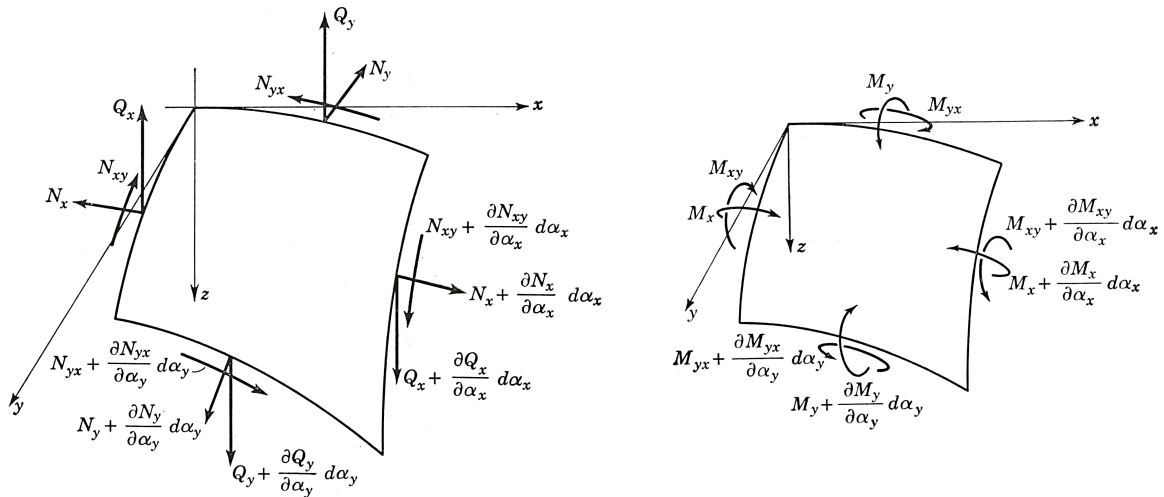


Figure 3.2: Forces on a shell element[1]

by:

$$\begin{aligned}
\frac{\partial}{\partial \alpha_x}(N_x a_y) - N_y \frac{\partial a_y}{\partial \alpha_x} + N_{xy} \frac{\partial a_x}{\partial \alpha_y} + \frac{\partial}{\partial \alpha_y}(N_{yx} a_x) - Q_y \frac{a_x a_y}{r_{xy}} - Q_x \frac{a_x a_y}{r_x} + p_x a_x a_y &= 0 \\
\frac{\partial}{\partial \alpha_y}(N_y a_x) - N_x \frac{\partial a_x}{\partial \alpha_y} + N_{yx} \frac{\partial a_y}{\partial \alpha_x} + \frac{\partial}{\partial \alpha_x}(N_{xy} a_y) - Q_x \frac{a_x a_y}{r_{xy}} - Q_y \frac{a_x a_y}{r_y} + p_y a_x a_y &= 0 \\
\frac{\partial}{\partial \alpha_x}(Q_x a_y) + \frac{\partial}{\partial \alpha_x}(Q_y a_x) + N_x \frac{a_x a_y}{r_x} + N_{xy} \frac{a_x a_y}{r_{xy}} + N_{yx} \frac{a_x a_y}{r_{xy}} + N_y \frac{a_x a_y}{r_y} + p_z a_x a_y &= 0 \\
-\frac{\partial}{\partial \alpha_y}(M_y a_x) + M_x \frac{\partial a_x}{\partial \alpha_y} - M_{yx} \frac{\partial a_y}{\partial \alpha_x} + \frac{\partial}{\partial \alpha_x}(M_{xy} a_y) + Q_y a_x a_y &= 0 \\
-\frac{\partial}{\partial \alpha_x}(M_x a_y) + M_y \frac{\partial a_y}{\partial \alpha_x} + M_{xy} \frac{\partial a_x}{\partial \alpha_y} - \frac{\partial}{\partial \alpha_y}(M_{yx} a_x) + Q_x a_x a_y &= 0
\end{aligned} \tag{3.3}$$

where α_x and α_y are curvilinear coordinates along the respective sides, and a_x and a_y are called Lamé parameters. The Lamé parameters are quantities which relate a change in arc length on the surface to the corresponding curvilinear coordinates [21].

3.5.2 Strains

The deformation of a shell element consists of strains both due to a change in curvature and axial deformation. The strains from the axial deformation are denoted as ε_1 and ε_2 for the strains in x and y directions respectively, and the new radii of curvatures are denoted as r'_x and r'_y , see Figure 3.3. The total expression for the strains, neglecting the small terms, is then given by [19]:

$$\begin{aligned}
\varepsilon_x &= \varepsilon_1 - z \left(\frac{1}{r'_x} - \frac{1}{r_x} \right) \\
\varepsilon_y &= \varepsilon_2 - z \left(\frac{1}{r'_y} - \frac{1}{r_y} \right) \\
\gamma_{xy} &= \gamma - 2z\chi_{xy}
\end{aligned} \tag{3.4}$$

where χ_{xy} represents the change in twisting curvature and γ is shear strain of the middle surface.

3.5.3 Stress-strain relations

The stress-strain relations are based on the Hook's law for flat plate element as shown in Eq. 3.5. In addition to the material being linearly elastic, it is also assumed that it is isotropic and homogeneous.

$$\begin{bmatrix} \sigma_x \\ \sigma_y \\ \tau_{xy} \end{bmatrix} = \begin{bmatrix} \frac{E}{1-\nu^2} & \frac{\nu E}{1-\nu^2} & 0 \\ \frac{\nu E}{1-\nu^2} & \frac{E}{1-\nu^2} & 0 \\ 0 & 0 & \frac{E}{2(1+\nu)} \end{bmatrix} \begin{bmatrix} \varepsilon_x \\ \varepsilon_y \\ \gamma_{xy} \end{bmatrix} \tag{3.5}$$

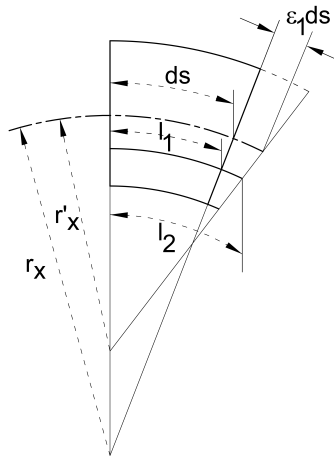


Figure 3.3: Deformed shell element[1]

Thus, the resulting forces on the shell element are obtained by inserting stresses from Eq. 3.5 into the expressions in Eq. 3.1 and substituting strains from Eq. 3.4, and are readily presented as:

$$\begin{aligned}
 N_x &= \frac{Eh}{1-\nu^2}(\varepsilon_1 + \nu\varepsilon_2) & N_y &= \frac{Eh}{1-\nu^2}(\varepsilon_2 + \nu\varepsilon_1) \\
 M_x &= -D(\chi_x + \nu\chi_y) & M_y &= -D(\chi_y + \nu\chi_x) \\
 N_{xy} = N_{yx} &= \frac{\gamma h E}{2(1+\nu)} & M_{xy} = -M_{yx} &= D(1-\nu)\chi_{xy}
 \end{aligned} \tag{3.6}$$

where D is the bending stiffness of the shell given by:

$$D = \frac{Eh^3}{12(1-\nu^2)}$$

and χ are the changes in curvature which are the terms in parentheses in Eq. 3.4.

3.5.4 Force-Displacement relations for shallow shells

The stress resultants in Eq. 3.6 are expressed in terms of the strains. Furthermore it is possible to express the strains in terms of displacements, u, v, w . The expressions are then further simplified by implementing shallow shell assumptions which are [1]:

- The slope of the shell is small compared with some reference plane.
- The curvature of the surface is small.
- The shell boundaries are such that the surface loads are carried primarily by the membrane stresses.
- Transverse deflection is much higher than in-plane deflection.

- The changes in curvature of the surface are small.

After applying this assumptions, it can be shown that the expressions in Eq. 3.6 become further extended to the following set of equations.

$$\begin{aligned}
N_x &= \frac{Eh}{1-\nu^2} \left[\frac{1}{a_x} \frac{\partial u}{\partial \alpha_x} - \frac{w}{r_x} + \nu \left(\frac{1}{a_y} \frac{\partial v}{\partial \alpha_y} - \frac{w}{r_y} \right) \right] \\
N_y &= \frac{Eh}{1-\nu^2} \left[\frac{1}{a_y} \frac{\partial v}{\partial \alpha_y} - \frac{w}{r_y} + \nu \left(\frac{1}{a_x} \frac{\partial u}{\partial \alpha_x} - \frac{w}{r_x} \right) \right] \\
N_{xy} &= \frac{hE}{2(1+\nu)} \left(\frac{1}{a_x} \frac{\partial v}{\partial \alpha_x} + \frac{1}{a_y} \frac{\partial u}{\partial \alpha_y} - \frac{2w}{r_{xy}} \right) \\
M_x &= -D \left(\frac{1}{a_x^2} \frac{\partial^2 w}{\partial \alpha_x^2} + \nu \frac{1}{a_y^2} \frac{\partial^2 w}{\partial \alpha_y^2} \right) \\
M_y &= -D \left(\frac{1}{a_y^2} \frac{\partial^2 w}{\partial \alpha_y^2} + \nu \frac{1}{a_x^2} \frac{\partial^2 w}{\partial \alpha_x^2} \right) \\
M_{xy} &= D(1-\nu) \left(\frac{1}{a_x a_y} \frac{\partial^2 w}{\partial \alpha_x \partial \alpha_y} \right)
\end{aligned} \tag{3.7}$$

Similarly, in Equation 3.3 due to the shallow shell assumption, a_x and a_y can be taken as constants, thus the terms like $\frac{\partial a_x}{\partial \alpha_y}$ are neglected. In addition, due to the assumption that loads are primarily carried by the in-plane stresses, the terms containing Q in the first two equations in Eq. 3.3 are small and therefore can be dropped. Applying this changes, it is possible to rewrite Equation 3.3 and in combination with Eq. 3.7 arrive at a single eight order partial differential equation for shallow shells, see [1, eq.1-28]. The solution for this equation involves eight constants in the homogeneous solution in addition to the particular solution. The homogeneous solution corresponds to the effect from the boundary conditions, while as the particular solution comes from the surface loading. The particular solution can usually, with a good accuracy, be substituted with the solutions from the membrane theory.

Shallow shells

The theory of shallow shells has a wide application in analytical calculations of different shell structures. Therefore, in this section a short description of shallow shells is presented. A shell could be defined as shallow if at any point of its middle surface the following inequalities hold [21]:

$$\left(\frac{\partial z}{\partial x} \right)^2 \ll 1 \quad \left(\frac{\partial z}{\partial y} \right)^2 \ll 1$$

where $z(x, y)$ is the equation of the middle surface. Following Figure 3.4 the simplification in shallow shells can be illustrated as follows:

$$ds \cong \sqrt{(dx)^2 + \left(\frac{\partial z}{\partial x} \right)^2}$$

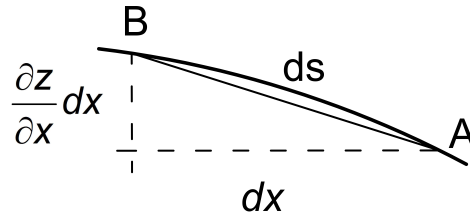


Figure 3.4: Shallow shell illustration

In shallow shells this is simplified to:

$$ds \approx dx$$

i.e, the intrinsic geometry of a shallow shell is identical to the geometry of a plane of its projection [21]. This implies that the curvilinear coordinates can be replaced by the Cartesian coordinates x and y with Lamé parameters, a_x and a_y as 1.

3.6 Membrane theory

The membrane theory is based on the omission of the bending stresses [19]. This reduces the equilibrium equations in Eq. 3.3 to only three unknowns, N_x , N_y and N_{xy} . Thus Eq. 3.3 is reduced to just the first three equations with the three variables as unknowns. The problem is then statically determinate, and it can be easily solved for a given loading and geometry. For example, the resulting in-plane force for a cylindrical shell that is loaded with a constant pressure can be expressed as:

$$N_\varphi = \sigma t = \int_0^{\pi/2} pr \cos \varphi d\varphi = pr \quad (3.8)$$

Which is derived from the vertical equilibrium of the half circle in Figure 3.5.

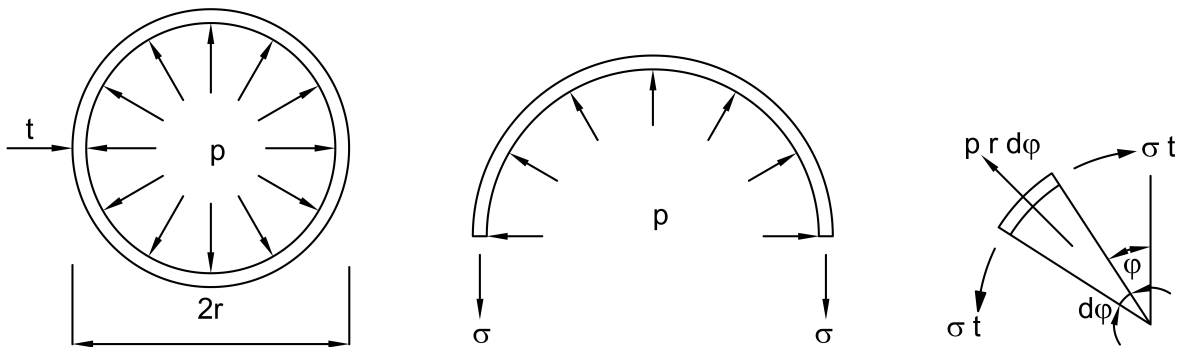


Figure 3.5: Cylinder shell with membrane theory [10]

Similarly for a sphere like structure loaded with a constant pressure, it can be shown that the in-plane stresses are expressed as:

$$\sigma_x = \sigma_\theta = \frac{pr}{2t} \quad (3.9)$$

The bending effects from the boundary conditions in shells tend to damp quickly, thus a large portion of the shell surface is dominated by the membrane forces. Therefore, the membrane theory can sometimes provide a reasonable basis for design. However, the membrane theory can only be used upon the fulfilment of the following conditions [1]:

- The displacements from membrane forces do not give rise to bending stresses.
 - The loading is distributed smoothly over the surface of the shell.
 - The boundaries can supply the forces and permit the displacements required by the membrane stress resultants.
 - The stress is uniformly distributed through the thickness of the shell.
-

Chapter 4

Cylindrical shells

4.1 General

Cylindrical shells are one of the most used structural elements in engineering. They are used both as storage facilities for resources such as gas and water, and as roofing for buildings. A cylindrical shell is an efficient structural form which is both easy to analyse and construct. Analysing a cylindrical shell with constant thickness involves only a system of equations with constant coefficients, thus it can be solved in a general manner.

4.2 Governing differential equation

The membrane theory which is presented in the previous chapter gives a sufficient solution for a shell or part of a shell surface that is free to expand. However, in parts of the shell close to a boundary where the free expansion is limited, bending stress will develop. Considering the small thickness of the thin shells, even small moments can cause significant stresses in the shell. Therefore, in order to fully analyse a shell structure, it is necessary to use both the membrane and bending theories.

In further analysis of the cylindrical shell, the notation shown in Figure 4.1 will be used.

General circular cylindrical shells with arbitrary loading and boundary conditions can only be fully analysed using FEM (finite element method). However, in some cases it is possible to get a good approximation by dividing the problem into different known state of stress [21]. In this thesis, only axisymmetrically loaded circular cylindrical shells will be considered. The symmetric nature of the problem allows for neglecting the membrane shear forces $N_{x\varphi}$ and $N_{\varphi x}$ and the twisting moments $M_{x\varphi}$ and $M_{\varphi x}$. Thus, from the remaining five equilibrium equations only three are left. These three equations adopting

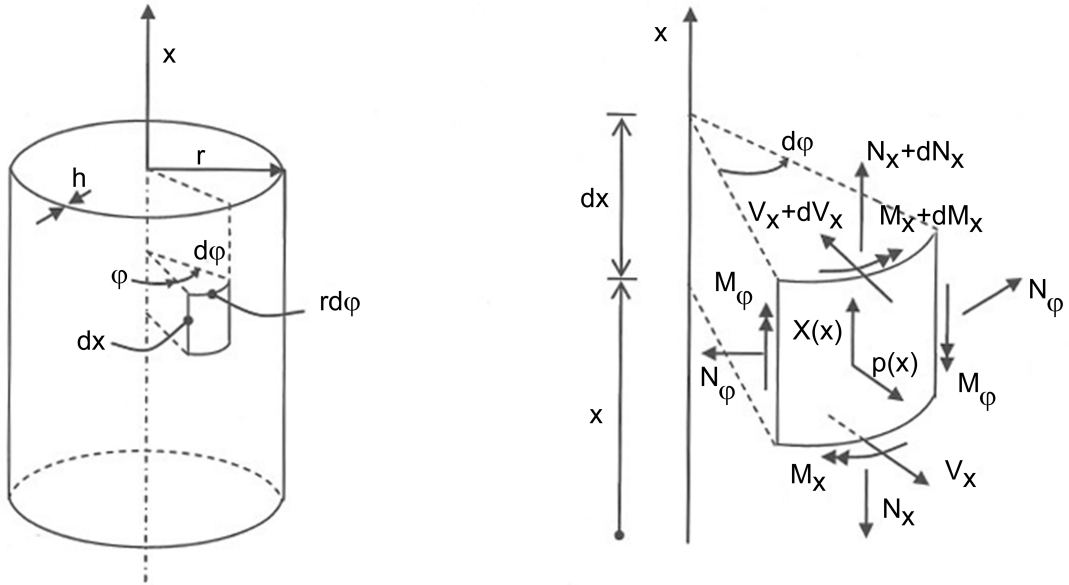


Figure 4.1: Forces on a cylindrical shell [20]

the notations in Figure 4.1 are as follows:

$$\begin{aligned}
 \sum F_x = 0 & \quad \frac{dN_x}{dx} + X(x) = 0 \\
 \sum M_{\text{tangential}} = 0 & \quad \frac{dM_x}{dx} - V_x = 0 \\
 \sum F_{\text{radial}} = 0 & \quad \frac{dV_x}{dx} + \frac{1}{r}N_\phi = P(x)
 \end{aligned} \tag{4.1}$$

From Eq. 4.1, it is clear that the first equation is not coupled with any of the two equations, thus could be solved independently. Further by combining the two coupled equations, the governing differential equation is found.

$$\frac{d^2M_x}{dx^2} + \frac{1}{r}N_\phi = p(x) \tag{4.2}$$

This can further be written in terms of displacements by employing strain-displacement relations, thus

$$N_\phi = E\varepsilon_\phi h \tag{4.3}$$

where ε_ϕ comes from the deformation in the circumferential direction. It is straight forward to show that the relationship between the hoop strain and the radial deformation is given by:

$$\varepsilon_\phi = \frac{w}{r} \tag{4.4}$$

Furthermore, neglecting the change of curvature in the circumferential direction, from the plate theory, it is known that:

$$M_x = D \frac{d^2w}{dx^2}$$

Substituting these equation into Eq. 4.2, leads to the following expression.

$$\frac{d^4w}{dx^4} + \frac{Eh}{Dr^2}w = \frac{p(x)}{D} \quad (4.5)$$

The particular solution of Equation 4.5 is the displacement from the membrane theory, which by combining equations 4.4, 4.3 and 3.8 becomes:

$$w_p = \frac{pr^2}{Eh} \quad (4.6)$$

Equation 4.6 is valid for loading p expressed with up to a third degree polynomial. In order to solve the homogeneous equation conveniently, a new expression called an elastic length is defined [14].

$$L_e = \frac{\sqrt{rh}}{\sqrt[4]{3(1-\nu^2)}}$$

and similarly a corresponding dimensionless coordinate $\xi = \frac{x}{L_e}$ is introduced. Now, the governing differential equation can be written as:

$$\frac{d^4w}{dx^4} + \frac{4}{L_e^4}w = 0 \quad (4.7)$$

The solution of this equation, introducing ξ , is given by:

$$w_h = C_1e^{-\xi} \cos \xi + C_2e^{-\xi} \sin \xi + C_3e^{\xi} \cos \xi + C_4e^{\xi} \sin \xi \quad (4.8)$$

The four constants are found by considering the boundary conditions at both ends. The boundary conditions correspond to the translational and rotational degree of freedoms at each end.

4.2.1 Damping length

The necessary length in which the bending effects are sufficiently damped out is denoted as damping length. Based on an acceptable error margin for the bending induced stresses, this length could roughly be approximated as [14]:

$$L_c = 2.41\sqrt{rh}$$

This implies that a cylindrical shell with a length smaller than

$$2L_c = 4.82\sqrt{rh}$$

such that the bending effects overlap can be characterized as short.

4.2.2 Analysis of long cylindrical shells

A cylindrical shell is characterized as long when boundary effects from one end doesn't overlap with the ones from the opposite end. When dealing with long cylindrical shells, Equation 4.8 become reduced to only two terms. The last two terms of the equation are multiplied by e^ξ which indicates an exponential increase in deflection when moving further from the boundary. However, its known that the boundary effect damps out further up the cylindrical wall. This leads to the conclusion that C_3 and C_4 must be zero. The expression in 4.8 can now be written as:

$$w_h = C_1 e^{-\xi} \cos \xi + C_2 e^{-\xi} \sin \xi \quad (4.9)$$

The remaining task is to find C_1 and C_2 from a given set of boundary conditions. Furthermore, the stress resultants can be found by differentiating the displacement. The proceeding arrangement of the solutions is done differently among the different academicians who had discussed this theorem, see Ref. [1, 2, 19, 21]. However, it is mostly about presenting the solutions in the most convenient way. In order to shorten the expressions, here the notation in Ref. [14] is followed, and accordingly define the following functions:

$$\begin{aligned} g_1 &= e^{-\xi} \cos \xi \\ g_2 &= e^{-\xi} \sin \xi \\ g_3 &= g_1 + g_2 \\ g_4 &= g_1 - g_2 \end{aligned}$$

For a given M_0 and V_0 at the edge $x = 0$, the corresponding C_1 and C_2 can be found as:

$$\begin{bmatrix} C_1 \\ C_2 \end{bmatrix} = \frac{L_e^2}{2D} \begin{bmatrix} 1 & 1 \\ -1 & 0 \end{bmatrix} \begin{bmatrix} M_0 \\ V_0 L_e \end{bmatrix} \quad (4.10)$$

By differentiating and including the g - functions, the load effects can then readily be presented as:

$$\begin{bmatrix} w \frac{2D}{L_e^2} \\ N_\varphi \frac{L_e^2}{2r} \\ \frac{dw}{dx} \frac{2D}{L_e} \\ M_x \\ V_x L_e \end{bmatrix} = \begin{bmatrix} g_4(\xi) & g_1(\xi) \\ g_4(\xi) & g_1(\xi) \\ -2g_1(\xi) & -g_3(\xi) \\ g_3(\xi) & g_2(\xi) \\ -2g_2(\xi) & g_4(\xi) \end{bmatrix} \begin{bmatrix} M_0 \\ V_0 L_e \end{bmatrix} \quad (4.11)$$

It should be noted that the total solution for the deformations and the circumferential force (N_φ) is found by the summation of both the homogeneous and the particular solution.

4.2.3 Analysis of short cylindrical shells

The difference when solving the equations for short cylindrical shells compared to the long cylindrical shells is that one has to deal with four unknowns, two at each end. As a

result the matrix in Equation 4.11 becomes a 4×4 matrix. If the notation in Figure 4.2 is used, a new coordinate η that starts from the edge $x = L$ is defined such that

$$\eta = \frac{L - x}{L_e}$$

Equation 4.11 can be rewritten to:

$$\begin{bmatrix} w \frac{2D}{L_e^2} \\ N_\varphi \frac{L_e^2}{2r} \\ \frac{dw}{dx} \frac{2D}{L_e} \\ M_x \\ V_x L_e \end{bmatrix} = \begin{bmatrix} g_4(\xi) & g_1(\xi) & g_4(\eta) & g_1(\eta) \\ g_4(\xi) & g_1(\xi) & g_4(\eta) & g_1(\eta) \\ -2g_1(\xi) & -g_3(\xi) & 2g_1(\eta) & g_3(\eta) \\ g_3(\xi) & g_2(\xi) & g_3(\eta) & g_2(\eta) \\ -2g_2(\xi) & g_4(\xi) & 2g_2(\eta) & -g_4(\eta) \end{bmatrix} \begin{bmatrix} M_{01} \\ V_{01} L_e \\ M_{02} \\ V_{02} L_e \end{bmatrix} \quad (4.12)$$

The positive directions are according to what is shown in Figure 4.3.

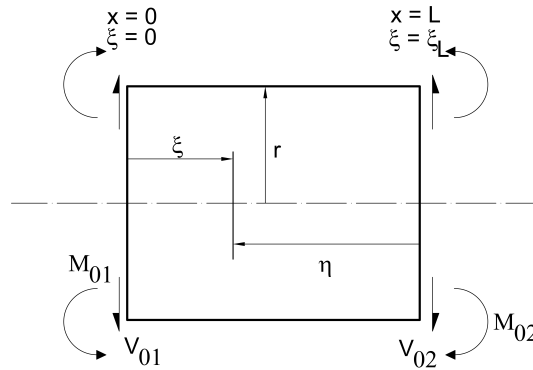


Figure 4.2: Definition of the coordinates

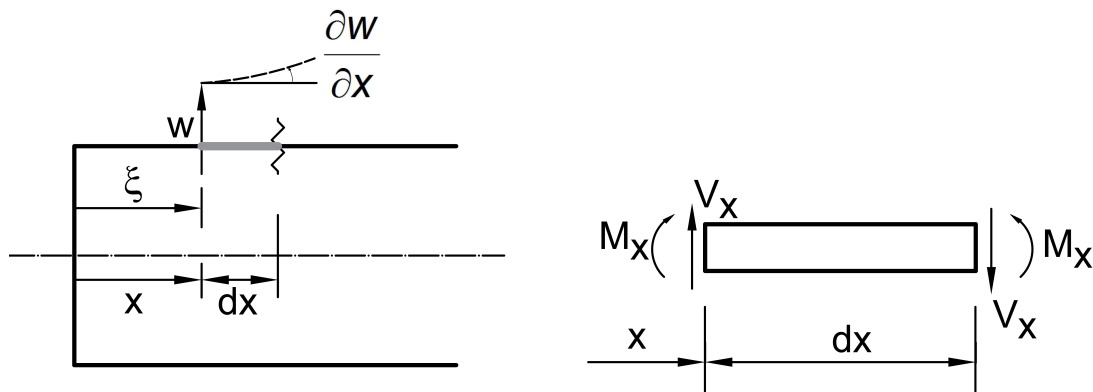


Figure 4.3: Illustration of the positive directions

So far the focus has been on finding the distribution of the load effects along the wall of the cylindrical shell. However, cylindrical shells, specially those used for storage facilities are often closed at both ends. Thus, for a complete analysis of the cylindrical shells, the contact areas with other surfaces must be dealt with. Generally the problem is solved by using compatibility requirements at the interface.

4.3 Circular flat plates

Cylindrical shells are often enclosed by circular flat plates at the top or/and bottom edge. The derivation of the governing differential equation for circular flat plates is similar to that of a rectangular flat plate. Adopting a polar coordinate system and considering only an axisymmetrical loading yields the following governing differential equation [21]:

$$\frac{d^4 w}{dr^4} + \frac{2}{r} \frac{d^3 w}{dr^3} - \frac{1}{r^2} \frac{d^2 w}{dr^2} + \frac{1}{r^3} \frac{dw}{dr} = \frac{p}{D} \quad (4.13)$$

Having the following solution for solid plates:

$$w = C_3 r^2 + C_4 + \frac{P_0 r^2}{16D} (3 + \nu) \quad (4.14)$$

Then the stress results can readily be found for different boundary conditions. Table 4.1 shows the expressions for the most common loading and boundary conditions.

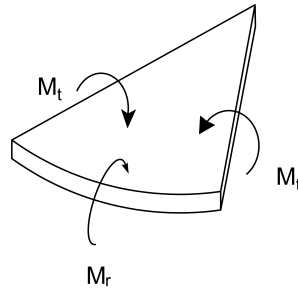
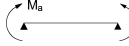
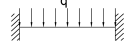
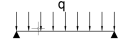


Figure 4.4: Moments in a circular flat slab

Table 4.1: Expressions for symmetrical bending of circular plates [1]

	General formulas			
ω	$\frac{qr^4}{64D} + C_1 \frac{r^2}{4} + C_2 \log \frac{r}{a} + C_3$	$\frac{M_a}{2D(1+\nu)}(a^2 - r^2)$	$\frac{q}{64D}(a^2 - r^2)^2$	$\frac{q}{64D}(a^2 - r^2) \left(\frac{5+\nu}{1+\nu} a^2 - r^2 \right)$
$\frac{d\omega}{dr}$	$\frac{qr^3}{16D} + C_1 \frac{r}{2} + C_2 \frac{1}{r}$	$-\frac{M_a r}{D(1+\nu)}$	$-\frac{qr}{16D}(a^2 - r^2)$	$-\frac{qr}{16D} \left(\frac{3+\nu}{1+\nu} a^2 - r^2 \right)$
$\frac{d^2\omega}{dr^2}$	$\frac{3qr^2}{16D} + \frac{C_1}{2} + C_2 \frac{1}{r^2}$	$-\frac{M_a}{D(1+\nu)}$	$-\frac{q}{16D}(a^2 - 3r^2)$	$-\frac{q}{16D} \left(\frac{3+\nu}{1+\nu} a^2 - 3r^2 \right)$
C_1		$-\frac{2M_a}{D(1+\nu)}$	$-\frac{qa^2}{8D}$	$-\frac{qa^2}{8D} \frac{3+\nu}{1+\nu}$
C_2		0	0	0
C_3		$\frac{M_a a^2}{2D(1+\nu)}$	$\frac{qa^4}{64D}$	$\frac{qa^4}{64D} \frac{5+\nu}{1+\nu}$
M_r	$-D \left(\frac{d^2\omega}{dr^2} + \frac{\nu}{r} \frac{d\omega}{dr} \right)$	$+M_a$	$\frac{q}{16} [a^2(1+\nu) - r^2(3+\nu)]$	$\frac{q}{16} (3+\nu)(a^2 - r^2)$
M_t	$-D \left(\frac{1}{r} \frac{d\omega}{dr} + \nu \frac{d^2\omega}{dr^2} \right)$	$+M_a$	$\frac{q}{16} [a^2(1+\nu) - r^2(1+3\nu)]$	$\frac{q}{16} [a^2(3+\nu) - r^2(1+3\nu)]$
M_a		$+M_a$	$-\frac{qa^2}{8}$	0
$M_{r,t}(x=0)$		$+M_a$	$\frac{qa^2}{16}(1+\nu)$	$\frac{qa^2}{16}(3+\nu)$

4.4 Example 1: Cylindrical water reservoir enclosed by a circular flat plate

This numerical example will be used to illustrate the practical application of the analytical solution procedure involving cylindrical shells. The structure that is considered in this example is an idealized water reservoir that has a form of a circular cylindrical shell. The cylindrical shell is connected to a circular flat slab at the top edge and is considered fully fixed at the bottom edge, see Figure 4.5.

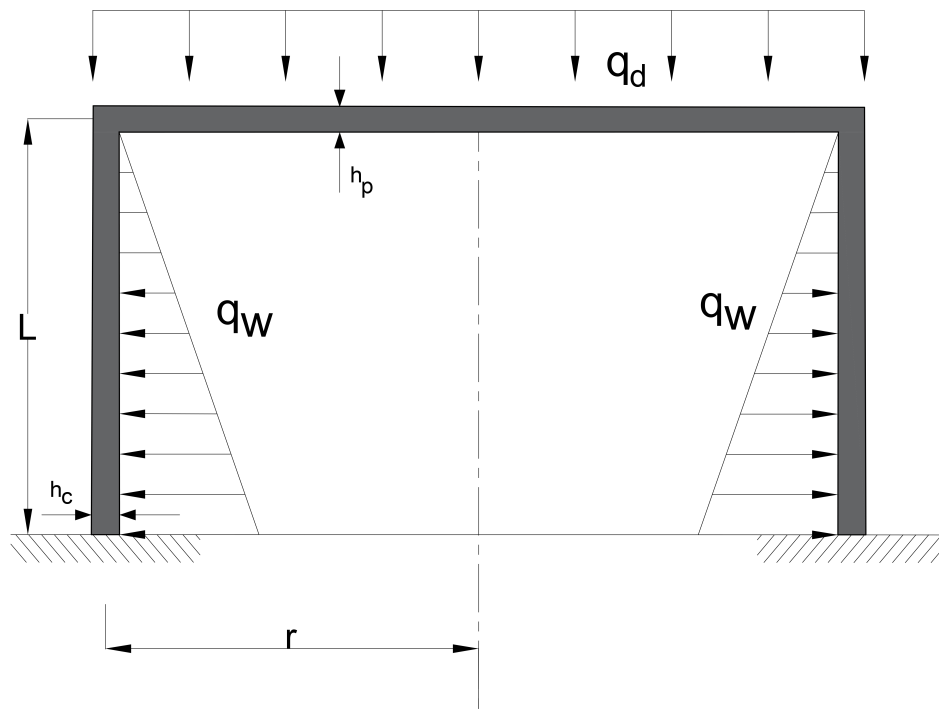


Figure 4.5: Illustration of the structure in example 1

Geometry :

$$\begin{aligned} h_c &= 0.2 \text{ m} \\ h_p &= 0.2 \text{ m} \\ r &= 6 \text{ m} \\ L &= 5 \text{ m} \end{aligned}$$

Material :

$$\begin{aligned} E &= 2 \cdot 10^7 \frac{\text{kN}}{\text{m}^2} \\ \rho &= 25 \frac{\text{kN}}{\text{m}^3} \\ \nu &= 0.2 \end{aligned}$$

Stiffness:

$$D_c = D_p = \frac{Eh^3}{12(1-\nu^2)} = \frac{2 \cdot 10^7 \cdot 0.2^3}{12(1-0.2^2)} = 1.389 \cdot 10^4 \text{ kNm}$$

Load:**Snow**

Following Eurocode 1 part 1-3 [15], and choosing an arbitrary location, snow load is given by:

$$S = \mu C_e C_t S_k = 0.8 \cdot 1 \cdot 1 \cdot 3.5 = 2.8 \quad \frac{kN}{m^2}$$

Self weight

$$g = \rho h_p = 25 \cdot 0.2 = 5 \quad \frac{kN}{m^2}$$

Using one of the Ultimate Limit State (ULS) combination from Eurocode 0 [17], the total design load is given by:

$$q_d = 1.2 \cdot g + 1.5 \cdot S = 1.2 \cdot 5 + 1.5 \cdot 2.8 = 10.2 \quad \frac{kN}{m^2}$$

Water pressure

The water pressure at the bottom of the tank (assuming load factor 1) is:

$$P_0 = \gamma_w L = 10 \cdot 5 = 50 \quad \frac{kN}{m^2}$$

If x axis is defined as a coordinate starting at the the bottom of the tank and upwards along the side of the tank, the linearly varying water pressure is given by:

$$q_w(x) = P_0 \left(1 - \frac{x}{L}\right) = 50 \left(1 - \frac{x}{L}\right)$$

Elastic length:

$$L_e = \frac{\sqrt{r h}}{\sqrt[4]{3(1 - \nu^2)}} = \frac{\sqrt{6 \cdot 0.2}}{\sqrt[4]{3(1 - 0.2^2)}} = 0.841 \quad m$$

Damping length:

$$2L_c = 4.82 \sqrt{r h_c} = 4.82 \sqrt{6 \cdot 0.2} = 5.28 \quad m$$

Since $2L_c > L$, the boundary effects from both ends must be solved together.

4.4.1 Circular plate**Particular solution**

First the connection between the circular plate and the cylindrical wall is considered as pinned. Thus, the plate is simply supported with uniformly distributed load q_d at the top. From Table 4.1, with $a = r$, the rotation at the boundary is given by:

$$\theta_q = \frac{dw}{dr} = -\frac{q_d r^3}{16 D_p} \left(\frac{3 + \nu}{1 + \nu} - 1 \right) = -\frac{10.2 \cdot 6^3}{16 \cdot 1.389 \cdot 10^4} \left(\frac{3 + 0.2}{1 + 0.2} - 1 \right) = -0.0165$$

Homogeneous solution

Then a unit moment is applied along the boundary of the circular plate. This moment

comes from the monolithic connection between the plate and the wall. The rotation of the plate due to this unit moment is found from Table 4.1 as:

$$\theta_M = \frac{dw}{dr} = -\frac{M_a r}{D_p(1+\nu)} = -\frac{M_a \cdot 6}{1.389 \cdot 10^4(1+0.2)} = -3.6 \cdot 10^{-4} M_a$$

4.4.2 Cylindrical wall

Particular solution

The radial displacement at the top edge due to the water pressure is given by Equation 4.6

$$w_p^T = \frac{q_w(L)r^2}{Eh_c} = 0$$

Similarly the radial displacement at the bottom edge is

$$w_p^B = \frac{q_w(0)r^2}{Eh_c} = \frac{50 \cdot 6^2}{2 \cdot 10^7 \cdot 0.2} = 4.5 \cdot 10^{-4} \text{ m}$$

The rotation due to the linearly varying water pressure is constant and is given by:

$$\theta_p = \frac{dw_p}{dx} = \frac{d}{dx} \left(\frac{q_w(x)r^2}{Eh_c} \right) = -\frac{50 \cdot 6^2}{5 \cdot 2 \cdot 10^7 \cdot 0.2} = -9 \cdot 10^{-5}$$

Homogeneous solution

As previously mentioned, the homogeneous solution must be evaluated by taking in consideration the edge effects from both ends, see Equation 4.12. First the values of the g – *functions* at the lower and upper edges must be evaluated. Thus, for both ξ and η equal to zero and $\frac{L}{L_e}$,

$$\begin{aligned} g_1(0) = 1 & \quad g_1\left(\frac{5}{0.841}\right) = 2.604 \cdot 10^{-3} \\ g_2(0) = 0 & \quad g_2\left(\frac{5}{0.841}\right) = 2.712 \cdot 10^{-4} \\ g_3(0) = 1 & \quad g_3\left(\frac{5}{0.841}\right) = 2.875 \cdot 10^{-3} \\ g_4(0) = 1 & \quad g_4\left(\frac{5}{0.841}\right) = 2.333 \cdot 10^{-3} \end{aligned}$$

Inserting these values in Equation 4.12 for the corresponding values of ξ and η renders the following set of equations:

$$\begin{aligned} w_h^T &= 5.94 \cdot 10^{-8} M_{01} + 6.63 \cdot 10^{-8} V_{01} L_e + 2.546 \cdot 10^{-5} M_{02} + 2.546 \cdot 10^{-5} V_{02} L_e \\ \theta_h^T &= -1.577 \cdot 10^{-7} M_{01} - 8.704 \cdot 10^{-8} V_{01} L_e + 6.055 \cdot 10^{-5} M_{02} + 3.027 \cdot 10^{-5} V_{02} L_e \\ w_h^B &= 2.546 \cdot 10^{-5} M_{01} + 2.546 \cdot 10^{-5} V_{01} L_e + 5.94 \cdot 10^{-8} M_{02} + 6.63 \cdot 10^{-8} V_{02} L_e \\ \theta_h^B &= -6.055 \cdot 10^{-5} M_{01} - 3.027 \cdot 10^{-5} V_{01} L_e + 1.577 \cdot 10^{-7} M_{02} + 8.704 \cdot 10^{-8} V_{02} L_e \end{aligned}$$

4.4.3 Compatibility requirements

Bottom edge displacement: $w_h^B = -w_p^B$

Bottom edge is fixed against displacement

$$2.546 \cdot 10^{-5} M_{01} + 2.546 \cdot 10^{-5} V_{01} L_e + 5.94 \cdot 10^{-8} M_{02} + 6.63 \cdot 10^{-8} V_{02} L_e = -4.5 \cdot 10^{-4} \quad (4.15)$$

Bottom edge rotation: $\theta_h^B = -\theta_p$

Bottom edge is fixed against rotation

$$-6.055 \cdot 10^{-5} M_{01} - 3.027 \cdot 10^{-5} V_{01} L_e + 1.577 \cdot 10^{-7} M_{02} + 8.704 \cdot 10^{-8} V_{02} L_e = 9 \cdot 10^{-5} \quad (4.16)$$

Top edge displacement: $w_h^T + w_p^T = 0$

The axial stiffness of the circular plate is considered infinite.

$$5.94 \cdot 10^{-8} M_{01} + 6.63 \cdot 10^{-8} V_{01} L_e + 2.546 \cdot 10^{-5} M_{02} + 2.546 \cdot 10^{-5} V_{02} L_e = 0 \quad (4.17)$$

Top edge rotation: $\theta_p + \theta_h^T = \theta_q + \theta_M$

$$\begin{aligned} -1.577 \cdot 10^{-7} M_{01} - 8.704 \cdot 10^{-8} V_{01} L_e + 6.055 \cdot 10^{-5} M_{02} + 3.027 \cdot 10^{-5} V_{02} L_e \\ - 9 \cdot 10^{-5} = -0.0165 - 3.6 \cdot 10^{-4} M_a \end{aligned} \quad (4.18)$$

$$M_a = M_{02}$$

Inserting this in Equation 4.18 and rearranging gives:

$$-1.577 \cdot 10^{-7} M_{01} - 8.704 \cdot 10^{-8} V_{01} L_e + 4.206 \cdot 10^{-4} M_{02} + 3.027 \cdot 10^{-5} V_{02} L_e = -0.0164 \quad (4.19)$$

Equations 4.15, 4.16, 4.17 and 4.19 constitute a set of four linear equations with four unknowns.

$$\begin{bmatrix} 2.546 \cdot 10^{-5} & 2.546 \cdot 10^{-5} & 5.94 \cdot 10^{-8} & 6.63 \cdot 10^{-8} \\ -6.055 \cdot 10^{-5} & -3.027 \cdot 10^{-5} & 1.577 \cdot 10^{-7} & 8.704 \cdot 10^{-8} \\ 5.94 \cdot 10^{-8} & 6.63 \cdot 10^{-8} & 2.546 \cdot 10^{-5} & 2.546 \cdot 10^{-5} \\ -1.577 \cdot 10^{-7} & -8.704 \cdot 10^{-8} & 4.206 \cdot 10^{-4} & 3.027 \cdot 10^{-5} \end{bmatrix} \begin{bmatrix} M_{01} \\ V_{01} L_e \\ M_{02} \\ V_{02} L_e \end{bmatrix} = \begin{bmatrix} -4.5 \cdot 10^{-4} \\ 9 \cdot 10^{-5} \\ 0 \\ -0.0164 \end{bmatrix}$$

When the set of linear equations are solved for the stress resultants, and the value for L_e is inserted, the following results are obtained:

$$\begin{bmatrix} M_{01} \\ V_{01} \\ M_{02} \\ V_{02} \end{bmatrix} = \begin{bmatrix} 14.61 & \frac{kNm}{m} \\ -38.40 & \frac{kN}{m} \\ -42.02 & \frac{kNm}{m} \\ 50.02 & \frac{kN}{m} \end{bmatrix}$$

Inserting these results into the different expressions for the load effects gives the distribution of the effects along the cylindrical wall and the circular slab.

4.4.4 Distribution of the load effects

As mentioned earlier the total load effects are obtained by summing up both the particular and homogeneous solutions.

Load effects in the circular slab

The expressions for both the radial and tangential moments are given in Table 4.1:

$$\begin{aligned} M_r &= M_{02} + \frac{q}{16}(3 + \nu)(a^2 - (6 - r)^2) = -42.02 + 2.04(36 - (6 - r)^2) \\ M_t &= M_{02} + \frac{q}{16}(a^2(3 + \nu) - (6 - r)^2(1 + 3\nu)) = -42.02 + 0.64(115.2 - 1.6(6 - r)^2) \end{aligned} \quad (4.20)$$

Notice that the axis is switched so that r starts at the edge and goes towards the center of the slab. The distribution of both the moments in the slab are plotted in Figure 4.6. Positive moment value results in tension stresses at the bottom of the slab. The red line represents the center of the circular flat plate.

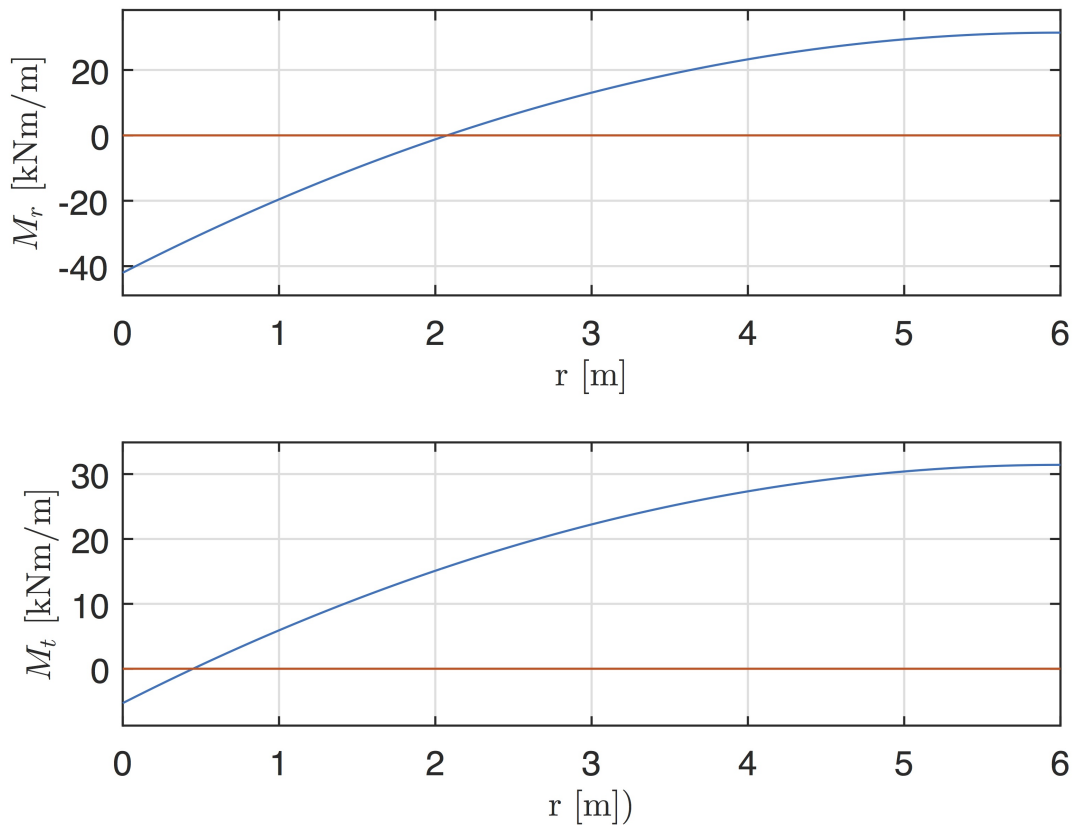


Figure 4.6: Slab moments

Due to symmetry conditions, the shear force V_t is neglected while as V_r is given by [21, eq.4.22] with $C_2 = 0$:

$$V_r = -\frac{q(6 - r)}{2} = -\frac{10.2(6 - r)}{2} \quad (4.21)$$

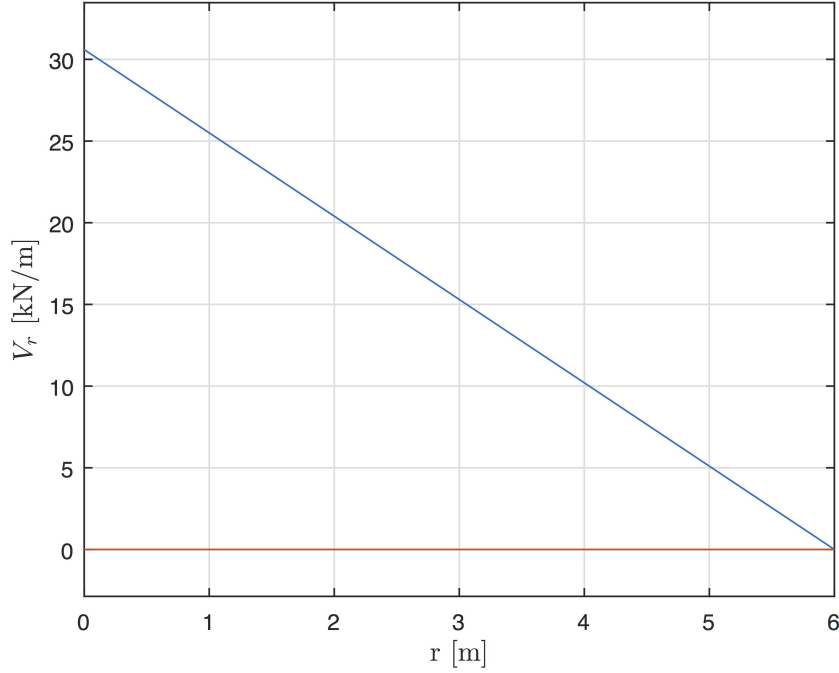


Figure 4.7: Shear force in the slab

The corresponding shear force distribution in the slab is plotted in Figure 4.7

Load effects in the cylindrical wall

The expression for the moment M_x is given in Equation 4.12 as:

$$\begin{aligned} M_x &= M_{01}g_3(\xi) + V_{01}L_e g_2(\xi) + M_{02}g_3(\eta) + V_{02}L_e g_2(\eta) \\ &= 14.61g_3(\xi) - 32.29g_2(\xi) - 42.02g_3(\eta) + 42.07g_2(\eta) \end{aligned} \quad (4.22)$$

Similarly the expression for the shear force V_x is given by:

$$\begin{aligned} V_x &= -\frac{2M_{01}}{L_e}g_2(\xi) + V_{01}g_4(\xi) + \frac{2M_{02}}{L_e}g_2(\eta) - V_{02}g_4(\eta) \\ &= -34.74g_2(\xi) - 38.40g_4(\xi) - 99.93g_2(\eta) - 50.02g_4(\eta) \end{aligned} \quad (4.23)$$

The corresponding distributions are plotted in Figures 4.8 and 4.9 respectively. $x = 0$ corresponds to the bottom of the cylindrical wall which is assumed to be fully fixed. The red line in the diagrams represent the center of the cylindrical wall.

The circumferential force N_φ has contributions both from the particular and homogeneous solutions. The particular solution is obtained from Equation 4.3 which by inserting the value for ξ_φ from the radial displacement, is given by:

$$N'_\varphi = E \frac{w_p}{r} h = p(x)r = 6(50 - 10x) \quad (4.24)$$

The homogeneous solution is given in Equation 4.12 as:

$$\begin{aligned} N_\varphi^h &= (M_{01}g_4(\xi) + V_{01}L_e g_1(\xi) + M_{02}g_4(\eta) + V_{02}L_e g_1(\eta)) \frac{2r}{L_e^2} \\ &= 247.88g_4(\xi) - 547.92g_1(\xi) - 712.93g_4(\eta) + 713.72g_1(\eta) \end{aligned} \quad (4.25)$$

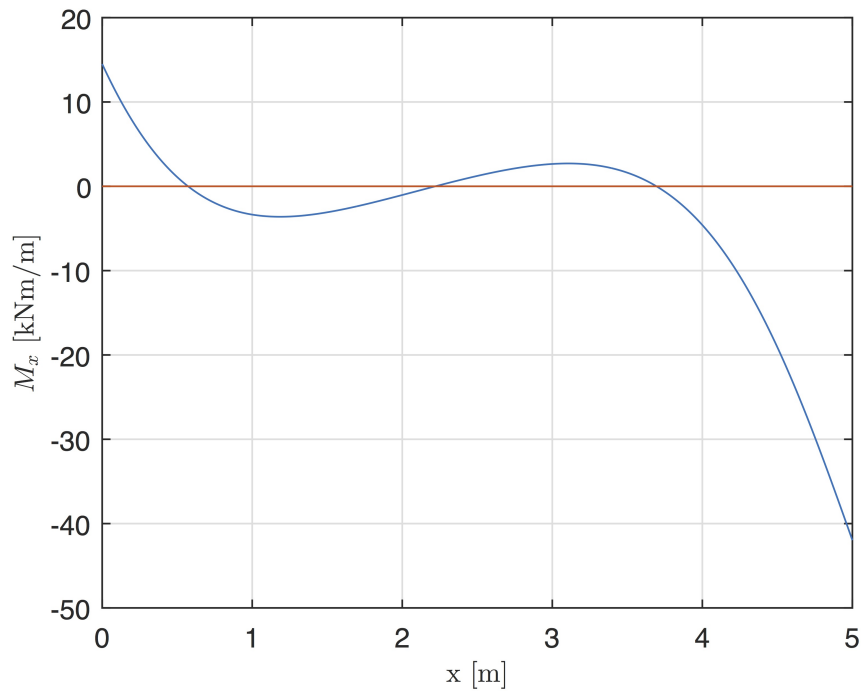


Figure 4.8: Moment in the cylindrical wall

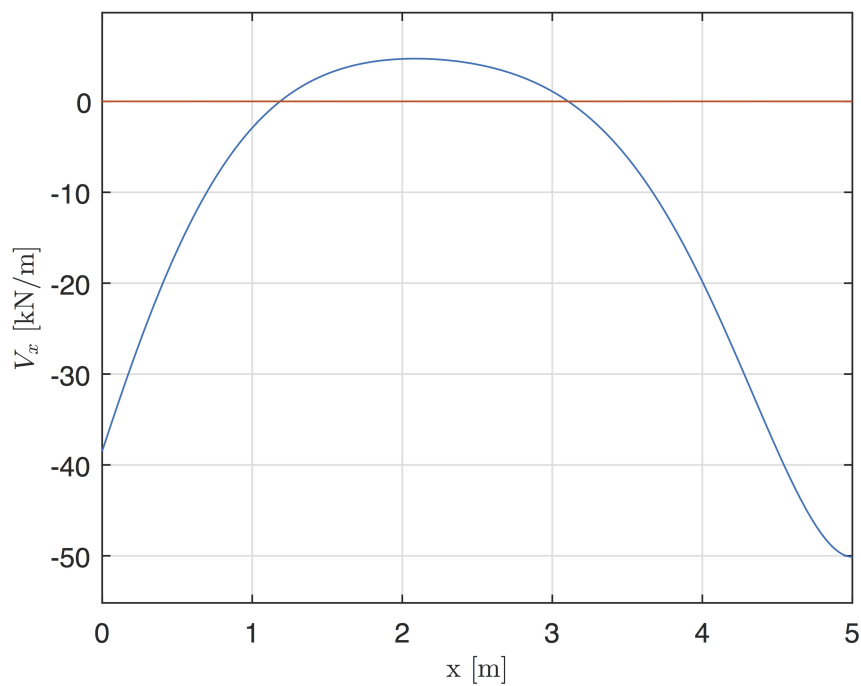


Figure 4.9: Shear force in the cylindrical wall

The total circumferential force is then given by:

$$N_\varphi = 247.88g_4(\xi) - 547.92g_1(\xi) - 712.93g_4(\eta) + 713.72g_1(\eta) + 300 - 60x \quad (4.26)$$

The distribution is plotted in Figure 4.10:

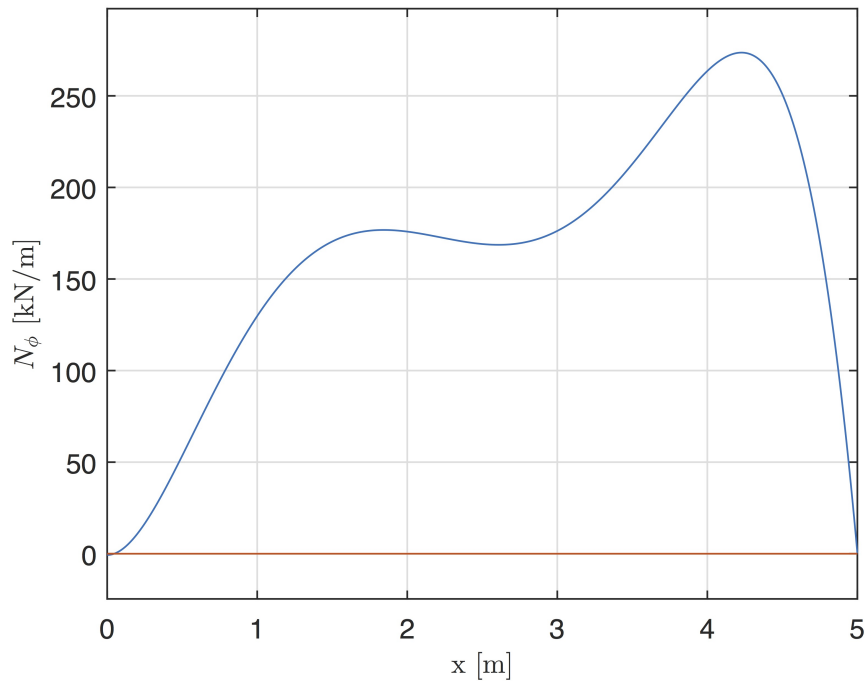


Figure 4.10: Circumferential force in the cylindrical wall

4.4.5 Remarks on the result from the analytical calculations

Both the moments in the circular slab changes from a positive value at the center to a negative value at the edge. Due to the vertically downward directed loading on the slab and the partially fixed edges, this result is as expected. From the diagrams for the stress resultants in the cylindrical wall, it is evident that the boundary effects from both edges are considered. The bending moment in the cylindrical shell is largest at the edges, and it quickly decreases towards the center of the wall which is dominated by the particular solution. The diagram for the circumferential force shows the presence of tension stresses in the circumferential direction in the entire length of the wall except at the edges which are zero. This agrees well with the type of edge constraints that are assumed.

Chapter 5

Shells of revolution

5.1 General

Shells of revolution, next to cylindrical shells, are one of the most practically used shell surfaces in concrete structures. Some of the application of this types of shells are tanks, containers, domes, and are often used in combination with cylindrical shells. Shells of revolution are obtained by the rotation of a plane curve about the axis lying in the plane of the curve [19]. The curve is called the meridian and its plane is denoted as the meridian plane. In this section, only the spherical dome will be considered. A spherical dome has a positive Gaussian curvature, thus the edge effects generally damp quickly.

A differential element shown in Figure 5.1 is cut out by two adjacent meridians and parallel circles. The position of a meridian is defined by the angles θ and φ . The angle θ is measured from a datum meridian plane, and the angle φ is made by the normal to the surface and the axis of rotation. The meridian plane and a plane perpendicular to the meridian are the planes of principal curvature at a given point on the surface. The corresponding radii of curvatures are denoted as r_1 and r_2 respectively. Furthermore, the radius of the parallel circle is denoted by:

$$r_0 = r_2 \sin \varphi$$

5.2 Membrane theory of shells of revolution

As mentioned earlier, neglecting the bending effects from the boundary conditions, a membrane theory of shells can be developed. In membrane theory, the external load is taken up by the in-plane forces N_θ and N_φ as shown in Figure 5.1. For axisymmetrically loaded shells, the in-plane shear forces are neglected and the external loading is decomposed into the local Y and Z axes only. The external load components in these directions, following Figure 5.1, are expressed as:

$$\begin{aligned} p_\varphi r_1 r_0 d\varphi d\theta \\ p_z r_1 r_0 d\varphi d\theta \end{aligned} \tag{5.1}$$

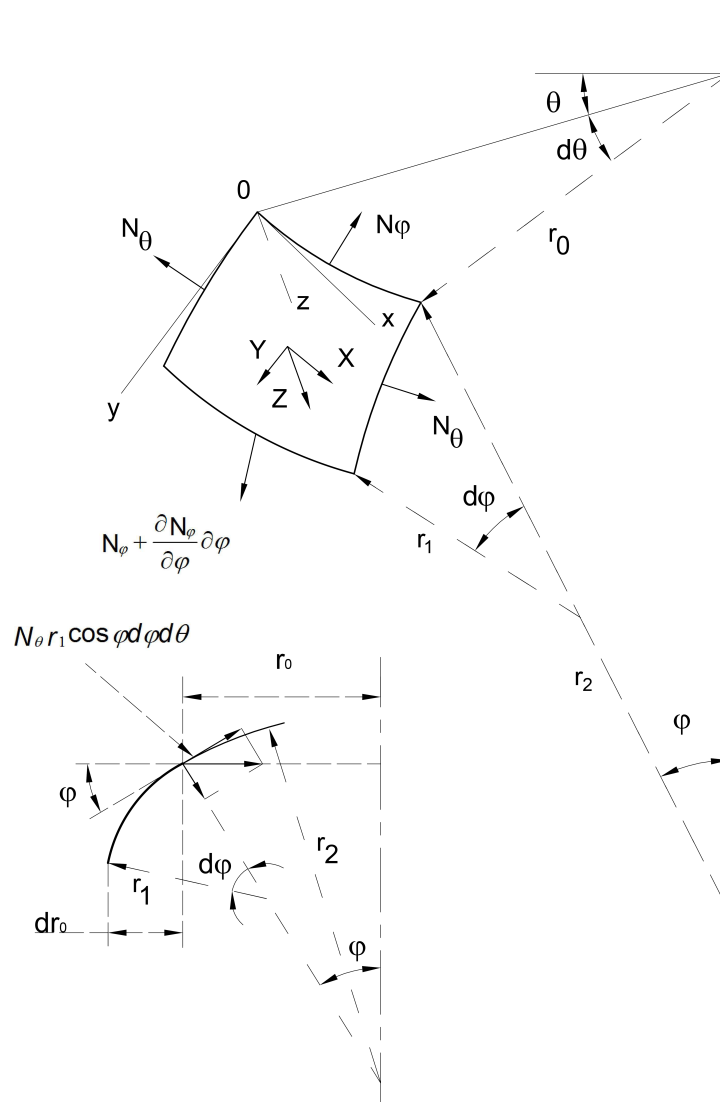


Figure 5.1: Differential element of axisymmetric shells of revolution[19]

Similarly the in-plane forces can also be decomposed in Y and Z directions so that the equilibrium equations, $\sum Y = 0$ and $\sum Z = 0$ are considered. This two equations are then expressed as:

$$\begin{aligned} \frac{d(N'_\phi r_0)}{d\phi} - N'_\theta \frac{dr_0}{d\phi} + p_\phi r_0 r_1 &= 0 \\ \frac{N'_\theta}{r_2} + \frac{N'_\phi}{r_1} + p_z &= 0 \end{aligned} \quad (5.2)$$

where N'_θ and N'_ϕ denotes the membrane forces. These two equations can then be solved with respect to these two unknowns. Next, doing some rearranging of the variables and mathematical manipulations, the following two expressions for the two unknowns can be

found [1].

$$\begin{aligned}
 N'_\theta &= -\frac{r_0}{\sin \varphi} \left(\frac{N'_\varphi}{r_1} + p_z \right) \\
 N'_\varphi &= -\frac{1}{2\pi r_0 \sin \varphi} \int_0^\varphi (p_\varphi \sin \varphi + p_z \cos \varphi)(2\pi r_0)r_1 d\varphi
 \end{aligned} \tag{5.3}$$

The expression within the integral represents the total vertical load, which is summed up over a complete parallel circle defined by φ and along the meridian. This is illustrated in Figure 5.2.

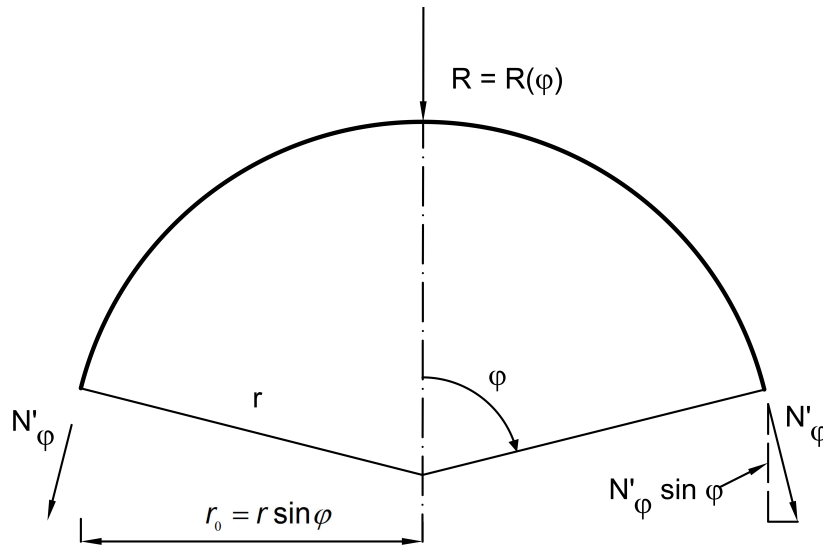


Figure 5.2: Illustration of the equivalent vertical load [14]

Hence, N'_φ can be directly written as:

$$N'_\varphi = -\frac{R}{2\pi r_0 \sin \varphi}$$

and therefore N'_θ as:

$$N'_\theta = \frac{R}{2\pi r_1 \sin^2 \varphi} - p_z \frac{r_0}{\sin \varphi}$$

Usually, for practical reasons, the meridional force N'_φ as shown in Figure 5.2, can not be provided by support force in the same direction. Such structures are usually supported by vertical walls and some kind of ring reinforcement at the edge to take up the horizontal force:

$$H_\varphi = N'_\varphi \cos \varphi$$

The hoop forces N_θ are usually not enough to offset the force H_φ , thus bending stresses along the meridian must develop. Such junctions will closely be discussed later in this chapter.

5.2.1 Displacements from the membrane theory

The deformations w and v due to loads in Z and Y directions respectively are considered. Thus, the total deformation of arc AB in Figure 5.3 can be written as:

$$\frac{dv}{d\varphi}d\varphi - wd\varphi$$

Dividing this by the initial length $r_1d\varphi$ gives the strain of the shell in the meridional direction as:

$$\varepsilon_\varphi = \frac{1}{r_1} \frac{dv}{d\varphi} - \frac{w}{r_1} \quad (5.4)$$

The corresponding strain in the circumferential direction is proportional to the change of radius r_0 . Thus it is given by:

$$\varepsilon_\theta = \frac{v \cos \varphi - w \sin \varphi}{r_0} \quad (5.5)$$

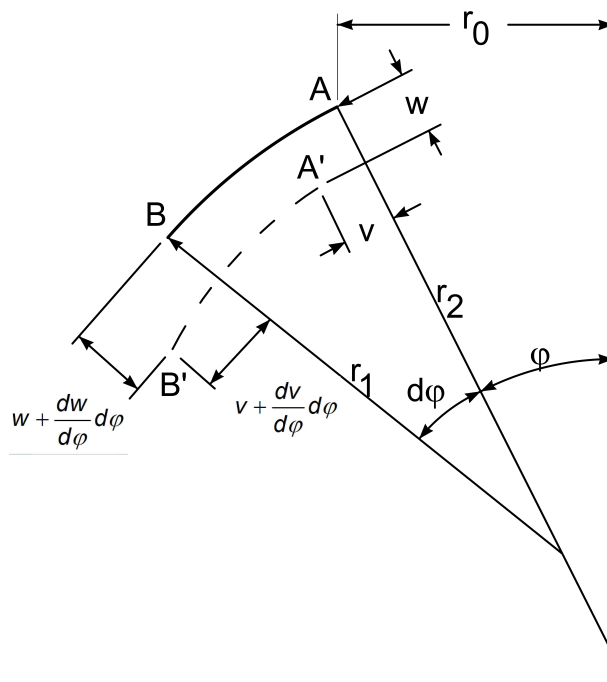


Figure 5.3: Displacements from the membrane theory [14]

Using Hooke's law the strains can be written in terms of stresses/forces and are expressed as:

$$\begin{aligned} \varepsilon_\varphi &= \frac{1}{Eh} (N_\varphi - \nu N_\theta) \\ \varepsilon_\theta &= \frac{1}{Eh} (N_\theta - \nu N_\varphi) \end{aligned} \quad (5.6)$$

Combining equations 5.4, 5.5 and 5.6, a differential equation that can be solved for v is obtained.

$$\frac{dv}{d\varphi} - v \cot \varphi = \frac{1}{Eh} [N_\varphi(r_1 + \nu r_2) - N_\theta(r_2 + \nu r_1)] \quad (5.7)$$

This has the general solution:

$$v = \sin \varphi \left(\int \frac{f(\varphi)}{\sin \varphi} d\varphi + C \right) \quad (5.8)$$

Where $f(\varphi)$ is the expression on the right hand side of the differential equation in 5.7. Then w can be found by differentiating v and inserting it into Eq. 5.4. Thus, substituting ε_φ from Eq. 5.6 w is given by:

$$w = v \cot \varphi - \frac{r_2}{Eh} (N'_\theta - \nu N'_\varphi) \quad (5.9)$$

Moreover, for the compatibility requirements with other surfaces, the horizontal displacement and rotation at the edge is of concern. The relationship between radial displacement and circumferential strain is as defined in Eq. 4.4. Thus,

$$\Delta_H = r_0 \varepsilon_\theta = \frac{r_2 \sin \varphi}{Eh} (N'_\theta - \nu N'_\varphi) \quad (5.10)$$

Assuming a rigid support at the edge, $v = 0$, the rotation could be written as:

$$\Delta_\varphi = \frac{1}{r_1} \frac{dw}{d\varphi} \quad (5.11)$$

For a spherical dome like structure loaded under its own weight, the membrane solutions from Eq. 5.10 and Eq. 5.11 are for example given by:

$$\begin{aligned} \Delta_H &= \frac{r^2 q}{Eh} \left(\frac{1 + \nu}{1 + \cos \varphi} - \cos \varphi \right) \\ \Delta_\varphi &= -\frac{r q}{Eh} (2 + \nu) \sin \varphi \end{aligned} \quad (5.12)$$

5.3 Bending theory in shells of revolution

As stated earlier bending in shells occur due to the supporting conditions. In this section, the governing differential equation will be developed, and its solution for spherical dome shells will be presented.

5.3.1 Governing differential equation

For the development of the governing differential equations, the external loading is dropped as it is already handled in the membrane theory. Furthermore, the reduction due to symmetry is implemented. Thus three equilibrium equations are left and these will be

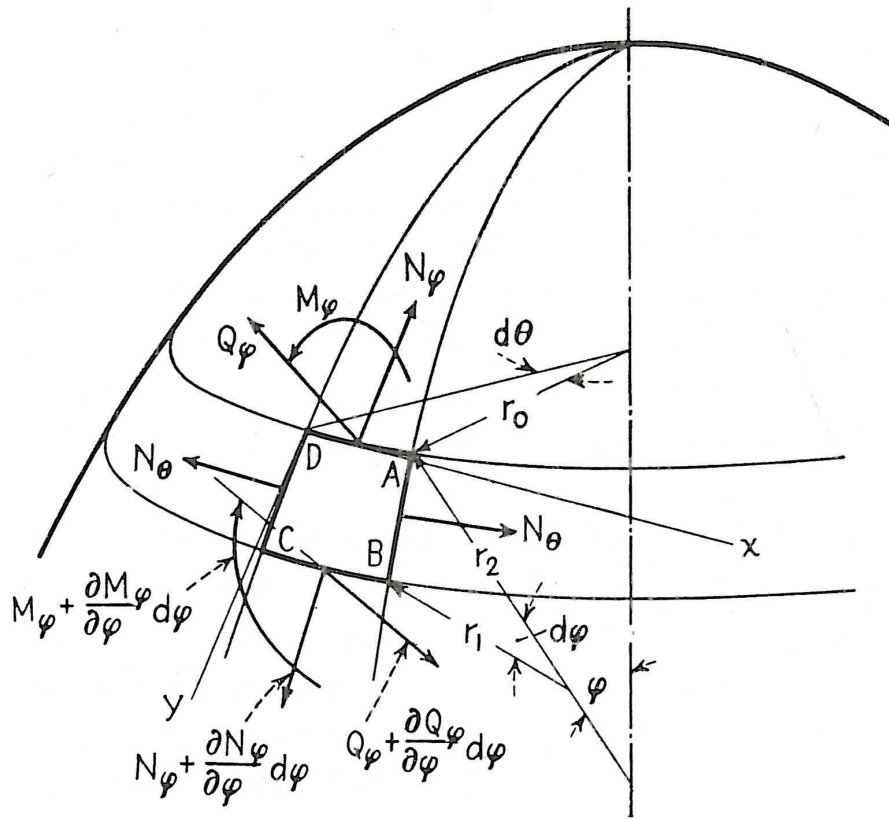


Figure 5.4: Forces on a shell element [19]

developed for the element in Figure 5.4.

Equilibrium of forces in the direction of tangent and normal to the meridian are the same as the first expression in Eq. 5.2 with an additional term due to the shear forces. The resulting shear force is given by $Q_\varphi r_0 d\theta$, and its component in the direction of tangent to the meridian is given by $Q_\varphi r_0 d\theta d\varphi$. Dropping the $d\theta d\varphi$, the term $-Q_\varphi r_0$ is then added to Eq. 5.2. Similarly $\frac{d(Q_\varphi r_0)}{d\varphi}$ is added to the second equation.

$$\begin{aligned} \frac{d(N_\varphi r_0)}{d\varphi} - N_\theta \frac{dr_0}{d\varphi} - Q_\varphi r_0 &= 0 \\ \frac{N_\theta}{r_2} + \frac{N_\varphi}{r_1} + \frac{d(Q_\varphi r_0)}{d\varphi} &= 0 \end{aligned} \quad (5.13)$$

The third equilibrium equation is obtained by taking moment equilibrium of the forces on the element with respect to the tangent to the parallel circle. Thus after some simplifications including elimination of small terms, this is given by:

$$\frac{d}{d\varphi}(M_\varphi r_0) - M_\theta r_1 \cos \varphi - Q_\varphi r_1 r_0 = 0 \quad (5.14)$$

Following Figure 5.5, it is also possible to express N_φ from vertical equilibrium similar as it is done before

$$N_\varphi = -Q_\varphi \cot \varphi \quad (5.15)$$

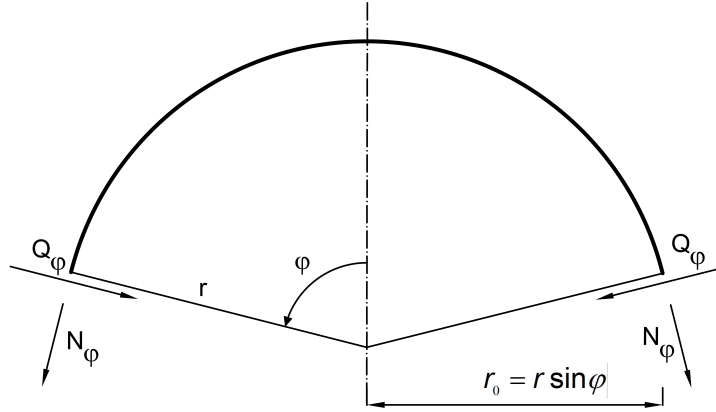


Figure 5.5: Vertical equilibrium [14]

Substituting Eq. 5.15 into the second equation of Eq. 5.13 and solving for N_φ , the following expression is obtained:

$$N_\theta = -\frac{1}{r_1 \sin \varphi} \frac{d(Q_\varphi r_0)}{d\varphi} + \frac{Q_\varphi r_0 \cot \varphi}{r_1 \sin \varphi} \quad (5.16)$$

If the following two variables are introduced

$$V = \frac{1}{r_1} \left(v + \frac{dw}{d\varphi} \right) \quad (5.17)$$

$$U = r_2 Q_\varphi$$

The two equations can then be written as:

$$\begin{aligned} N_\varphi &= -\frac{1}{r_2} U \cot \varphi \\ N_\theta &= -\frac{1}{r_1} \frac{dU}{d\varphi} \end{aligned} \quad (5.18)$$

Then, differentiating Eq. 5.9 once and substituting it in the first of Eq. 5.17, the following expression for V is obtained.

$$V = \frac{\cot \varphi}{r_1 E h} [(r_1 + \nu r_2) N_\varphi - (r_2 + \nu r_1) N_\theta] - \frac{d}{r_1 d\varphi} \left[\frac{r_2}{E h} (N_\theta - \nu N_\varphi) \right] \quad (5.19)$$

Inserting N_φ and N_θ from Eq. 5.18, and taking $r_1 = r_2 = r$, that is for a sphere like structure, the first differential equation is found.

$$\frac{d^2 U}{d\varphi^2} + \frac{dU}{d\varphi} \cot \varphi - U(\cot^2 \varphi - \nu) = E h r V \quad (5.20)$$

The second differential equation is found by expressing the bending moments in the third equilibrium equation 5.14 with curvatures, see Eq. 3.6. It can be shown that the curvatures expressed in terms of V are given by:

$$\begin{aligned} \chi_\varphi &= \frac{d}{r d\varphi} V \\ \chi_\theta &= \frac{\cot \varphi}{r} V \end{aligned} \quad (5.21)$$

Thus, the second differential equation becomes:

$$\frac{d^2V}{d\varphi^2} + \frac{dV}{d\varphi} \cot \varphi - V(\cot^2 \varphi + \nu) = -\frac{r^2}{D}Q_\varphi \quad (5.22)$$

The exact solution for these two simultaneous differential equations is fairly complicated. However, there exists a simplified version of the equations that could be solved easily. The assumption for this simplification is based on the bending deformation being small. Thus, all functions characterizing the stress and strain components in a shell near its edge, as well as their first derivatives, are small compared with their higher derivatives [21]. This assumption is especially correct for shells that can't be characterized as shallow. Implementing this simplifications, the two equations are written as:

$$\begin{aligned} \frac{d^2U}{d\varphi^2} &= EhrV \\ \frac{d^2V}{d\varphi^2} &= -\frac{r^2}{D}Q_\varphi \end{aligned} \quad (5.23)$$

This can further be rewritten to a single differential equation as:

$$\frac{d^4Q_\varphi}{d\varphi^4} + 4\lambda^4Q_\varphi = 0 \quad (5.24)$$

where

$$\lambda^4 = 3(1 - \nu^2) \left(\frac{a}{h}\right)^2 \quad (5.25)$$

The solution of this equation is similar to that of a cylindrical shell. Defining the angle measured from the edge ($\varphi = \varphi_0$) as:

$$\psi = \varphi_0 - \varphi$$

The correctly damped solution is given by:

$$Q_\varphi = e^{-\lambda\psi}(C_1 \cos \lambda\psi + C_2 \sin \lambda\psi) \quad (5.26)$$

The term $\lambda\psi$ is denoted as t and the g - functions are as defined before. Then, it is possible to show that for a given M_0 and horizontal force R_0 at the edge $\psi = 0$, the corresponding C_1 and C_2 can be expressed as:

$$\begin{bmatrix} C_1 \\ C_2 \end{bmatrix} = \begin{bmatrix} -\sin \varphi & 0 \\ \sin \varphi & \frac{Ehr}{2\lambda^3 D} \end{bmatrix} \begin{bmatrix} R_0 \\ M_0 \end{bmatrix} \quad (5.27)$$

By differentiating Eq. 5.26 and rearranging the variables, the load effects can readily be found as [14]:

$$\begin{bmatrix} R_\varphi \sin \varphi \\ M_\varphi \frac{Ehr}{2\lambda^3 D} \\ Q_\varphi \\ N_\varphi \tan \varphi \\ N_\theta \frac{1}{\lambda} \\ M_\theta \frac{Ehr}{2\nu\lambda^3 D} \\ \Delta_\varphi \frac{Eh}{2\lambda^2} \\ \Delta_H \frac{Eh}{\lambda r \sin \varphi} \end{bmatrix} = \begin{bmatrix} g_4(t) & g_2(t) \\ 2g_2(t) & g_3(t) \\ -g_4(t) & g_2(t) \\ g_4(t) & -g_2(t) \\ 2g_1(t) & g_4(t) \\ 2g_2(t) & g_3(t) \\ -g_3(t) & -g_1(t) \\ 2g_1(t) & g_4(t) \end{bmatrix} \begin{bmatrix} R_0 \sin \varphi \\ M_0 \frac{Ehr}{2\lambda^3 D} \end{bmatrix} \quad (5.28)$$

Since R_0 is introduced as an integration constant instead of Q_0 , the particular solution needs to be modified. A term that corresponds to $R_0 = 0$ must be added to the membrane theory solutions. To do this, a horizontal component of the support force N_φ must be eliminated, thus a force $H = N_\varphi \cos \varphi$ is applied at the edge. Solving Eq. 5.28 for Δ_φ and Δ_H with $M_0 = 0$ and $R_0 = -H$ renders the following solutions:

$$\begin{aligned} \Delta_H^R &= \frac{\lambda r \sin \varphi}{Eh} 2R_0 \sin \varphi \\ \Delta_\varphi^R &= -\frac{2\lambda^2}{Eh} R_0 \sin \varphi \end{aligned} \quad (5.29)$$

Thus, the final particular solutions are obtained as

$$\begin{aligned} \Delta_H^p &= \Delta_H + \Delta_H^R \\ \Delta_\varphi^p &= \Delta_\varphi + \Delta_\varphi^R \end{aligned} \quad (5.30)$$

It should again be noted that the total solution for deformation and membrane forces are obtained by the summation of the homogeneous and particular solutions.

5.4 Ring beams

At a connection between a spherical shell roof and a circular cylindrical wall, there is often an edge reinforcement in the form of a circular ring beam. In the following derivation of the theoretical background for ring beams, it is assumed that the width of the beam b is small compared to r , so that the 'curved-beam' effect is neglected. It can be shown that for any practical concrete structure, this assumption is justifiable [2]. First, the deformations of a circular ring beam which is loaded by distributed force H acting in the radial direction through the centroid of the cross section, is to be derived, see Figure 5.6. Similar as it is done in Eq. 3.8, that is equilibrium of the half circle, following Figure 5.6 the ring force T can be written as:

$$T = Hr$$

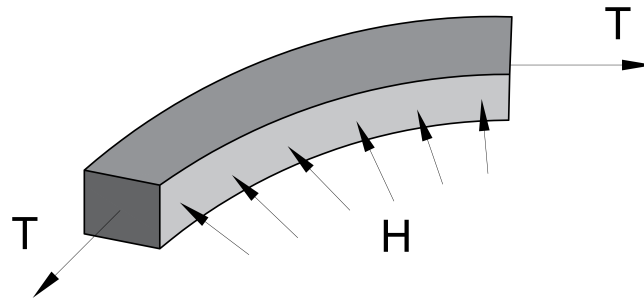


Figure 5.6: Ring beam with distributed force the in radial direction

which gives a strain in circumferential direction

$$\varepsilon_{\theta} = \frac{T}{EA}$$

Following Eq. 4.4 the radial deformation can now be expressed in terms of H as:

$$\Delta_H = \frac{r^2}{EA} H \quad (5.31)$$

Again, the same ring beam is loaded with distributed moment M_r acting in the radial direction. Similarly the moment M_{θ} of the beam can be expressed as:

$$M_{\theta} = M_r r$$

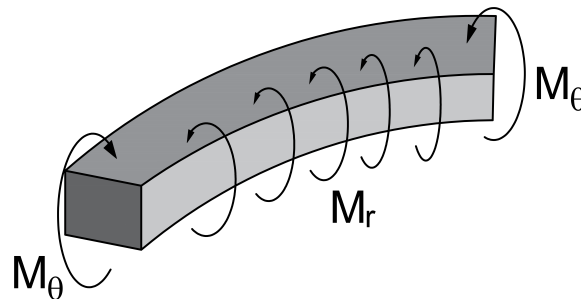


Figure 5.7: Ring beam with distributed moment in the radial direction

Following beam theory the corresponding stress is found as:

$$\sigma(y) = \frac{M_{\theta}}{I} y$$

Using Hook's law the strains are obtained as

$$\varepsilon_{\theta} = \frac{M_{\theta} y}{EI}$$

Thus,

$$\Delta_H = \frac{r^2 y}{EI} M_r \quad (5.32)$$

And as rotation is defined by $\Delta_{\varphi} = \frac{\Delta_H}{y}$, it follows that:

$$\Delta_{\varphi} = \frac{r^2}{EI} M_r \quad (5.33)$$

5.5 Example 2: An idealized cylindrical concrete gas vessel enclosed by a spherical shell at the top

In this example a connection between a spherical shell roof, a ring beam and a cylindrical wall is to be illustrated. The structure that is to be analysed is an idealized concrete gas pressure vessel that has a form of a circular cylindrical shell. The vessel is enclosed by a spherical shell at the top, and it is considered fully fixed at the bottom, see Figure 5.8.

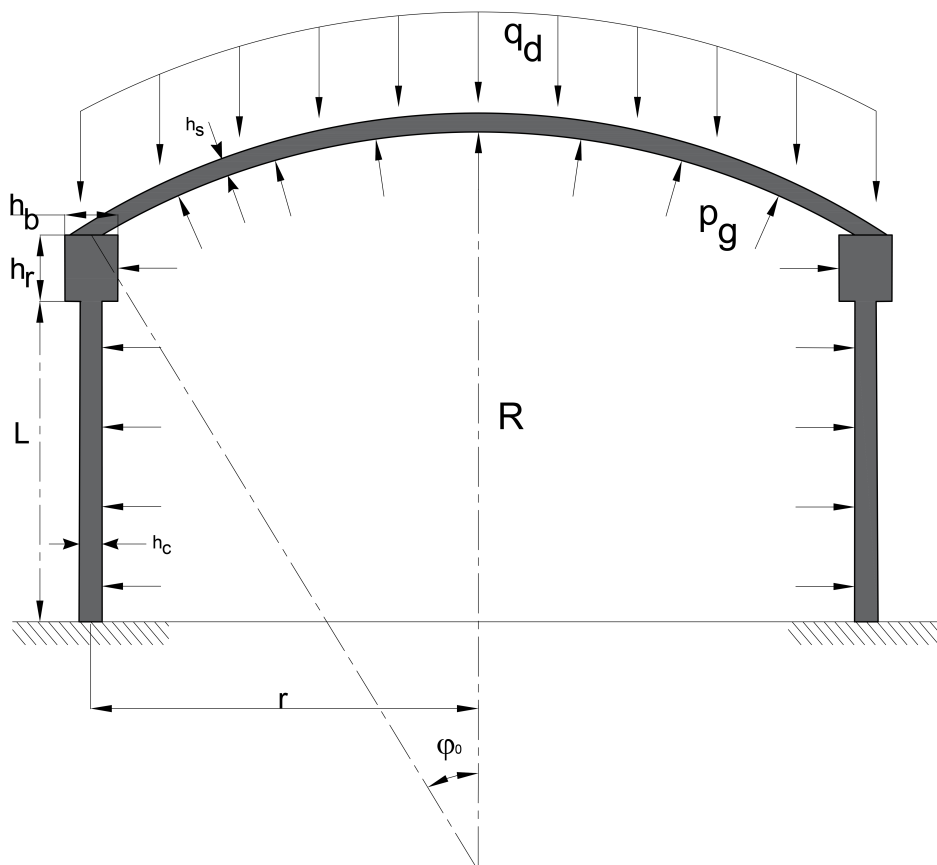


Figure 5.8: Illustration of the structure in example 2

Geometry :

$$h_c = 0.2 \text{ m}$$

$$h_s = 0.2 \text{ m}$$

$$r = 5 \text{ m}$$

$$L = 6 \text{ m}$$

$$h_r = b = 0.3 \text{ m}$$

$$r_1 = r_2 = R = 12 \text{ m}$$

$$\varphi_0 = 24.6^\circ$$

Material :

$$E = 2 \cdot 10^7 \frac{\text{kN}}{\text{m}^2}$$

$$\rho = 25 \frac{\text{kN}}{\text{m}^3}$$

$$\nu = 0.2$$

Stiffness:

$$D_c = D_s = \frac{Eh^3}{12(1-\nu^2)} = \frac{2 \cdot 10^7 \cdot 0.2^3}{12(1-0.2^2)} = 1.389 \cdot 10^4 \quad kNm$$

$$EI = E \frac{bh^3}{12} = 1.35 \cdot 10^4 \quad kNm^2$$

Load:

Snow

Following Eurocode 1 part 1-3 [15], the snow load is given by:

$$S = \mu C_e C_t S_k = 0.8 \cdot 1 \cdot 1 \cdot 3.5 = 2.8 \quad \frac{kN}{m^2}$$

The snow load is given per square meter of of the plane in the horizontal projection, but here for simplification it is considered to have the same distribution as self weight.

Self weight

$$g = \rho h_p = 25 \cdot 0.2 = 5 \quad \frac{kN}{m^2}$$

Again, using one of the Ultimate Limit State (ULS) combination from Eurocode 0 [17] the total design load is given by

$$q_d = 1.2 \cdot g + 1.5 \cdot S = 1.2 \cdot 5 + 1.5 \cdot 2.8 = 10.2 \quad \frac{kN}{m^2}$$

Gas pressure

The gas pressure acts perpendicular to all the internal surfaces of the vessel. In this example the following assumed design value is chosen.

$$p_g = 150 \quad \frac{kN}{m^2}$$

As the gas pressure load acts against the snow load and the self weight, a design load combination with the reduced partial safety factors should have been used. Since the gas pressure is not explicitly given however this is not considered in here. All the external loads on the spherical shell can now be decomposed in to the local Y and Z directions as:

$$\begin{aligned} p_\varphi &= q_d \sin \varphi = 10.2 \sin \varphi \\ p_z &= q_d \cos \varphi - p_g = 10.2 \cos \varphi - 150 \end{aligned}$$

Elastic length:

$$L_e = \frac{\sqrt{rh}}{\sqrt[4]{3(1-\nu^2)}} = \frac{\sqrt{5 \cdot 0.2}}{\sqrt[4]{3(1-0.2^2)}} = 0.768 \quad m$$

Damping length:

$$2L_c = 4.82 \sqrt{rh_c} = 4.82 \sqrt{5 \cdot 0.2} = 4.82 \quad m$$

Since $2L_c < L$, the boundary effects from both ends can be treated separately.

5.5.1 Cylindrical wall

Particular solution

The displacement from the gas pressure is constant and is given by Equation 4.6

$$w_p = \frac{p_g r^2}{E h_c} = \frac{150 \cdot 5^2}{2 \cdot 10^7 \cdot 0.2} = 9.375 \cdot 10^{-4}$$

The gas pressure doesn't result into any rotation in the cylindrical wall, thus:

$$\theta_p = \frac{dw_p}{dx} = 0$$

Homogeneous solution

The homogeneous solution is given by Equation 4.11. The numerical values of the relevant g - functions at ξ equal to zero is one. Thus, inserting these values in Equation 4.11 renders the following set of linear equations:

$$\begin{aligned} w_h &= \frac{L_e^2}{2D_c} (M_{0c} + V_0 L_e) = 1.631 \cdot 10^{-5} V_0 + 2.123 \cdot 10^{-5} M_{0c} \\ \theta_h &= \frac{L_e}{2D_c} (-2M_{0c} - V_0 L_e) = -2.123 \cdot 10^{-5} V_0 - 5.530 \cdot 10^{-5} M_{0c} \end{aligned}$$

5.5.2 Spherical shell

Particular solution

The expressions for the displacement and rotation at the sphere edge are functions of the meridian and circumferential forces. Therefore, these forces must first be determined using Equation 5.3.

$$\begin{aligned} N'_\varphi &= -\frac{1}{2\pi \cdot 12^2 \sin 24.6} \int_0^{\varphi_0} (10.2 \sin^2 \varphi + (10.2 \cos \varphi - 150) \cos \varphi) 2\pi 12^2 \sin \varphi d\varphi \\ &= 835.891 \frac{kN}{m} \end{aligned}$$

$$N'_\theta = -835.891 - 12 \cdot (10.2 \cos 24.6 - 150) = 852.819 \frac{kN}{m}$$

The horizontal displacement is then found from Equation 5.10 as:

$$\Delta_H = \frac{12 \sin 24.6}{2 \cdot 10^7 \cdot 0.2} (852.819 - 0.2 \cdot 835.891) = 8.563 \cdot 10^{-4} \text{ m}$$

And the rotation is given by Equation 5.11, from which by combining 5.7, 5.9 and 5.10 can be rewritten as:

$$\begin{aligned} \Delta_\varphi &= \frac{\cot \varphi}{r_1 E h_s} [N'_\varphi (r_1 + \nu r_2) - N'_\theta (r_2 + \nu r_1)] \frac{d}{r_1 d\varphi} \left(\frac{\Delta_H}{\sin \varphi} \right) \\ &= \frac{\cot 24.6}{12 \cdot 2 \cdot 10^7 \cdot 0.2} [12036.8 - 12280.6] \frac{d}{12 d\varphi} (\varphi = 24.6) \left(\frac{\Delta_H}{\sin \varphi} \right) = -2.802 \cdot 10^{-5} \text{ rad} \end{aligned}$$

The modification due to the actual support conditions is given by Equation 5.29

$$\lambda = \sqrt[4]{3(1 - 0.2^2) \left(\frac{12}{0.2}\right)^2} = 10.09$$

$$\Delta_H^R = \frac{10.09 \cdot 12 \cdot \sin 24.6}{2 \cdot 10^7 \cdot 0.2} \cdot 2(-835.891 \cos 24.6) \sin 24.6 = -0.0080 \quad m$$

$$\Delta_\varphi^R = -\frac{210.09^2}{2 \cdot 10^7 \cdot 0.2} (-835.891 \cdot 10^3 \cos 24.6) \sin 24.6 = 0.0161 \quad rad$$

The total particular solution is then obtained by summing up both of the contributions.

$$\Delta_H^p = 8.563 \cdot 10^{-4} - 0.0080 = -0.0071 \quad m$$

$$\Delta_\varphi^p = -2.802 \cdot 10^{-5} + 0.0161 = 0.01607 \quad rad$$

Homogeneous solution

The deformations from the homogeneous solution are given in Equation 5.28

$$\begin{aligned} \Delta_H^h &= \frac{\lambda r \sin \varphi}{Eh} (2g_1(t)R_0 \sin \varphi + g_4(t)M_{0s} \frac{EhR}{2\lambda^3 D_s}) \\ &= 1.0491 \cdot 10^{-5} R_0 + 2.1195 \cdot 10^{-5} M_{0s} \\ \Delta_\varphi^h &= \frac{2\lambda^2}{Eh} (-g_3(t)R_0 \sin \varphi - g_1(t)M_{0s} \frac{EhR}{2\lambda^3 D_s}) \\ &= -2.119 \cdot 10^{-5} R_0 - 8.5622 \cdot 10^{-5} M_{0s} \end{aligned}$$

5.5.3 Ring beam

The radial displacement of the ring beam can be found by adding the contributions from both the radial force and moment, Equations 5.31 and 5.32 respectively. First from equilibrium, the radial force and moment are given by:

$$H = -(V_0 + R_0) + h_r p_g = 45 - V_0 - R_0$$

$$M_r = M_{0s} - M_{0c} + (V_0 - R_0) \frac{h_r}{2} = M_{0s} - M_{0c} + 0.15V_0 - 0.15R_0$$

Then, the radial displacements at the top and bottom of the ring beam are:

$$\begin{aligned} w_{top} &= \frac{r^2}{EA} (45 - V_0 - R_0) + \frac{r^2 h_r}{2EI} (M_{0s} - M_{0c} + 0.15V_0 - 0.15R_0) \\ &= -5.5556 \cdot 10^{-5} R_0 + 2.7778 \cdot 10^{-4} M_{0s} + 2.7778 \cdot 10^{-5} V_0 \\ &\quad - 2.7778 \cdot 10^{-4} M_{0c} + 6.25 \cdot 10^{-4} \\ w_{bottom} &= \frac{r^2}{EA} (45 - V_0 - R_0) - \frac{r^2 h_r}{2EI} (M_{0s} - M_{0c} + 0.15V_0 - 0.15R_0) \\ &= 2.7778 \cdot 10^{-5} R_0 - 2.7778 \cdot 10^{-4} M_{0s} - 5.5556 \cdot 10^{-5} V_0 \\ &\quad + 2.7778 \cdot 10^{-4} M_{0c} + 6.25 \cdot 10^{-4} \end{aligned}$$

The rotation of the beam is expressed in Equation 5.33

$$\begin{aligned}\theta_{ring} &= \frac{r^2}{EI} (M_{0s} - M_{0c} + 0.15V_0 - 0.15R_0) \\ &= -2.7778 \cdot 10^{-4} R_0 + 1.8519 \cdot 10^{-3} M_{0s} + 2.7778 \cdot 10^{-4} V_0 - 1.8519 \cdot 10^{-3} M_{0c}\end{aligned}$$

5.5.4 Compatibility requirements

Sphere shell/Ring beam:

The horizontal displacement at the top of the ring beam must be the same as the total horizontal displacement at the edge of the sphere shell.

$$\Delta_H^p + \Delta_H^h = w_{top}$$

$$\begin{aligned}& -0.0071 + 1.0491 \cdot 10^{-5} R_0 + 2.1195 \cdot 10^{-5} M_{0s} \\ &= -5.5556 \cdot 10^{-5} R_0 + 2.7778 \cdot 10^{-4} M_{0s} + 2.7778 \cdot 10^{-5} V_0 - 2.7778 \cdot 10^{-4} M_{0c} + 6.25 \cdot 10^{-4}\end{aligned}$$

After rearranging the different terms, the first compatibility equation is obtained:

$$6.6047 \cdot 10^{-5} R_0 - 2.5658 \cdot 10^{-4} M_{0s} - 2.7778 \cdot 10^{-5} V_0 + 2.7778 \cdot 10^{-4} M_{0c} = 7.743 \cdot 10^{-3} \quad (5.34)$$

Similarly, requiring compatibility of the rotation between the two surfaces leads to the second compatibility equation.

$$\Delta_\varphi^p + \Delta_\varphi^h = \varphi_{ring}$$

$$2.5658 \cdot 10^{-4} R_0 - 1.9375 \cdot 10^{-3} M_{0s} - 2.7778 \cdot 10^{-4} V_0 + 1.8519 \cdot 10^{-3} M_{0c} = -0.016 \quad (5.35)$$

Cylindrical shell/Ring beam:

Compatibility of the horizontal displacement gives:

$$w_p + w_h = w_{bottom}$$

$$\begin{aligned}& -2.7778 \cdot 10^{-5} R_0 + 2.7778 \cdot 10^{-4} M_{0s} + 7.1839 \cdot 10^{-5} V_0 - 2.5656 \cdot 10^{-4} M_{0c} \\ &= -3.125 \cdot 10^{-4}\end{aligned} \quad (5.36)$$

And the last equations is obtained from requiring the compatibility of the rotation between the cylindrical shell and the bottom of the ring beam.

$$\theta_p + \theta_h = -\theta_{ring}$$

$$2.7778 \cdot 10^{-4} R_0 - 1.8519 \cdot 10^{-3} M_{0s} - 2.5656 \cdot 10^{-4} V_0 + 1.9071 \cdot 10^{-3} M_{0c} = 0 \quad (5.37)$$

Equations 5.34, 5.35, 5.36 and 5.37 constitute a set of four linear equations with four unknowns.

$$\begin{aligned}
 & \begin{bmatrix} 6.6047 \cdot 10^{-5} & -2.5658 \cdot 10^{-4} & -2.7778 \cdot 10^{-5} & 2.7778 \cdot 10^{-4} \\ 2.5658 \cdot 10^{-4} & -1.9375 \cdot 10^{-3} & -2.7778 \cdot 10^{-4} & 1.8519 \cdot 10^{-3} \\ -2.7778 \cdot 10^{-5} & 2.7778 \cdot 10^{-4} & 7.1839 \cdot 10^{-5} & -2.5656 \cdot 10^{-4} \\ 2.7778 \cdot 10^{-4} & -1.8519 \cdot 10^{-3} & -2.5656 \cdot 10^{-4} & 1.9071 \cdot 10^{-3} \end{bmatrix} \begin{bmatrix} R_0 \\ M_{0s} \\ V_0 \\ M_{0c} \end{bmatrix} \\
 & = \begin{bmatrix} 7.743 \cdot 10^{-3} \\ -0.016 \\ -3.125 \cdot 10^{-4} \\ 0 \end{bmatrix}
 \end{aligned}$$

When the set of linear equations are solved, the following results are obtained:

$$\begin{bmatrix} R_0 \\ M_{0s} \\ V_0 \\ M_{0c} \end{bmatrix} = \begin{bmatrix} 307.32 & \frac{kNm}{m} \\ 123.98 & \frac{kN}{m} \\ -182.51 & \frac{kNm}{m} \\ 51.07 & \frac{kN}{m} \end{bmatrix}$$

Inserting these results into the different expressions for the load effects renders the distribution of the effects along the cylindrical wall and the spherical shell.

5.5.5 Distribution of the load effects

Load effects in the spherical shell

The expressions for both the moment and shear force distribution are given in Equation 5.28:

$$\begin{aligned}
 M_\varphi &= \frac{2\lambda^3 D_s}{EhR} \left(2g_2(t)(R_0 - H)\sin\varphi + g_3(t)M_0 \frac{EhR}{2\lambda^3 D_s} \right) \\
 Q_\varphi &= \frac{2\lambda^3 D_s}{EhR} \left(-g_4(t)(R_0 - H)\sin\varphi + g_2(t)M_0 \frac{EhR}{2\lambda^3 D_s} \right)
 \end{aligned}$$

Notice that the additional horizontal load H , which previously was applied at the edge is also included here. The distribution of both the moment and the shear force in the spherical shell are plotted in Figures 5.9 and 5.10 respectively. $\phi = 0$ corresponds to the center of the spherical shell.

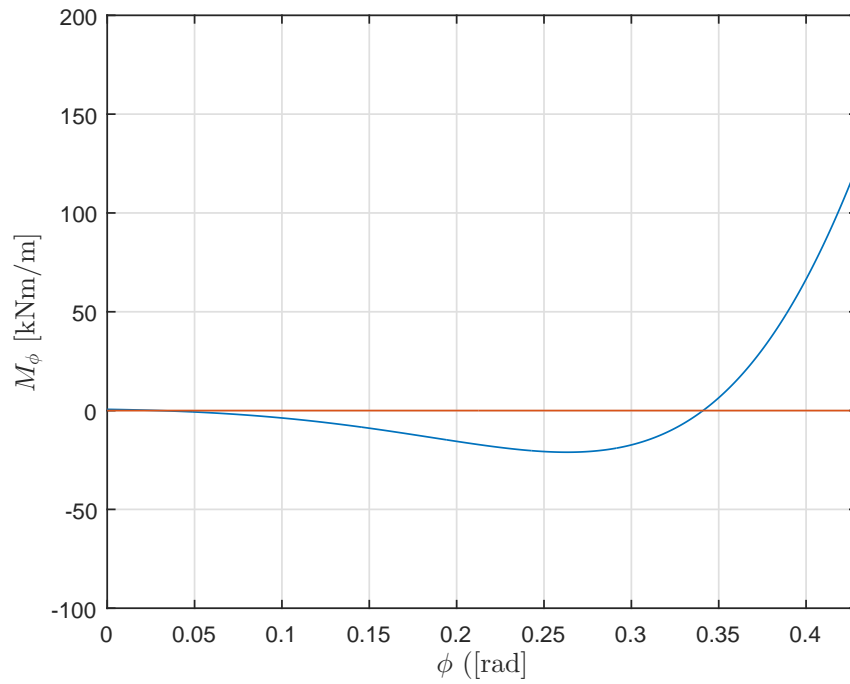


Figure 5.9: Meridian moment

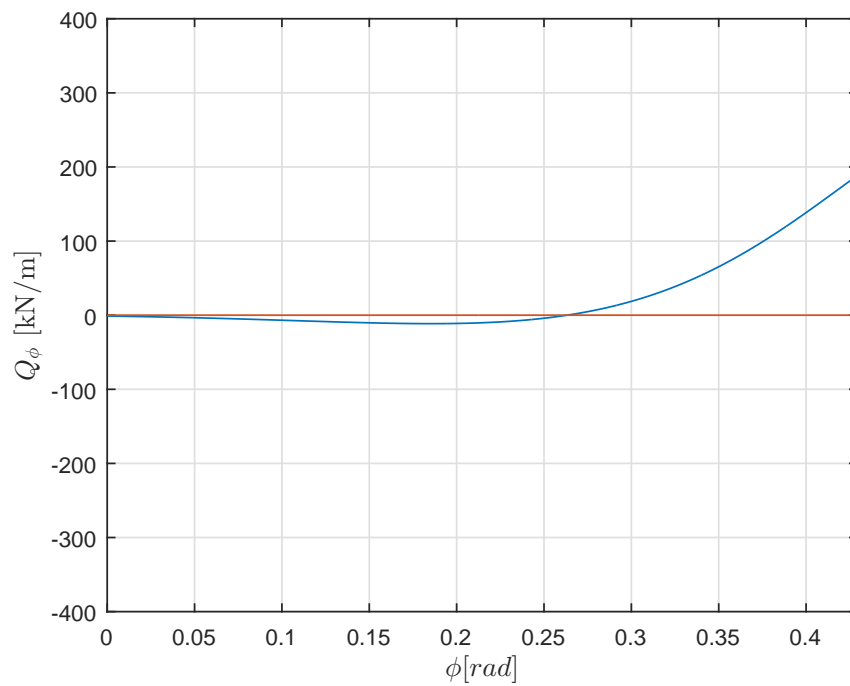


Figure 5.10: Shear force in the spherical shell

The in-plane forces are found by adding the contributions from both the particular and homogeneous solutions.

$$N_\varphi = \frac{1}{\tan \varphi} (g_4(t)(R_0 - H) \sin \varphi - g_2(t) M_{0s} \frac{EhR}{2\lambda^3 D_s})$$

$$N_\theta = \lambda(2g_1(t)(R_0 - H) \sin \varphi + g_4(t) M_{0s} \frac{EhR}{2\lambda^3 D_s})$$

The distribution of the in-plane forces are plotted in 5.11

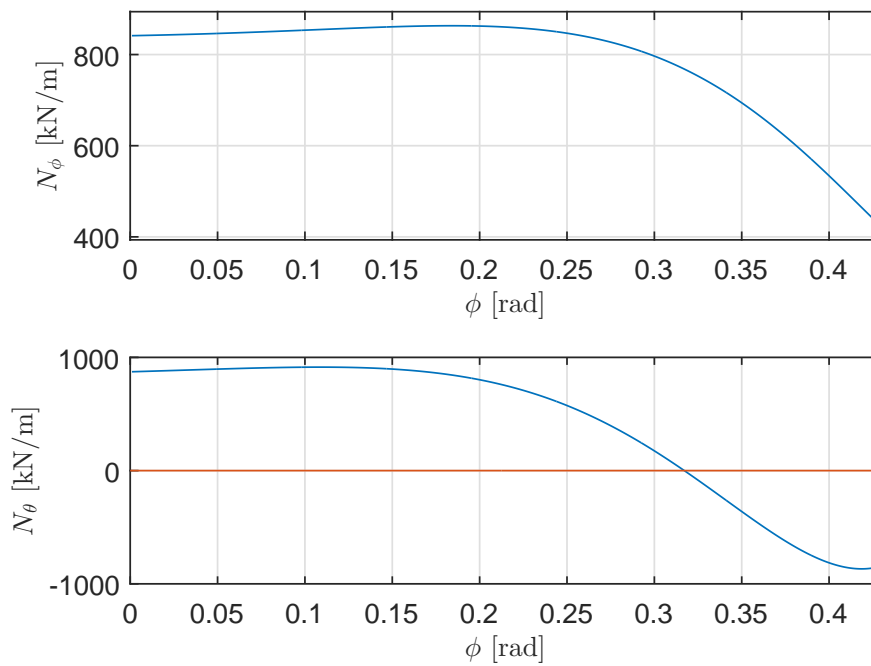


Figure 5.11: The in-plane forces

Load effects in the cylindrical wall

The expression for the moment M_x is given in Equation 4.11 as:

$$M_x = M_{0c}g_3(\xi) + V_0L_e g_2(\xi)$$

Similarly the expression for the shear force V_x is given by:

$$V_x = -\frac{1}{L_e}(-2M_{0c}g_2(\xi) + V_0L_e g_4(\xi))$$

The corresponding distributions are plotted in Figures 5.12 and 5.13 respectively. $x = 0$ corresponds to the the top of the cylindrical wall thus bottom of the ring beam.

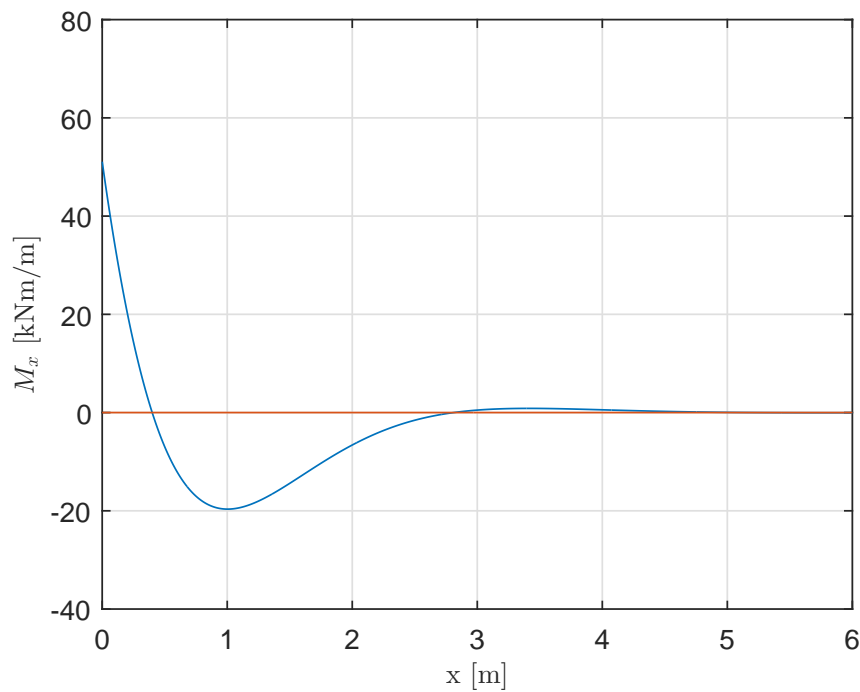


Figure 5.12: Moment in the cylindrical wall

Again the circumferential force N_φ has contributions both from the particular and homogeneous solutions.

$$N_\varphi = \frac{2r}{L_e^2}(M_{0c}g_4(\xi) + V_0L_e g_1(\xi)) + E\frac{w_p}{r}h$$

The distribution is plotted in Figure 5.14:

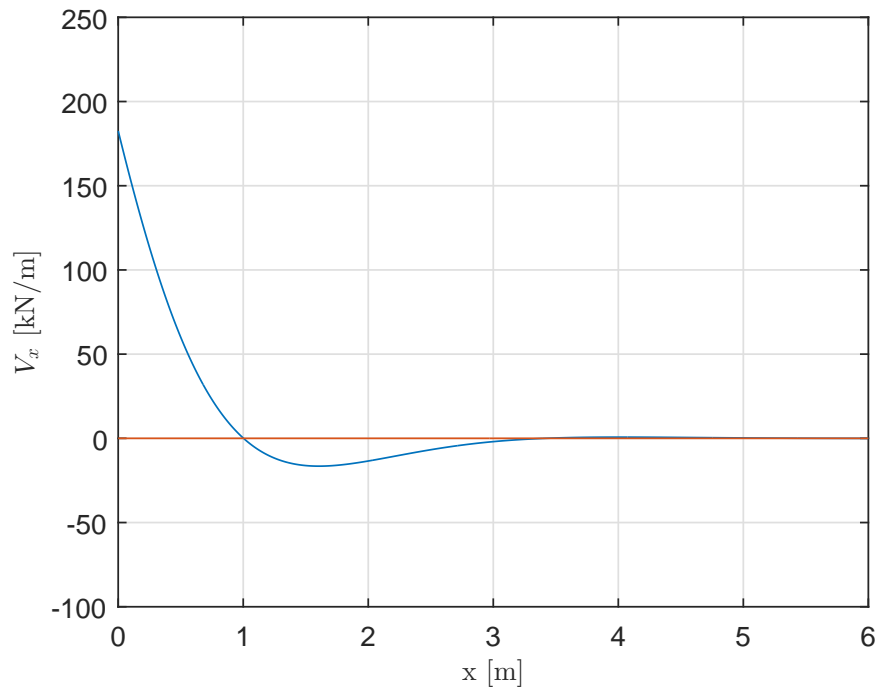


Figure 5.13: Shear force in the cylindrical wall

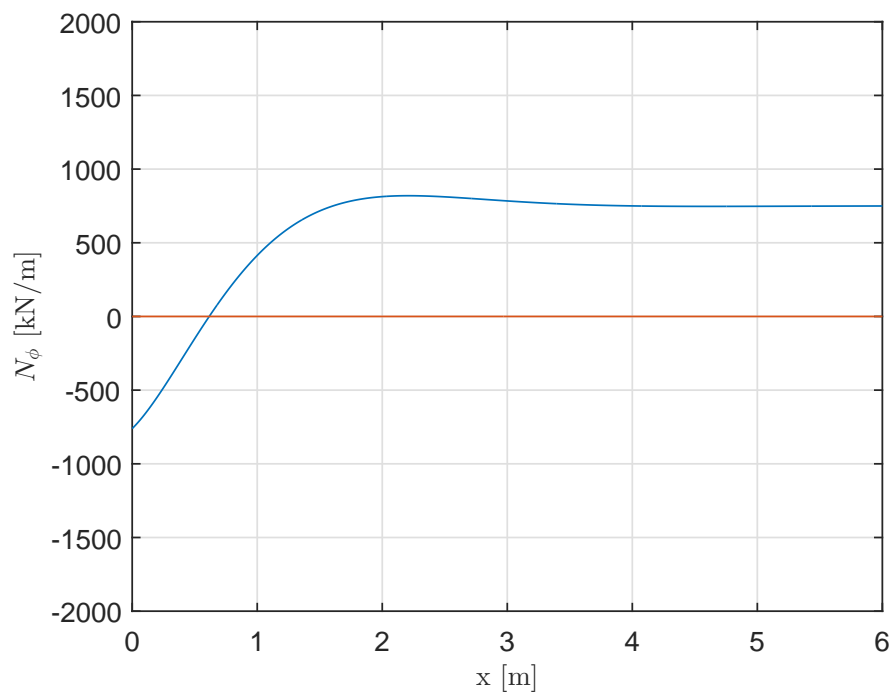


Figure 5.14: Circumferential force in the cylindrical wall

Since the cylindrical shell is long enough for the edge influences not to overlap, the load effects from both edges are calculated separately. The cylindrical wall is considered fully fixed at the bottom, thus both the rotation and the displacement is zero. Applying those boundary conditions, and following the same procedures as it is done so far, it can be shown that the load effects at the edge are as follows.

$$M_{x0} = \frac{p_g L_e^2}{2} = \frac{150 \cdot 0.768^2}{2} = 44.24 \frac{kNm}{m}$$

$$V_{x0} = -p_g L_e = -150 \cdot 0.768 = -115.2 \frac{kN}{m}$$

$$N_{\varphi 0} = 0$$

5.5.6 Remarks on the result from the analytical calculations

The moment diagrams of the spherical shell show that there are large moments concentrated at the junction with the ring beam. As expected the bending effects in shells are mainly associated with the boundary effects, this is illustrated in Figure 5.9. The moment diagram gets exponentially damped towards the center of the sphere. Due to the internal uniform pressure, the in-plane forces in the sphere are relatively large, and so are the circumferential force in the cylindrical wall. This in-plane forces result in tension stresses in most of the structure, thus to take up these stresses a considerable amount of steel reinforcement is required. Concrete cylindrical tanks are often used as storage tanks for liquefied natural gas (LNG) and as containment vessels. However for such purposes they are mostly reinforced by pre-stressing tendons. Moreover, they are internally supplemented by several layers that consist of different materials that regulate temperature and prevent leakage. From the circumferential (hoop) force both in the sphere and the cylindrical wall, it is also evident that the ring beam is in the state of compression in the ring direction.

Chapter 6

Conical shells

6.1 General

The cone is another example of shells of revolution which is often used in concrete structures. Similar to cylindrical shells, conical shells have a zero Gaussian curvature. In conical shells the meridional angle φ is constant, thus a new variable for the coordinate of the meridian must be introduced. The new variable is denoted as y and it measures the distance from the apex of the cone, See Figure 6.1.

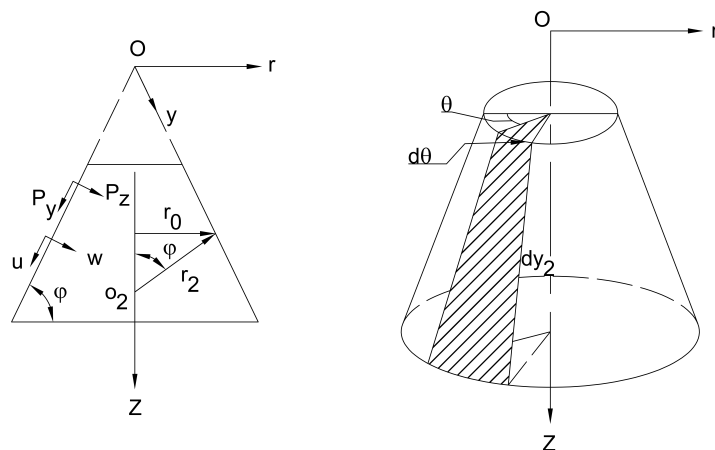


Figure 6.1: Notations used in the description of conical shells [21]

6.1.1 Membrane theory of conical shells

The equilibrium equations with membrane forces only are given by [21]:

$$\begin{aligned} \frac{\partial}{\partial y}(N_y y) + \frac{1}{\cos \varphi} \frac{\partial y}{\partial \theta} - N_\theta + y p_y &= 0 \\ \frac{1}{\cos \varphi} \frac{\partial N_\theta}{\partial \theta} + \frac{1}{y} \frac{\partial}{\partial y}(N_{\theta y} y^2) + y p_\theta &= 0 \\ \frac{1}{y} \tan \varphi N_\theta + p_z &= 0 \end{aligned} \quad (6.1)$$

For axisymmetrically loaded conical shells, the shear forces $N_{\theta y}$, load p_θ and all differentials of $\partial \theta$ are neglected. Thus, the remaining set of equations are as follows:

$$\begin{aligned} \frac{\partial}{\partial y}(N_y y) - N_\theta &= -y p_y \\ N_\theta &= -p_z y \cot \varphi \end{aligned} \quad (6.2)$$

combining these two equations yields

$$\frac{\partial}{\partial y}(N_y y) = -y(p_y - p_z \cot \varphi) \quad (6.3)$$

Equation 6.3 solved for N_y gives:

$$N_y = - \left[\frac{1}{y} \int (p_y + p_z \cot \varphi) y dy + \frac{C}{y} \right] \quad (6.4)$$

Furthermore the displacements can be found as before using strain-force relations. If it is assumed a rigid support at the edge, it can be shown that the displacement w at the edge is given by:

$$w = \varepsilon_\theta y \cot \varphi \quad (6.5)$$

Substituting for ε_θ from Eq. 5.6 gives

$$w = \frac{y \cot \varphi}{Eh} (N_\theta - \nu N_y) \quad (6.6)$$

6.2 Bending theory of conical shells

The governing differential equation of conical shells is the same as the one that is developed for general shells of revolutions. Introducing the notations and variables which are defined for conical shells, the expressions in Eq. 5.23 are rewritten as [21, eq. 16.55]:

$$\begin{aligned} \frac{d^2 U}{dy^2} &\approx \frac{Eh}{r_2} V \\ \frac{d^2 V}{dy^2} &\approx -\frac{U}{Dr_2} \end{aligned} \quad (6.7)$$

Again, combining these two equations and introducing

$$\beta = \sqrt[4]{\frac{3(1-\nu^2)}{r_2^2 h^2}} \quad (6.8)$$

the simplified single differential equations (for $\varphi > 35^\circ$) is given by

$$\frac{d^4 U}{dx^4} + 4\beta^4 U = 0 \quad (6.9)$$

Expressing the integration constants in terms of edge loads M_0 and Q_0 as before, the following solution is found.

$$U = \mp M_0 2\beta r_2 e^{-\beta x} \sin \beta x + Q_0 r_2 e^{-\beta x} (\cos \beta x - \sin \beta x) \quad (6.10)$$

where x is the coordinate measured from the edge of interest. The upper and lower sign refers to the top and bottom edge of the cone respectively.

The definition of x is following Figure 6.3 given by:

For the top edge: $x = y - y_1$

For the bottom edge: $x = y_2 - y$

The load effects can then be derived using the different relations developed in previous chapter. If we denote $\beta x = \kappa$ and then define g - *functions* as before, the load effects can be written as:

$$\begin{bmatrix} \frac{N_y}{2\beta \cot \varphi} \\ \frac{N_\theta}{2\beta^2 r_2} \\ M_y \\ \frac{dw}{dy} \beta D \end{bmatrix} = \begin{bmatrix} \pm g_2(\kappa) & -g_4(\kappa) \\ g_4(\kappa) & \pm 2g_1(\kappa) \\ g_3(\kappa) & \pm 2g_2(\kappa) \\ \pm g_1(\kappa) & g_3(\kappa) \end{bmatrix} \begin{bmatrix} M_0 \\ \frac{Q_0}{2\beta} \end{bmatrix} \quad (6.11)$$

Together with

$$\begin{aligned} M_\theta &= \nu M_y \\ \Delta_H &= r_2 \sin \varphi \frac{1}{Eh} (N_\theta - \nu N_y) \end{aligned} \quad (6.12)$$

The positive directions of the edge effects M_0 and Q_0 are as defined in Figure 6.2. The total solution of a conical shell with external loading is the sum of the membrane and homogeneous solution.

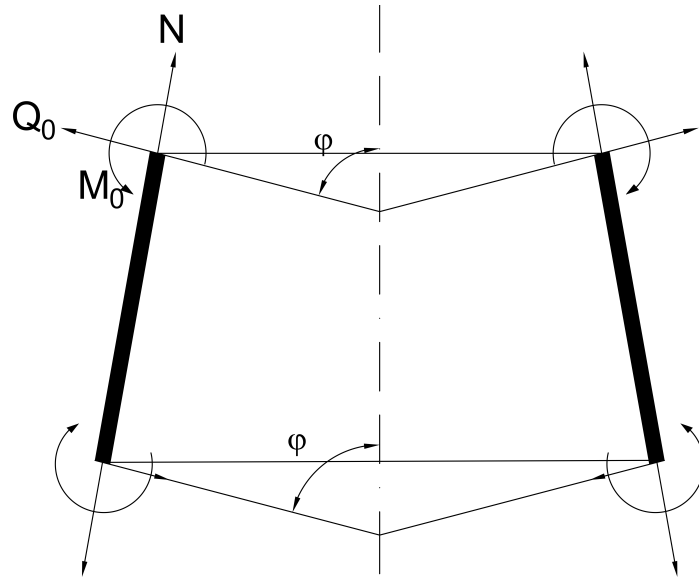


Figure 6.2: Positive directions of the edge effects on a cone [21]

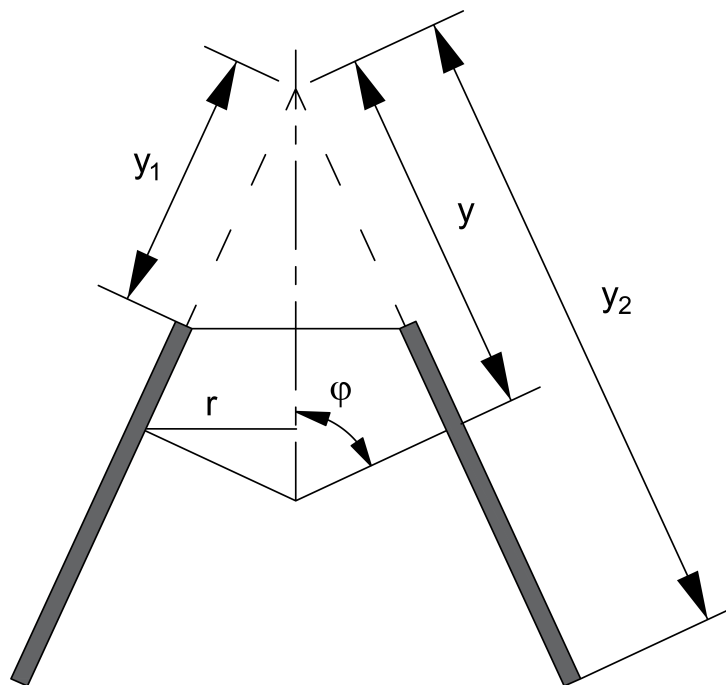


Figure 6.3: Illustration for the definition of x

Chapter 7

FEA

7.1 Analytical vs numerical solution

When different mathematical techniques, as it done so far in this paper, are used to develop a response to a mathematical model of a structure, the solution is called an analytical solution. This solution can represent the behaviour of that mathematical model under any circumstances. While this kind of approach to finding a solution gives the closest/exact results, it often tends to be tedious and time consuming when dealing with complex models. This challenge is usually solved using another method called the numerical analysis method. This method is based on discretization of the model into smaller elements where the results are obtained by performing thousands of repetitive calculations by utilizing computers. However it should be noted that the results obtained from the numerical method are not exact, it's an approximate solution that satisfies the equilibrium within a predefined tolerance. One of the most widely used numerical methods in civil engineering is called finite element method (FEM). It utilizes displacements as basic variables to calculate the strains and the stresses within the element. Even though FEM provides an approximated solution, it is usually good enough for solving daily engineering problems within an acceptable accuracy.

7.1.1 FEM

As mentioned above, finite element method (FEM) is one of the most used numerical analysis methods. It gives an approximate solution to boundary values for a set of partial differential equations which describes the equilibrium of the structure at hand. The general idea behind this method is first to simplify the structure into a model which represents the structural behaviour correctly, thus has the appropriate boundary conditions and material/physical properties. Then, discretize it into a finite number of simplified elements where it is easier to find solutions to. In a displacement based FEM, first the displacement field in each element is approximated by so called shape functions. Then strains and stresses are calculated from this displacements. Performing structural analysis using FEM can be summarized into the following steps[12]:

- **Pre-processing phase**

Most commercial FEA programs offer a wide variety of design tools for modelling and mesh generation algorithms.

- Design

Geometric properties, material properties, and boundary conditions of the structure together with the applied loads on the structure are defined here. Geometry property defines the outline of the structure and provides the geometric data for the analysis. The geometry can be drawn with the provided tools on the software or be imported from a CAD programs such as AutoCAD.

- Discretization

Discretizing the geometry by subdividing into small finite elements with simple shape, and creating a FE mesh with proper mesh density. The term finite indicates the fact that these elements are not infinitesimally small but are relatively small compared to the overall model size. Furthermore, an appropriate element type is chosen and applied surface loads are discretized in to each element nodes. The mesh will then contain all the parameters needed for the analysis. It is evident that the mesh formation and density will have an effect on the final solutions.

- **Solution phase**

A set of linear algebraic equations that describes the force-displacement relation of the structure are solved to obtain nodal results such as displacements and rotations.

- **Post-processing phase**

Here strains and stresses are computed from the obtained nodal displacements. Most post-processors are able to present the analysis results graphically in the form of contour plot, graphs, tables etc. Based on the obtained results the analyst can then evaluate the accuracy of the FE-solution and apply the appropriate measures as needed.

The process is illustrated in the process diagram shown in Figure 7.1.

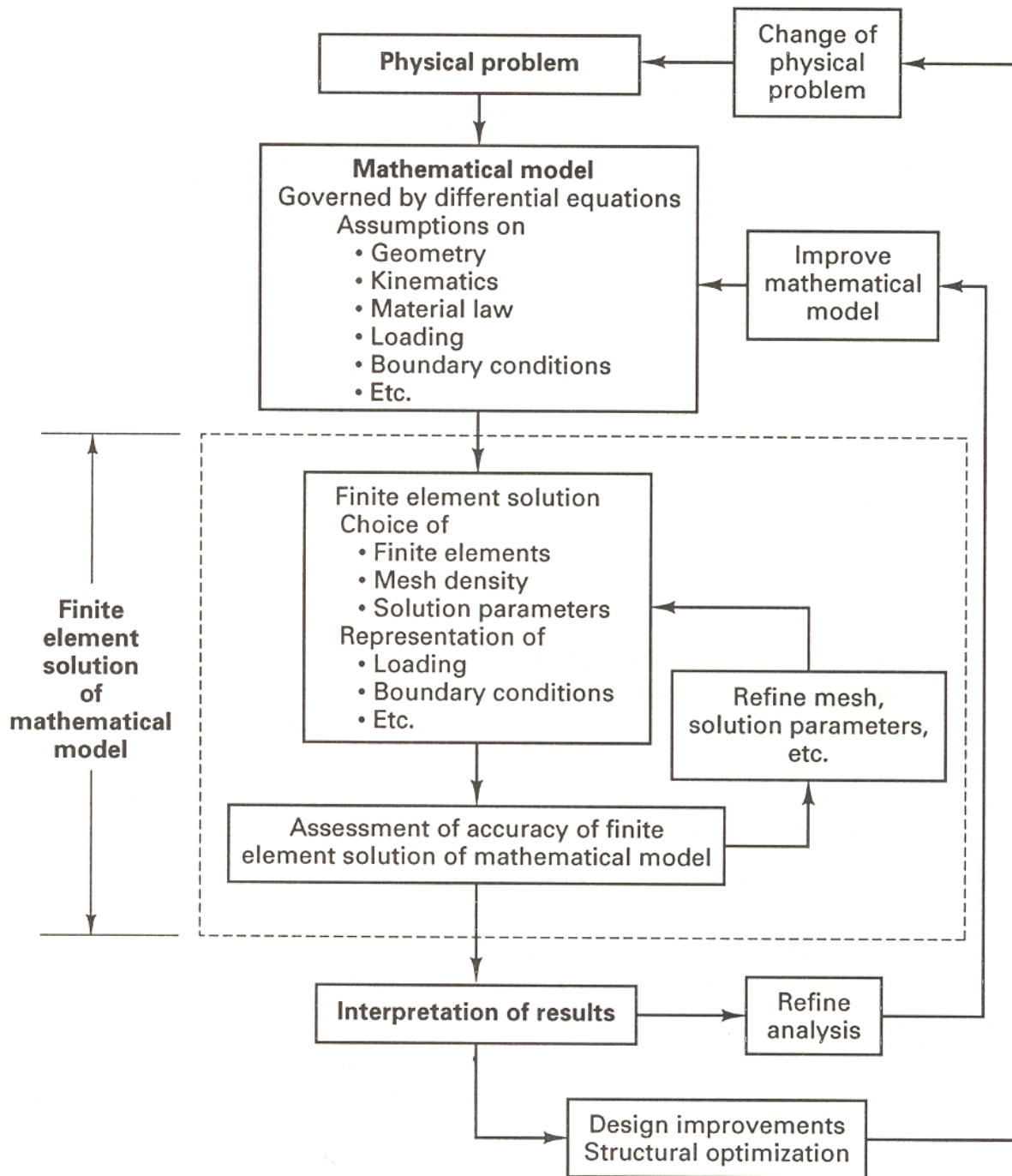


Figure 7.1: Finite element analysis procedures [12]

To illustrate these summarized steps the following simple example of a cantilever beam is considered [12].

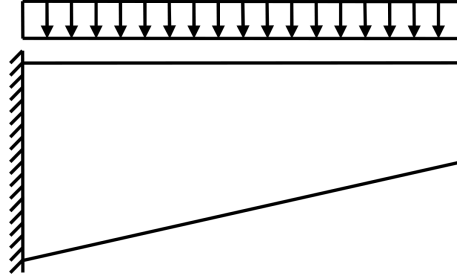


Figure 7.2: A uniformly loaded cantilever beam

Pre-processing phase:

As it is shown in Figure 7.2, the beam has a linearly varying height, and it is made of a linear-elastic material. The load is uniformly distributed on the top surface of the beam and the beam is fixed at one end.

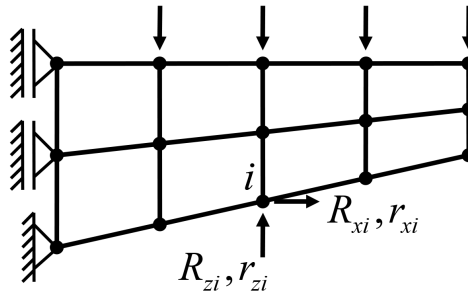


Figure 7.3: Discretized model

The model is then subdivided into 2×4 plane stress elements. Each element displacements are described by nodal interpolation functions, the displacement of an arbitrary point within the element can be determined uniquely by these nodal interpolation functions.

Solution phase:

Elements stiffness relationship can then be obtain by solving the governing differential equation and the corresponding boundary conditions of the elements.

$$S_e = K_e V_e + S_e^o \quad (7.1)$$

where, S_e is the element nodal forces, K_e is the element stiffness matrix, V_e is the element nodal displacement and S_e^o is the consistent nodal force vector of the element. By implementing nodal point compatibility for each element $V_e = a_e r$ and the nodal point equilibrium for all nodes $R + \sum_e R_e = 0$ the system stiffness relationship is found as

$$R = K r + R^o \quad (7.2)$$

Where,

$$\begin{aligned} K &= \sum_e a_e^T K_e a_e \\ R^o &= \sum_e a_e^T S_e^o \end{aligned} \quad (7.3)$$

And,

R denotes the structure nodal point forces due to external loads

r denotes the structure nodal point displacements

K denotes the structure (system) stiffness matrix

R^o denotes the nodal point forces due to external loads

a_e denotes the connectivity matrix

Applying boundary condition by suppressing restrained nodal displacements (setting the corresponding $r_i = 0$) gives the modified system stiffness relationship. The system displacement can then be obtained by solving the modified system stiffness relationship:

$$r = K^{-1}(R - R^o) \quad (7.4)$$

Post-processing phase

The corresponding strains and stresses are computed as following:

Strain:

$$\varepsilon = \frac{d}{dx}V = BV \quad (7.5)$$

Stress:

$$\sigma = E\varepsilon = EBV = CBar \quad (7.6)$$

7.2 DIANA

In this thesis, all the finite element analysis are performed in the FE-software DIANA. DIANA (DIplacement ANALyzer) is a multi-purpose finite element analysis software based on the displacement method. It has been under development at TNO DIANA in Delft in the Netherlands since 1970s [5]. DIANA provides the possibility of modelling in both 2D- and 3D-environment. Its capabilities of performing linear and nonlinear analysis, together with its broad material models and element libraries has made DIANA one of the most appealing software in the field of concrete and soil analysis. The different activities in DIANA that corresponds to the three phases of FEA are as follows.

7.2.1 Pre-processing phase and Discretization

The pre-processing in DIANA is done in its designated pre-processor called iDIANA. The pre-processor is equipped with some basic modelling tools. The modelling process starts out in 1D where the user defines the necessary points that outlines the object. These points can then be connected into 2D lines by using LINE command in iDIANA, and

subsequently from lines one can constitute surfaces and 3D bodies. The model is then meshed or discretized into the appropriate number of elements and the corresponding element type. Then, the prescribed loads and material properties are attached to the model. To finish the preprocessing phase the boundary conditions are applied by restraining either the rotational or/and translational degree of freedoms at specified nodes/points.

7.2.2 Solution phase

Following the Pre-processing phase, an input data file with the extension *.dat* is generated. This file contains vital information such as the geometric data, element properties, load cases, material properties and boundary conditions. When starting the analysis process this file is first read and checked by DIANA. As shown in Figure 7.4, there are a number of analysis types that can be performed in DIANA. In this study, the only analysis type that will be used are the structural linear static and structural nonlinear.

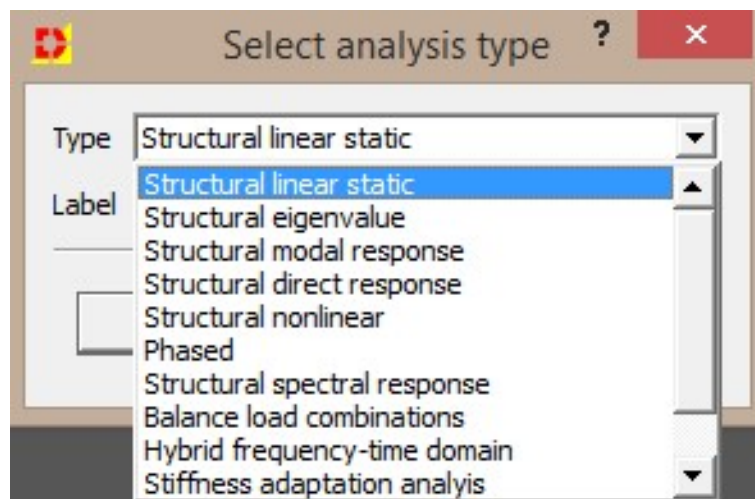


Figure 7.4: FEA options in DIANA

7.2.3 Post-processing phase

DIANA has some standard output parameters associated with each analysis type, but the user has also the possibility to specify the type of output he/she is interested in. Finally, the FEA results in DIANA can be presented in the form of graphs, tables, contour plots etc.

7.3 Linear static analysis in DIANA

For the purpose of the comparison with the previously obtained analytical solutions and studying the way DIANA deals with axisymmetrical shells, the two previously calculated

examples are analysed in DIANA. From the above presented theoretical background of FEM, it's clear that choosing the appropriate type of element and mesh density is important. To do so an insight into the overall structural behaviour of shells which is gained from the analytical method is useful. In DIANA, axisymmetric shells can be modelled by using axisymmetric elements. For these elements only the cross-sectional geometry of xy-plane is created and then it is rotated about the global y-axis to create the associated full structure.

7.3.1 Axisymmetric elements in DIANA

DIANA has two classes of axisymmetric elements, solid rings and shells of revolution.

Displacement

Basic degrees of freedom (DOF) for axisymmetric elements are U_x and U_y and they represent the translation of each node in global X- and Y-directions. The axisymmetric shell elements however have an extra rotational degree of freedom φ_z .

Strains

The nodal displacements yield du_x and du_y of an infinitesimal part of the element defined by dx , dy and a unit thickness in the tangential direction. From these deformations DIANA derives the Green-Lagrange strains [5]:

$$\begin{bmatrix} \varepsilon_{xx} \\ \varepsilon_{yy} \\ \varepsilon_{zz} \\ \gamma_{xy} \end{bmatrix} = \begin{bmatrix} \frac{\partial U_x}{\partial x} \\ \frac{\partial U_y}{\partial y} \\ \frac{U_x}{r} \\ \frac{\partial U_x}{\partial y} + \frac{\partial U_y}{\partial x} \end{bmatrix} \quad (7.7)$$

and **Cauchy stresses**

$$\begin{bmatrix} \sigma_{xx} \\ \sigma_{yy} \\ \sigma_{zz} \\ \sigma_{xy} = \sigma_{yz} \end{bmatrix} \quad (7.8)$$

DIANA has basically two axisymmetric shell elements for modelling shells of revolution, the L6AXI and the CL9AX. The L6AXI is a straight two-noded element with three degrees of freedom, U_x , U_y and φ_z at each node. The CL9AX on the other hand is a three-noded curved element with the same degrees of freedom as the L6AXI at each node. The axisymmetric shell elements have a thickness which is small compared to their length, i.e. they are line shaped elements. In this example the analysis is done using both types of elements. To study the convergence rate of both elements, the results of the FEA are obtained for meshes going from the coarsest to the finest. Higher mesh densities

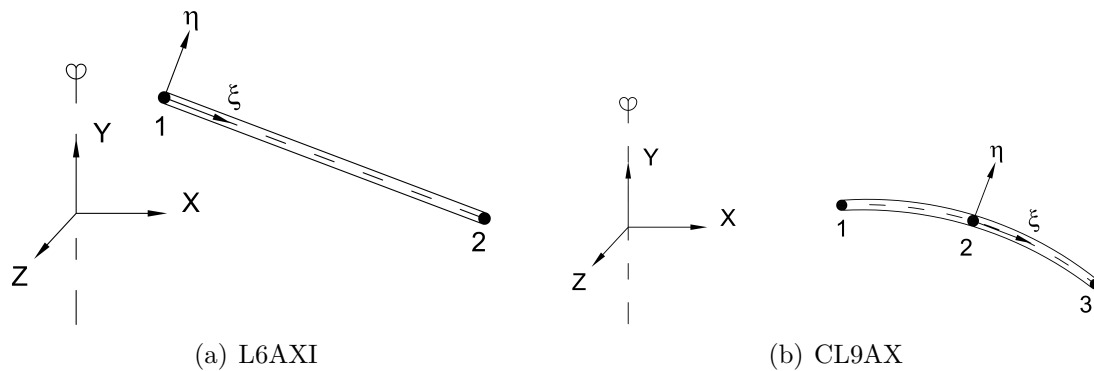


Figure 7.5: Axissymmetric elements in DIANA

are applied at the areas with high stress-concentrations on the basis of the analytical solution. It should however be noted that the analysis is performed using iDIANA release 9.4.4 Teacher edition, which is among others limited to 50 elements per line segment and 1000 elements overall.

7.3.2 Example 1 analysed in DIANA

The results that are obtained from the linear finite element analysis of the cylindrical water tank in example 1, using the two elements are presented in tables 7.1 and 7.2.

Table 7.1: Results from the linear FEA using L6AXI

	Mesh size	Element type	M_{02}	M_{01}	V_{02}	V_{01}	N_{φ}
Mesh 1	5000/20	L6AXI	-36.1	10.3	-45.7	-32.4	263
Mesh 2	5000/40	L6AXI	-38.9	12.1	-46, 5	-35, 3	261
Mesh 3	5000/80	L6AXI	-40.4	13.2	-46, 7	-36, 8	261
Mesh 4	5000/100	L6AXI	-40.7	13.4	-46, 7	-37, 7	261
Mesh 5	5000/160	L6AXI	-41.1	13.8	-46, 7	-37, 6	261
Mesh 6	5000/200	L6AXI	-41.3	13.9	-46, 6	-37, 7	261
Mesh 7	5000/500	L6AXI	-41.6	14.2	-46, 6	-38, 1	261
Mesh 8	5000/800	L6AXI	-41.7	14.2	-46, 6	-38, 2	261
Mesh 9	5000/980	L6AXI	-41.7	14.3	-46, 6	-38, 2	261
Analytical solution			-42.02	14.61	-50, 02	-38, 40	273.6

Percent deviation	0.76%	2.12%	6.84%	0.52%	4.61%
-------------------	-------	-------	-------	-------	-------

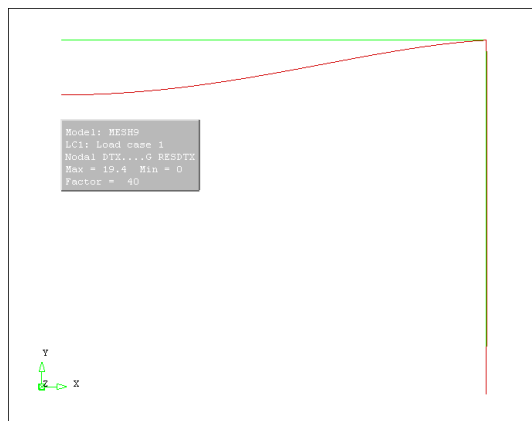
Again, M_{01} and V_{01} are given at the bottom of the cylindrical wall while as M_{02} and V_{02} are given at the junction with the circular flat plate. From the above results it can be said that the linear FEA solutions from DIANA are fairly close to those solutions obtained from analytical calculations. Furthermore, with finer meshes a more accurate result is obtained as expected. It is also clear to see that even though one arrives at solutions with

Table 7.2: Results from the linear FEA using CL9AX

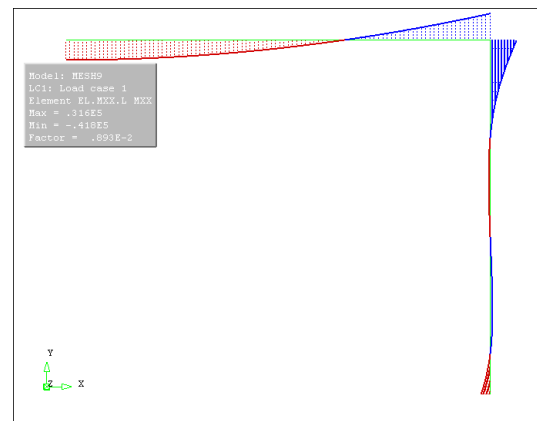
	Mesh size	Element type	M_{02}	M_{01}	V_{02}	V_{01}	N_{φ}
Mesh 1	5000/20	CL9AX	-41.8	14.1	-47.2	-38.2	263
Mesh 2	5000/40	CL9AX	-41.8	14.3	-46,7	-38.3	261
Mesh 3	5000/80	CL9AX	-41.8	14.3	-46,6	-38.4	261
Mesh 4	5000/100	CL9AX	-41.8	14.3	-46,6	-38.4	261
Mesh 5	5000/160	CL9AX	-41.8	14.3	-46,6	-38.4	261
Analytical solution			-42.02	14.61	-50,02	-38,40	273.6

Percent deviation	0.52%	2.12%	6.84%	0%	4.61%
-------------------	-------	-------	-------	----	-------

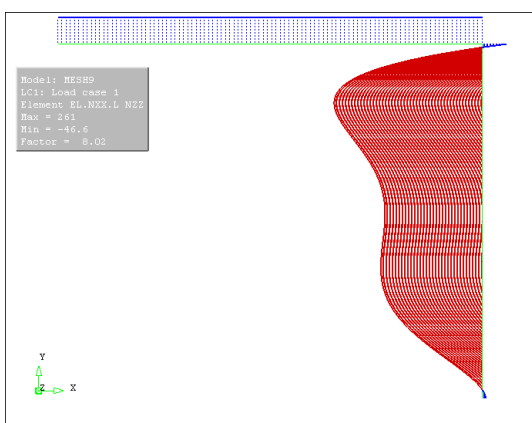
sufficient accuracy with both element types, the CL9AX element converges quicker than the L6AXI. As CL9AX is a higher order element, this is usually to be expected. Moreover the diagrams for some of the stress resultants are shown in Figure 7.6. Compared to the



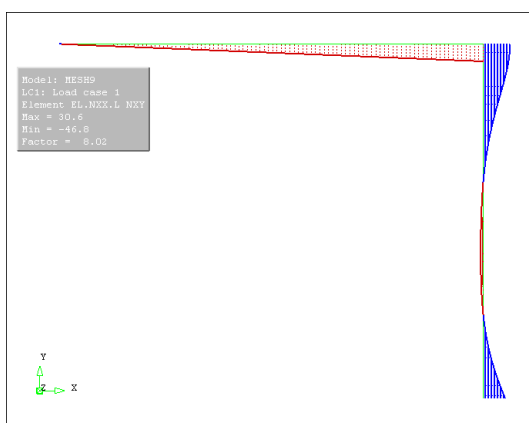
(a) Deformation shape of the structure in example 1



(b) Meridian moment



(c) Circumferential force



(d) Shear force

Figure 7.6: Stress resultant diagrams from linear FEA of example 1

stress resultant diagrams obtained from the analytical calculations (figures 4.5 to 4.9),

these diagrams are more or less the same. It should however be noted that the axial stiffness which are not taken in to account in the analytical calculations are accounted for in here. This is done to reflect the real structural behaviour of the system, and to include the deviations that might come from the assumption.

7.3.3 Example 2 analysed in DIANA

Similarly, the results obtained from the linear finite element analysis of the cylindrical gas vessel in example 2, using the two elements, are presented in tables 7.3 and 7.4.

Table 7.3: Results from the linear FEA using L6AXI

	Mesh size	Element type	M_{0s}	M_{0c}	R_0	V_0	N_φ
Mesh 1	5157/20	L6AXI	116	50.6	288	176	824
Mesh 2	5157/40	L6AXI	118	50	290	174	818
Mesh 3	5157/80	L6AXI	118	49.7	291	174	817
Mesh 4	5157/100	L6AXI	118	49.7	291	174	817
Mesh 5	5157/160	L6AXI	118	49.6	291	173	817
Mesh 6	5157/200	L6AXI	118	49.5	291	173	817
Mesh 7	5157/900	L6AXI	119	49.4	291	173	–
Analytical solution			123.98	51.07	307.32	182.51	819.30

Percent deviation	4.02%	3.27%	5.31%	5.21%	0.28%
-------------------	-------	-------	-------	-------	-------

Table 7.4: Results from the linear FEA using CL9AX

	Mesh size	Element type	M_{0s}	M_{0c}	R_0	V_0	N_φ
Mesh 1	5157/20	CL9AX	119	49.5	291	173	817
Mesh 2	5157/160	CL9AX	119	49.5	291	173	818
Mesh 3	5157/900	CL9AX	119	49.4	291	173	–
Analytical solution			123.98	51.07	307.32	182.51	819.30

Percent deviation	4.02%	3.27%	5.31%	5.21%	0.16%
-------------------	-------	-------	-------	-------	-------

Again, M_{0c} and V_0 are given at the bottom of the ring beam while as M_{0s} and R_0 are given at the top of the ring beam in the junction with spherical shell. N_φ is the largest circumferential force in the cylindrical wall. The results from the linear FEA are again fairly close to the results obtained from the analytical calculations. The highest deviation that is found is 5.31% compared to the results obtained from the analytical solution. The deformation shape shows that most of the spherical shell and the cylindrical wall deforms outwards while as the ring beam is pressed inwards, see Figure 7.7. This is analogous with the type of loading applied, which is dominated by a uniform gas pressure load directed outwards. From the diagrams for the bending moment and shear force, it can be seen that the stress resultant from both ends more or less damps out toward the middle of the cylindrical wall. This justifies the assumption of long cylindrical shell in the analytical calculations.

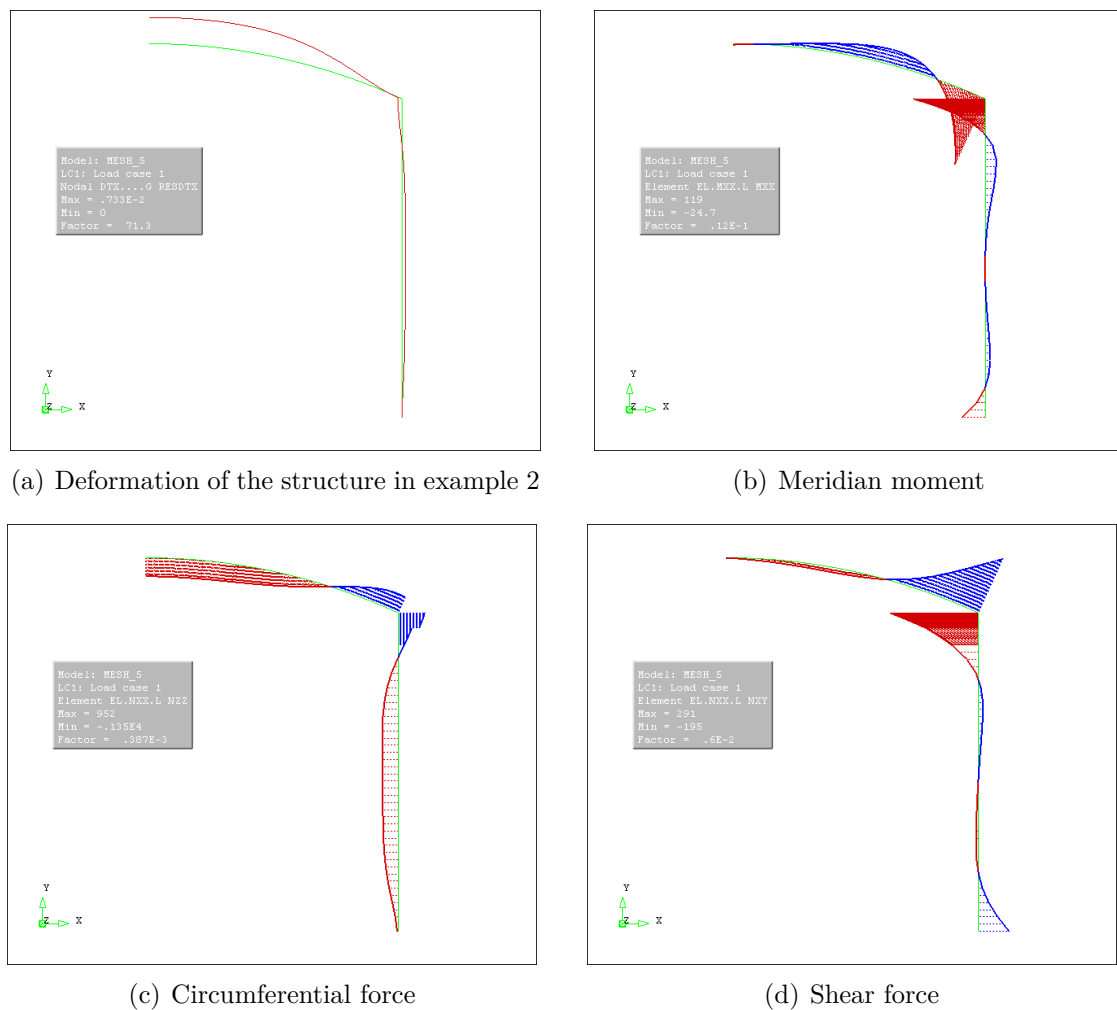


Figure 7.7: Stress resultant diagrams from linear FEA of example 2

7.4 Nonlinear finite element analysis

To further study the response of structures when the linear range is exceeded, a nonlinear analysis of the structure in example 1 is carried out. RC structures exhibit nonlinear behaviour mainly due to the tensile cracking of concrete. Before cracking the concrete is assumed to behave linear elastically until the ultimate tension strength is reached. After this limit the stresses are mainly carried out by the reinforcement. Therefore, before proceeding with the nonlinear analysis, the amount of necessary reinforcement is first calculated. This reinforcement will then be included in the finite element model. In the following subsections the different input parameters needed for the nonlinear FEA will be presented.

7.4.1 Reinforcement

Based on the load effects obtained from the analytical calculations, the necessary reinforcement is first calculated. The stress resultants in the shell are independent of each other, therefore the design calculations are done as for one way slabs according and according Eurocode 2. The detailed calculations can be found in Appendix A, here the results are summarized in Table 7.5.

Table 7.5: Structurally required amount of steel reinforcement in example 1 [$\frac{mm^2}{m}$]

Circular slab	Inner layer	Outer layer	Shear reinforcement
Radial	478.4	646.9	No need
Tangential	478.4	81.3	
Cylindrical wall			
Vertical	222.5	646.9	No need
Ring	314.6	314.64	

Table 7.6: Final amount of reinforcement including minimum requirements according to the Eurocodes [$\frac{mm^2}{m}$]

Circular slab	Inner layer	Outer layer	Shear reinforcement
Radial	481.3	665.3	No need
Tangential	481.3	452.4	
Cylindrical wall			
Vertical	452.4	665.3	No need
Ring	452.4	452.4	

7.4.2 Structural modelling

In order to include the steel reinforcement, the structural model first needs to be rebuilt into 2D (two dimensional). The model is then discretized into isoparametric axisymmetric regular solid ring elements. DIANA has total six types of such elements. Three of them are triangular elements with 3 (T6AXI), 6 (CT12A) and 15 (CT30A) nodes, while as the other three are quadrilaterals with 4 (Q8AXI) and 8 (CQ16A) nodes. The reinforcement in DIANA can be modelled either using truss elements or as embedded reinforcement which can be a bar or a grid. In the following example the 8-node quadrilateral element CQ16A with embedded grid reinforcement is chosen. This element is a higher order element that is based on quadratic interpolation functions. This element is chosen such that higher convergence rate could be achieved, and shear locking behaviour, which is associated with linearly interpolated plane elements, could be avoided. Furthermore the model is discretized into a uniform quadratic mesh with a chosen mesh size of 50 mm.

7.4.3 Material models

In order to perform the nonlinear analysis, the constitutive relations (stress-strain diagrams) for both the concrete and reinforcement must first be determined. In DIANA there are three material models available for modelling the reinforcement, the linear elasticity, plasticity and a user specified model. The plasticity material model employs Von Mises yield criterion. In the following example, the reinforcing steel is assumed to be elastic-perfectly plastic (ideal plasticity) in both compression and tension with no hardening effect.

The constitutive behaviour of concrete is characterized by tensile cracking, compressive crushing and long terms effects like shrinkage and creep. The latter two will not be considered in this study. The constitutive relation of concrete is modelled using a multi-linear diagram in compression similar to what is proposed in Eurocode 2, 3.1.5 [16], and a linear diagram in tension. There are two types of crack models available in DIANA, the multi-

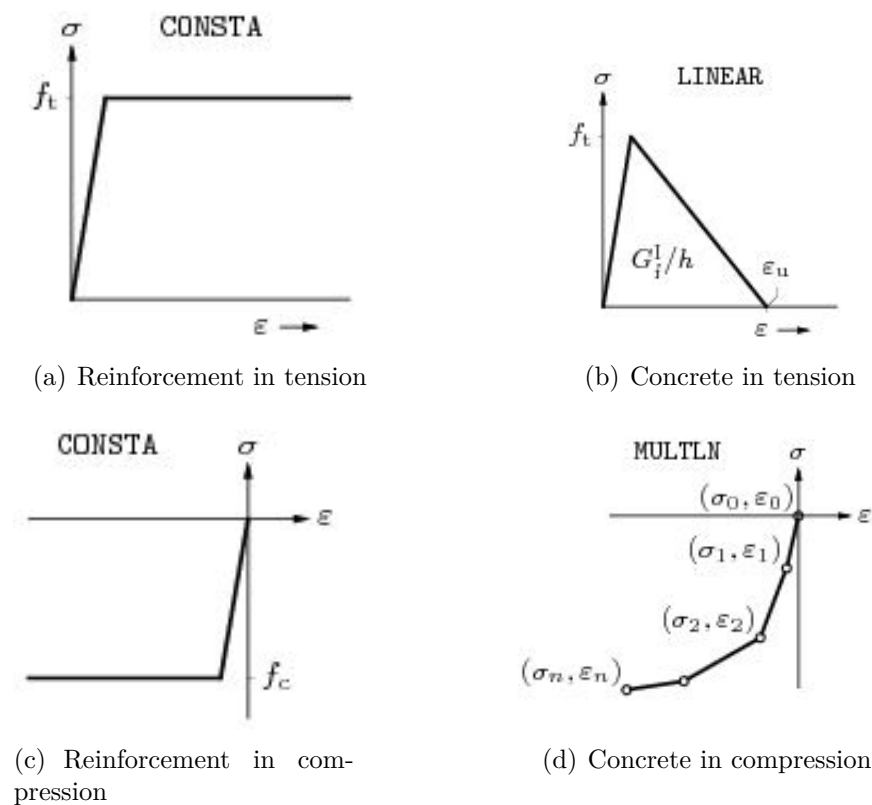


Figure 7.8: Material models that are applied [5]

directional fixed crack model and the total strain crack model. In the following example a crack model based on total strain with rotating crack model is chosen. In this model the tensile and compressive behaviours are described in one stress-strain relationship evaluated in the principal directions of the strain vector. This model tends to give numerically stable results, and according to the DIANA users manual [5], it is very well suited for SLS and ULS analysis of RC structures. After the development of cracks in the concrete, the tension stresses are carried by the reinforcement, however due to the bond between

the steel reinforcement and the concrete, some tension is still existent between cracks. This tension gradually decreases with increasing load, this can be modelled by adding a tension softening/stiffening effect based on either ultimate strain or fracture energy. In RC structures the ultimate crack strain can be taken as $\frac{\sigma_{steel}}{E_s}$, where σ_{steel} is the average stress in the steel reinforcement. In the following example this is for simplification taken as the design tensile strength of the steel reinforcement. Fracture energy G_f is the energy required to form a crack and is given by:

$$G_f = \frac{1}{2} \varepsilon_y^{cr} f_t h \quad (7.9)$$

where ε_y^{cr} is the ultimate strain, f_t the ultimate tensile strength and h is a crack bandwidth which is related to the element size. However, with relatively coarse finite element meshes this formulation has some shortcomings. The crack model that is used in this study is based on smeared crack approach, that is cracks are in a way smeared over an element instead of discrete cracks. Equation 7.9 is based on a uniform distribution of microcracks in the element, while as the actual microcracks in a relatively large element are concentrated in a small region of the element. Based on an exponential distribution function of the crack region, a more generally applicable model has for example been suggested by Kwak and Filippou [9].

$$G_f = \frac{1}{2} \varepsilon_y^{cr} f_t 2 \int_0^{b/2} f(x) dx \quad (7.10)$$

where $f(x)$ is given by

$$f(x) = e^{-\frac{2}{b} \ln \frac{b}{3} x}$$

where b is the element width. This model converges to the previous model when the element size is 3 inches (76.2 mm), that is three times the approximated maximum aggregate size 1 inch (25.4 mm). Thus in SI units the function becomes:

$$f(x) = e^{-\frac{2}{b} \ln \frac{b}{76.2} x}$$

7.4.4 Solution procedure

Unlike in linear FEA, in nonlinear FEA the relationship between force vector and displacement vector is not linear. Thus, a displacement vector that equilibrates the internal and external forces must be found by using an incremental-iterative solution procedure. In this procedure the load is applied successively in steps, and for each load step the equilibrium equation is to be fulfilled within the convergence limit that is chosen by the user. DIANA has different types of iteration methods and convergence criterion to choose from. In the following analysis the regular Newton-Raphson method is chosen. It is based on updating the stiffness matrix at each iteration rather than keeping it constant over several iterative cycles. Both the force and displacement convergence criteria are also employed so that they complement each other, as suggested in Ref. [4]. The solution procedure employed in the following example is summarized in Table 7.7.

Table 7.7: Solution procedure for the nonlinear FEA

Variable	Chosen value/method
Nonlinearity	Physical and Geometrical(Total Lagrange)
Load increment	0.1
Number of increments	30
Max. number of iterations	100
Iterative procedure	Regular Newton-Raphson with arc length control
Convergence criterion	Both force and displacement norm
Convergence Limit	0.01

7.4.5 Results from the Nonlinear FEA of the structure in example 1

The load-deflection diagram for a node at the center of the circular plate is shown in Figure 7.9. The nonlinear FEA is first performed applying the structurally required amount of steel reinforcement as shown in Table 7.5, this results in a load-deflections path plotted by the blue line. The path reaches its first peak value at load step 10 before it drops back. At this first peak the structure reaches a capacity of just over load factor one (1.02). The load factor 1.0 corresponds to the applied loading. Figure 7.10 shows the stresses in the concrete at load step 10, here it can be seen that the ultimate tension strength, which is given as $2 \frac{N}{mm^2}$, is reached in the global σ_{xx} , and σ_{yy} is about to approach this value.

Moreover, from the image with the crack patterns in Figure 7.11, one can see that the crack patterns at the top of the cylindrical wall changes dramatically from load step 10 to 11. The stress in the reinforcement for the same two load steps is also presented in Figure 7.12, the stresses in σ_{yy} jumps from $129 \frac{N}{mm^2}$ to just around the design strength of the steel reinforcement $435 \frac{N}{mm^2}$.

Nevertheless the structure is able to carry the design load or a load factor of 1.02 before it drops back. However, to obtain a more ductile behaviour of the structure, the necessary minimum reinforcement according to Eurocode 2 is applied. Now the load-deflection diagram is plotted as it is presented by the red line in Figure 7.9. Here it can be seen that the remaining path post the limit value also stays over the load factor one. As it is shown in Figure 7.13, the stress in the reinforcement post the peak is $228 \frac{N}{mm^2}$, which is far from the design strength of the steel reinforcement.

Generally the crack patterns are as expected concentrated on the areas with high stress concentrations. Similarly the stresses in the steel reinforcement reaches their maximum values at this areas. For practical purposes the steel reinforcement bars are usually applied with uniform distribution of the entire surface as it is done in this example. Therefore the stresses in the reinforcement are generally low over a large portion of the structure.

The concrete stresses for this discussion are sampled at integration points which gives

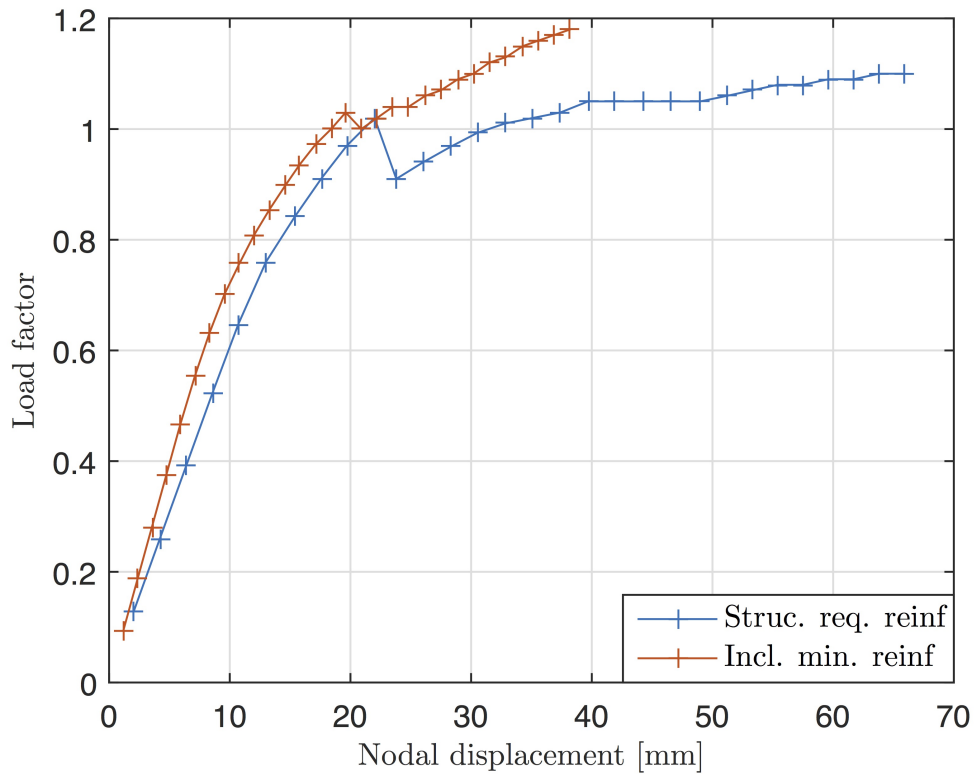


Figure 7.9: Load-deflection diagram at the center of the circular plate

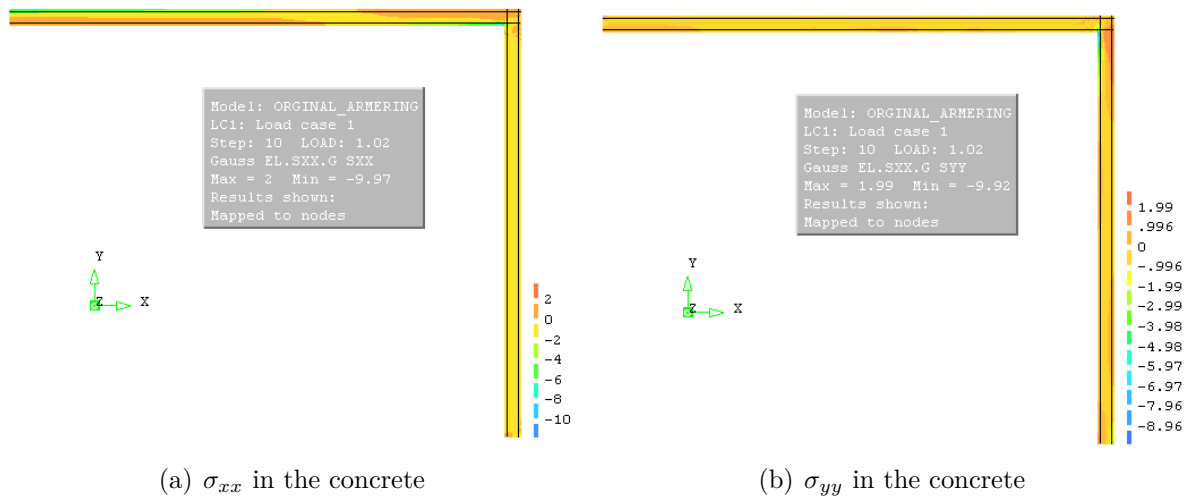


Figure 7.10: Stresses in the concrete at load step 10

highest accuracy for stresses. However it is possible to use some smoothing techniques so that accurate stresses could also be found elsewhere within each element, which is not done here.

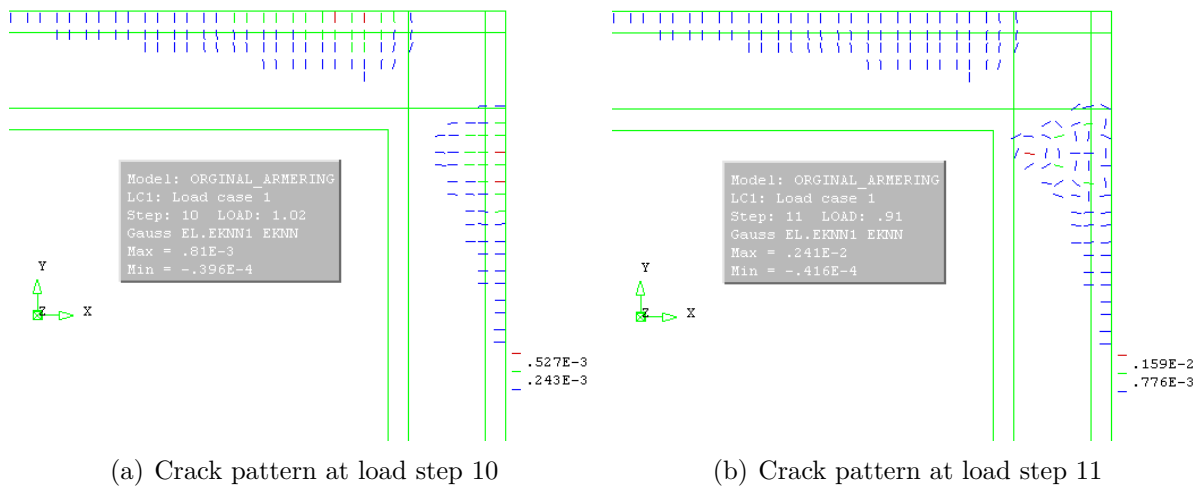


Figure 7.11: Crack patterns in example 1

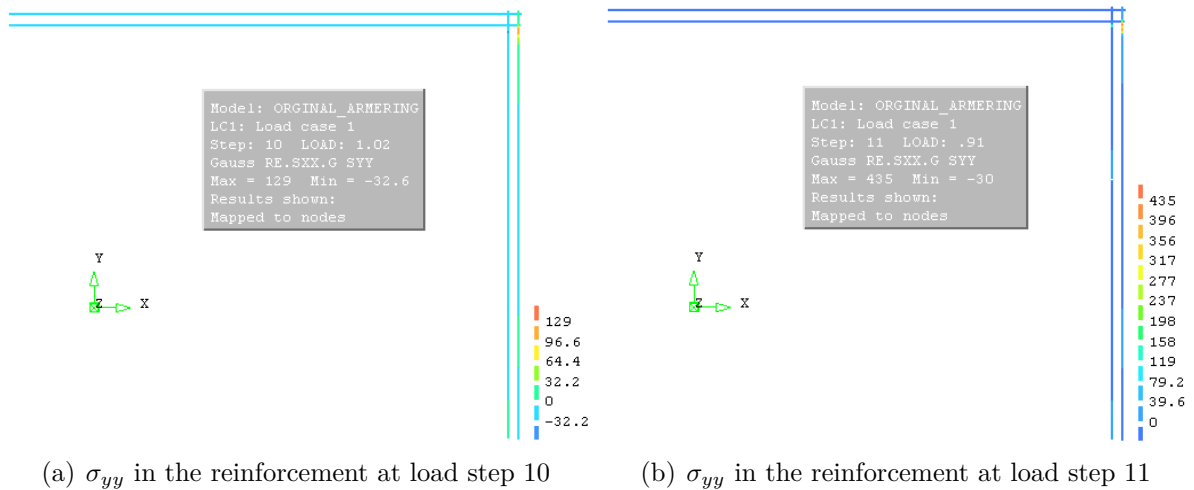


Figure 7.12: Stresses in the reinforcement

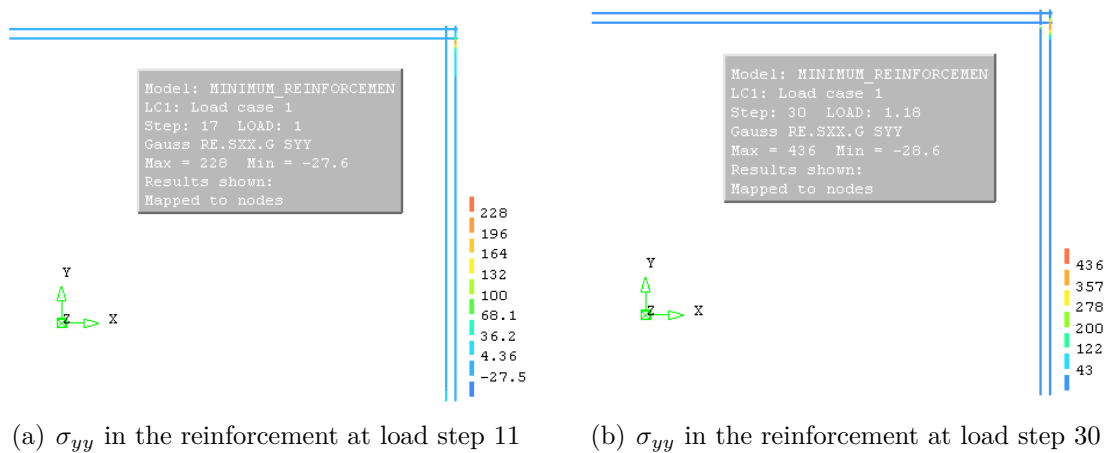


Figure 7.13: Stresses in the reinforcement after including min. reinforcement

7.5 Discussion

The linear FEA using both the L6AXI and CL9AX axisymmetric elements gives relatively good results as the mesh gets refined. From the tabulated values in Tables 7.1 to 7.4, it can be seen that the result from the linear FEA converges close to the analytical solutions. The deviation at its highest is just less than 7% of the analytical solution. There are different sources of errors that could add up and cause this deviation. Firstly there are lots of computations and assumptions involved in the analytical solution procedure. On the effort of avoiding calculation errors, the calculations are performed in the computational software Matlab. However there might still be some minor input errors which together with the assumptions made during the derivation of the procedure, could cause some uncertainty on the analytical solutions. Secondly, modelling errors and errors in the input parameters to the finite element model could also be sources of uncertainties in the FEA solutions. However the results are good enough to confirm that both solution methods give results in the vicinity of the same magnitude.

Following the linear FEA, the structure in example 1 is designed accordingly. The load carrying capacity of the RC structure is then verified by performing a nonlinear FEA. It should be noted that the combination of the material model and the solution procedure applied in the nonlinear FEA is one of the many alternatives that are available in DIANA. However based on the results obtained both in the form of stresses, crack patterns and load-deflection curves, it can be said that the results are sensible to what could be expected on the basis of the linear FEA. Moreover, based on the results, the structure is properly designed to carry the applied design load. As the analysis is based on ultimate limit state, the SLS requirements are not considered in the verification. Therefore the size of the crack width and deflection at the ultimate capacity could possibly be in contradiction to the SLS requirements.

Chapter 8

Cylindrical shell roofs

8.1 General

All of the previously discussed shell structures are axisymmetrical shells. However, cylindrical shell roofs are not, therefore in comparison, the computations involved in the analytical solution procedure are more lengthy and complicated. The analytical solution for cylindrical shell roofs is usually obtained using different approximation methods. In this chapter, just the general outline of the theory behind the analytical solution will be presented.

8.2 Background theory

Circular cylindrical shell roofs, which some times referred to as barrel shells, another type of shell elements that are frequently used for concrete roof structures. This cylindrical shell roofs are a part of a full cylindrical shell discussed in Chapter 4. Such open cylindrical shells are usually supported along the curvilinear edges (diaphragms) or/and along the longitudinal edges. The longitudinal edges are often stiffened by beams which act together with the shells to transfer the loading to the supporting structures such as columns and walls. If the shell is only continuously supported along the longitudinal edge, it acts like a barrel arch and could be analysed as such.

The analytical solution procedure is similar to that of other shells discussed previously. The combination of the membrane and bending theories are used to obtain the complete analytical solution. Following the classical thin shell theory formulations presented in Chapter 3, the membrane stress resultants adopting the notations in Eq. 8.2 are given by:

$$\begin{aligned}N'_\varphi &= -p_z r \\N'_{x\varphi} &= -\frac{1}{r} \int \frac{\partial N'_\varphi}{\partial \varphi} dx - \int p_\varphi dx + f_1(\varphi) \\N'_x &= -\frac{1}{r} \int \frac{\partial N'_{x\varphi}}{\partial \varphi} dx - \int p_x dx + f_2(\varphi)\end{aligned}\tag{8.1}$$

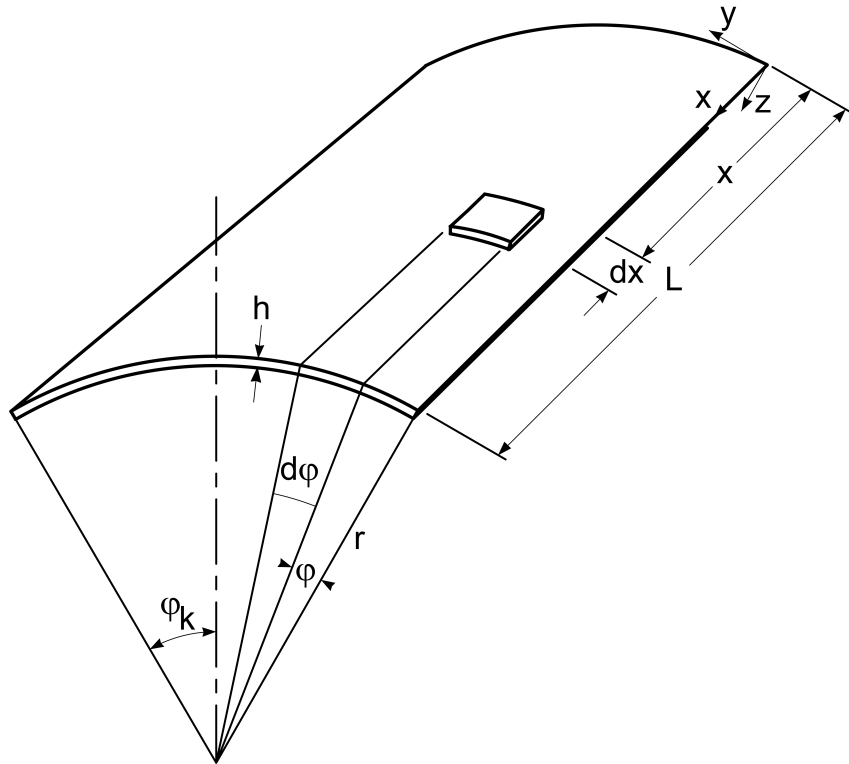


Figure 8.1: Notation and axis definition

The angle φ is measured from the longitudinal edge, and $f_1(\varphi)$ and $f_2(\varphi)$ are integration constants that can be determined from the boundary conditions along the curved edge. When the membrane stress resultants are determined, then the corresponding displacement u, v , and w could be found. As for the previously discussed shell structures, the membrane theory must be supplemented with compatible edge effects in order to represent the internal stress resultants correctly.

For cylindrical shell roofs the solution of the bending theory is rather complicated. For simplifying the mathematical difficulties involved in the bending theory, it is common to represent both the loading and boundary conditions in terms of a Fourier series. For example a uniform shell dead load could be represented as:

$$(p_d)_x = \frac{4}{\pi} p_d \sum_{n=1,3,5,\dots}^{\infty} \frac{1}{n} \sin \frac{n\pi x}{L}$$

Similarly a reaction line load along the longitudinal edge could be written as:

$$(T_L)_x = \frac{4}{\pi} p_d \sum_{n=1,3,5,\dots}^{\infty} \frac{1}{n} \sin \frac{n\pi x}{L}$$

Where P_d is the amplitude of the applied loading or forces. In the bending theory of cylindrical shell roofs, the shallow shell simplification mentioned earlier in this paper are commonly used. The eight order governing differential equation for cylindrical shell roofs is first to be developed. In this paper we will follow a shorter version of the procedure presented by David P. Billington [1]. The shallow shell simplifications has lead us to the

formulation of the expression in Eq. 3.7. These equations are a combination of the deep-beam and the slab equations. For shallow cylindrical shell roofs the different variables are defined as follows:

$$\begin{aligned} \alpha_x &= x & r_x &= \infty & N_y &= N_\varphi \\ \alpha_y &= \varphi & r_y &= r & N_{xy} &= N_{x\varphi} \\ a_x &= 1 & r_{xy} &= \infty & & \\ a_y &= r & & & & \end{aligned} \quad (8.2)$$

Adopting this variables in to Equations 3.7 and 3.3, it is possible to differentiate and arrive at the following single eight order differential equation for cylindrical shell roofs.

$$\nabla^8 w + \frac{12(1 - \nu^2)}{h^2} \nabla_R^4 w = \frac{1}{D} \nabla_R^2 f(p) + \nabla^4 f'(p) \quad (8.3)$$

where,

$$\begin{aligned} \nabla_R^4 w &= \frac{\partial^4 w}{r^2 \partial x^4} \\ \nabla^8 w &= \left(\frac{\partial^2}{\partial x^2} + \frac{\partial^2}{r^2 \partial \varphi^2} \right)^4 w \\ f(p) &= \frac{1}{r^2} \int \frac{\partial^2 p_x}{\partial \varphi^2} dx + r \int \frac{\partial^2 p_\varphi}{\partial x^2} d\varphi \\ f'(p) &= \frac{p_z}{D} - \frac{1}{D} \int p_\varphi d\varphi \end{aligned}$$

The particular solution of Eq. 8.3 can with a good accuracy be replaced by the membrane theory. However the solution for the homogeneous term still need to be obtained. This solution could be taken in the form:

$$w = \sum_{n=1,3..}^{\infty} A_n e^{M\varphi} \phi(k, x) \quad (8.4)$$

Where $k = \frac{n\pi}{L}$ and the term A_n represent the eight constants that depends on the boundary conditions along the longitudinal edge. Similarly, the function $\phi(k, x)$ depends on the boundary conditions along the curved edge, for a simply supported edge it can be taken as $\sin kx$. Substituting Equation 8.4 in to the complementary part of Eq. 8.3 yields eight complex roots represented by the variable M in Equation 8.4. In the case with symmetrical loading and geometry about the longitudinal axis, four unknowns are remained, thus could be solved using four equations. By partially differentiating w , the expression for the different stress resultants could be obtained. Applying the necessary edge effects for this expression gives us the equations needed to solve for the unknown constants. This procedure is suited for a tabulated solution, and one can find various versions of such tables in different books.

8.2.1 Edge beams

The longitudinal edges of cylindrical roof shells are often stiffened using edge beams. Long cylindrical roof shells are usually provided with high edge beams while as shorter shells are

provided with horizontal beams. This has to do with the fact that the principal structural action being in the longitudinal and transverse direction for long and short cylindrical roof shells respectively. The analysis method when dealing with the interaction between the shell and the edge beam is more or less similar to what is presented in chapter 5. The solution procedure is based on first letting the structural parts deform unrestricted, independent of each other, and then restoring compatibility at the interaction. These compatibility equations could be set up both in terms of displacement or equilibrium of forces. The set of equations are then to be solved for the unknowns.

8.3 Numerical examples analysed using linear and nonlinear FEA

In this section, two numerical examples of circular cylindrical concrete shell roofs are analysed. Linear and nonlinear FEA of both the examples is performed in DIANA. Furthermore the results from the linear FEA are compared with their corresponding analytical solutions. In the first example, a concrete shell roof structure which is fixed along its longitudinal edge and that has a span of 25 m is considered. Similarly, in the second example a concrete roof shell which is simply supported along its curved edge and free along the longitudinal edge is analysed.

8.3.1 Linear FEA

The shell structures in the following two examples are modelled using regular curved shell elements. These elements are based on isoparametric degenerated-solid approach where transverse shear deformation is included according to Mindlin-Reissner theory [5]. DIANA has total six types of such elements. Three of them are triangular elements with 3 (T15SH), 6 (CT30S) and 15 (CT45S) nodes, while as the other three are quadrilaterals with 4 (Q20SH), 8 (CQ40S) and 12 (CQ60S) nodes. In the following examples the 8 node quadrilateral element CQ40S is used. It is based on quadratic interpolation and Gauss integration over the $\xi - \eta$ element area. The element has three translational DOFs (U_x, U_y, U_z) and two rotational DOFs (ϕ_x, ϕ_y) at each node [5].

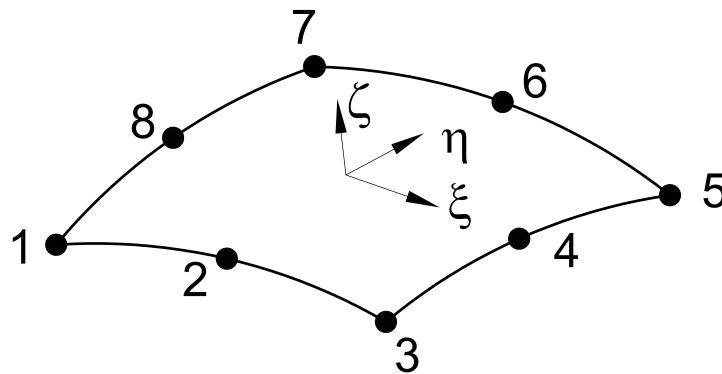


Figure 8.2: CQ40S

8.3.2 Reinforcement

Before proceeding with the nonlinear analysis, the amount of necessary steel reinforcement based on the stress resultants obtained from the linear FEA will be calculated. In general the principal moment and membrane force directions in shells do not coincide. Therefore, establishing bending and axial force interaction diagrams is not possible [20]. Usually a design method based on the six moments and membrane forces is used to calculate the amount of necessary reinforcement. In this paper, the so called Two layered approach (Membrane method) as presented in Ref. [20] will be used. This is a simplified method which is based on dividing the shell in to two layers (membranes) loaded with equivalent membrane forces. This method is considered good enough for finding the amount of necessary reinforcement that can be used as an initial input for more advanced computation or analysis. The detailed reinforcement calculation according to this method can be found in Appendix B.

8.3.3 Nonlinear FEA

Before conducting the nonlinear FEA, the calculated amount of steel reinforcement is first included in the structural model as embedded steel reinforcement. To account for the change of stresses across the thickness the number of integration points in ζ direction (see Figure 8.2) is increased from the default 3 to 9. The overall material model is the same as presented in Subsection 7.4.3. The ultimate crack strain of the RC structures is taken as $2.17 \cdot 10^{-3}$, which is the ultimate strain of the steel reinforcement.

8.3.4 Example 3: Circular cylindrical shell roof with fixed edges

Linear FEA

In this example a large RC shell roof structure loaded with a uniformly distributed external load is considered. The roof structure covers a rectangular area of 25m x 55m. The shape and support conditions are as the shown in Figure 8.3. Due to the symmetry of the structure and the loading, only a quarter of the shell is analysed.

Analytical solution

In a paper written by Chandrasekaran, Gupta and Carnnante [3], some design aids based on the analytical solution procedure for fixed support RC shells is proposed. In the same paper the accuracy of the analytical solution is verified by performing FEA of a numerical example in which a satisfactory comparison was achieved. The stress resultants from the analytical method are given in a rather lengthy closed-form expressions. In this study this expressions are implemented in the computational software Matlab so that for a given set of input parameters the results from the analytical method could easily be obtained (see script in Appendix D). Thus by applying the parameters from the current

Table 8.1: Geometric and material properties of the RC shell

Description	Value
Length	55 m
Width	25 m
Thickness (t)	0.176 m
Radius (R)	17.6 m
f_{ck}	$30 \frac{N}{mm^2}$
f_t	$2 \frac{N}{mm^2}$
E_{steel}	$2 \cdot 10^5 \frac{N}{mm^2}$
$E_{concrete}$	$3 \cdot 10^4 \frac{N}{mm^2}$
Total load	$9 \frac{kN}{m^2}$

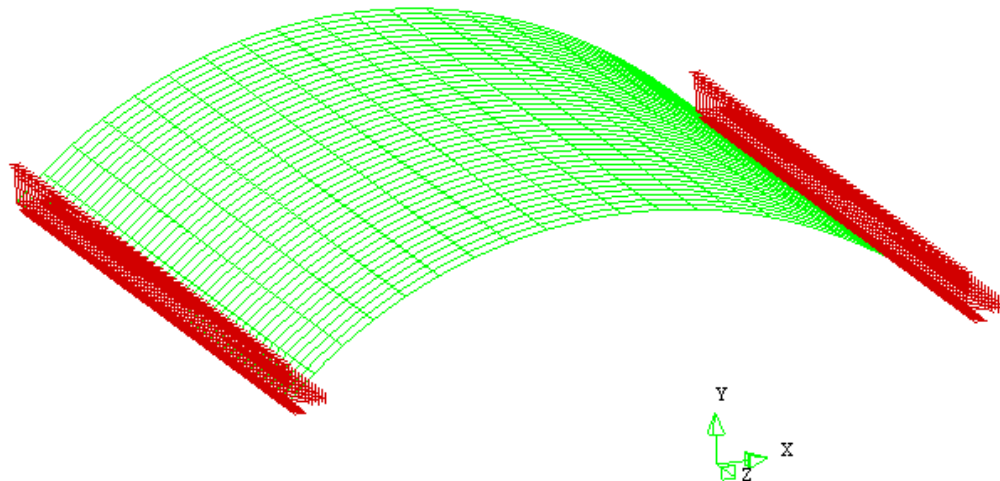


Figure 8.3: Illustration of the structure in example 3

numerical example, the stress resultants from the analytical method are readily acquired. In Figure 8.4, this results are plotted against the stress results from the linear FEA. As it is shown in the diagrams, most of the stress results show good agreement except for N_x . The longitudinal axial force N_x increasingly deviates from the analytical solution when moving further from the fixed edge in φ direction towards the midspan. The analytical solution method is based on the stress results varying only in φ direction. However, the results from the FEA show the existence of variation of different magnitude along the longitudinal axis. This variations could be due to the introduction of the discontinuities at both curved edges of the shell which are not accounted for in the analytical method. This is further investigated by adding an additional constraint in Z direction along the curved edge, the result of this on the different stress resultants are presented in Appendix C. Further from the curved edge, the disturbances of the edge gradually disappear and

the result from the FEA gets very close to those obtained from the analytical method. The results also show that there are large compression forces N_φ in the structure, due to the arch like structural behaviour of the shell most of the loading is carried in the arch direction.

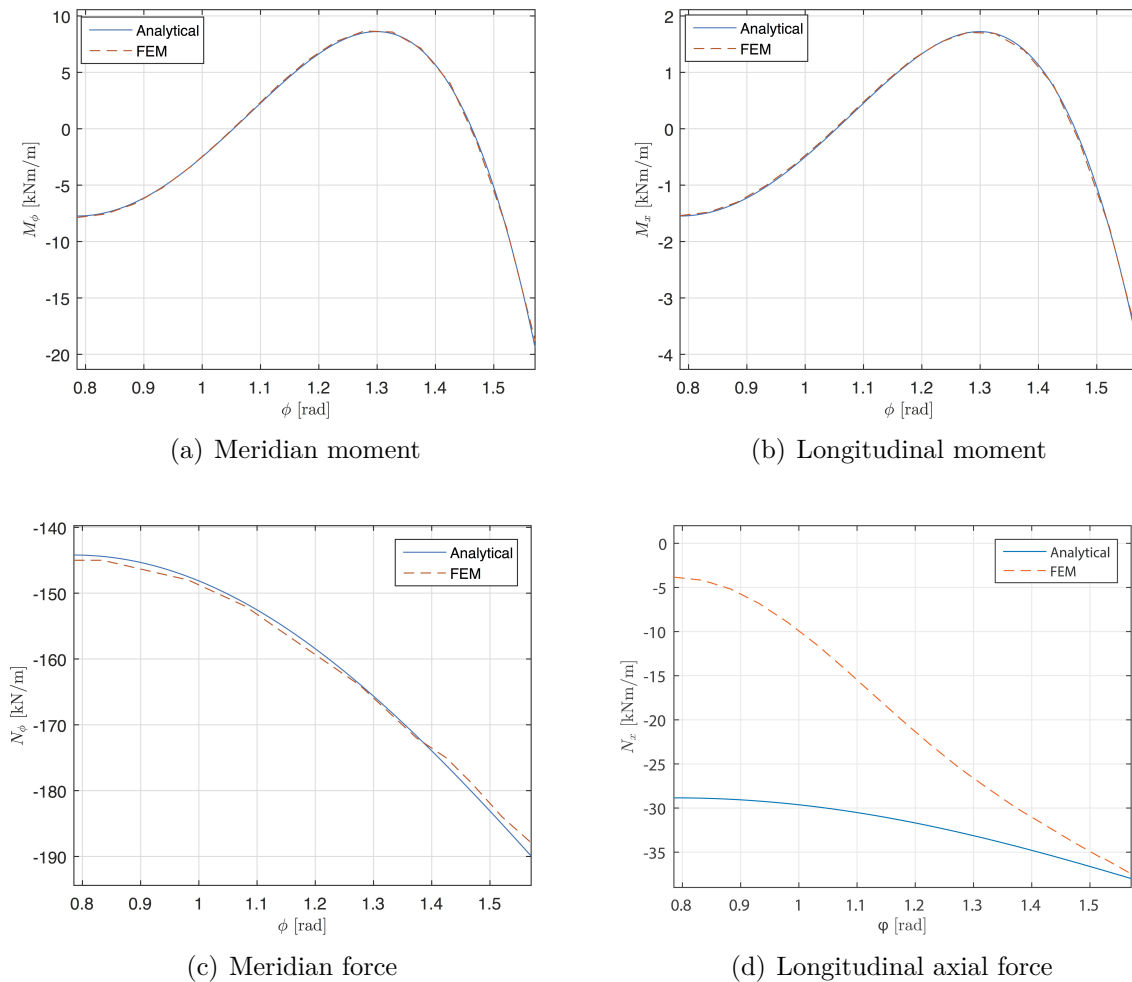


Figure 8.4: Comparison between analytical and FEA solutions

Nonlinear FEA

Again before proceeding to the nonlinear FEA the amount of required steel reinforcement is calculated. Though small compared to the other stress resultants, the linear FEA results shows the existence of the in-plane shear forces $N_{x\varphi}$ and twisting moment $M_{x\varphi}$. Thus, the two layered approach based on the six stress resultants is used to calculate the amount of required reinforcement. The design calculation according to this membrane method is shown in Appendix B. Here the amount of steel reinforcement that is to be applied are summarized in Table 8.2. This is a very little amount of reinforcement, and less than the minimum requirement according to the Eurocodes. However, for the purpose of studying

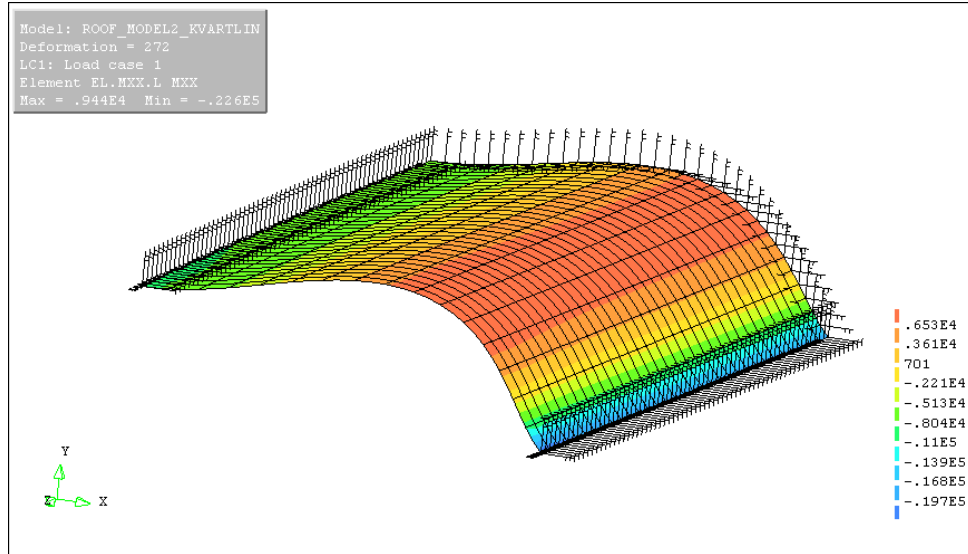


Figure 8.5: Shape of the deformed element model

Table 8.2: Initial reinforcement input [$\frac{mm^2}{m}$]

Reinforcement	Top	bottom
$A_{s\varphi}$	78.5	231.49
A_x	78.5	115.75

the structural response this will be applied as it is.

This reinforcement is added to the model as embedded grid reinforcement. Furthermore the solution procedure that is applied for the nonlinear FEA is as shown in Table 8.3. The quarter of the shell is discretized into a 18×36 elements which gives a quadratic mesh

Table 8.3: Solution procedure for the nonlinear analysis

Variable	Chosen value/method
Nonlinearity	Physical and Geometrical
Load increment	0.2
Number of increments	40
Max. number of iterations	100
Iterative procedure	Regular Newton-Raphson with arc length control
Convergence criterion	Both force and displacement norm
Convergence Limit	0.01

with a mesh size of 771.1 mm. This is the finest mesh where this particular version of

DIANA software is able to provide results for. As this is a relatively large element size, the tension stiffening model according to Equation 7.10 should be considered. However, when fracture energy is given as an input in DIANA, it calculates the ultimate crack strain by using Equation 7.9. Therefore, the new model according to Eq. 7.10 is not easy to implement when performing FEA with DIANA. The nonlinear FEA in this example will therefore be analysed only with the fractures energy calculated by Eq. 7.9 as an input. The results in the form of a load-deflection diagram at node 1 which is at the midspan is shown in Figure 8.6.

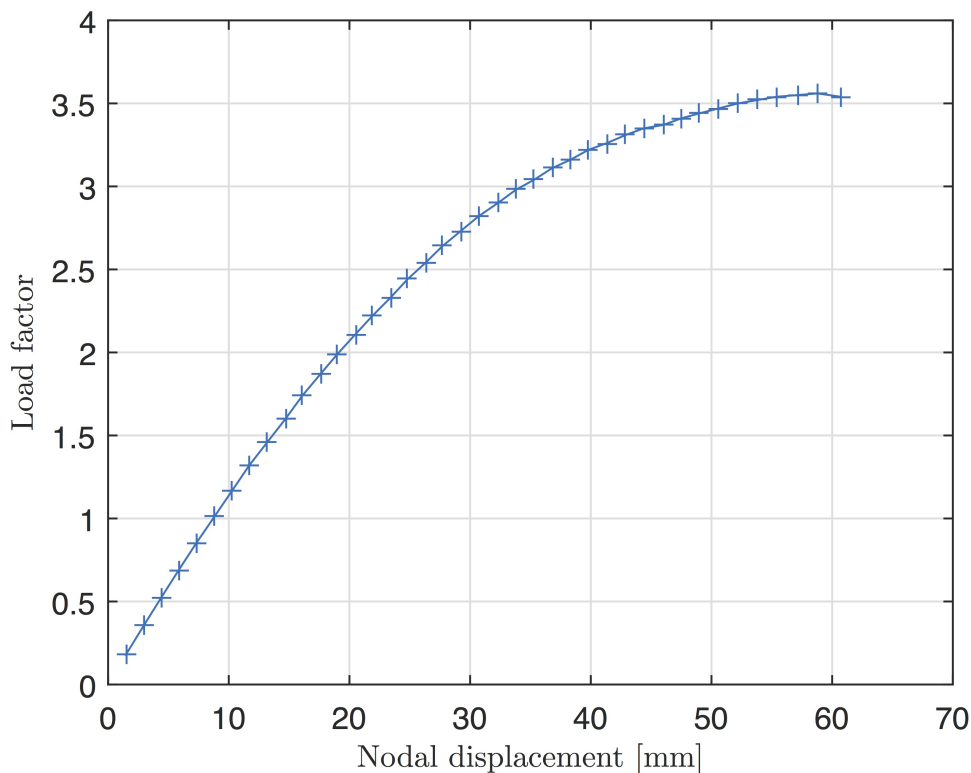


Figure 8.6: Load-displacement curve at the midspan in example 3, $\frac{R}{t} = 100$

The diagram shows that the structure has a sufficient capacity, which is more than three times the applied loading. This can be due to the fact that most of the loading is taken as compressive force in the circumferential direction. Therefore it is further possible to optimize the structure by reducing the thickness of the shell.

The analysis is then performed again with a reduced thickness of the RC shell such that $\frac{R}{t} = 150$, but with the same amount of reinforcement. Again the force-deflection diagram at the same node as previous is plotted and is shown in Figure 8.7. This time the maximum capacity is reduced to $1.04\times$ applied load. Compared to the previous structure the ultimate capacity is reduced by 70%.

As it can be seen from Figure 8.8, at the maximum capacity, the ultimate tension capacity of the concrete ($2 \frac{N}{mm^2}$) in the global Z and X directions are approached. The crack strain vectors which act perpendicular to the crack patterns are shown in Figure 8.9. The cracks are as expected, following the moment diagram, concentrated at the bottom surface near

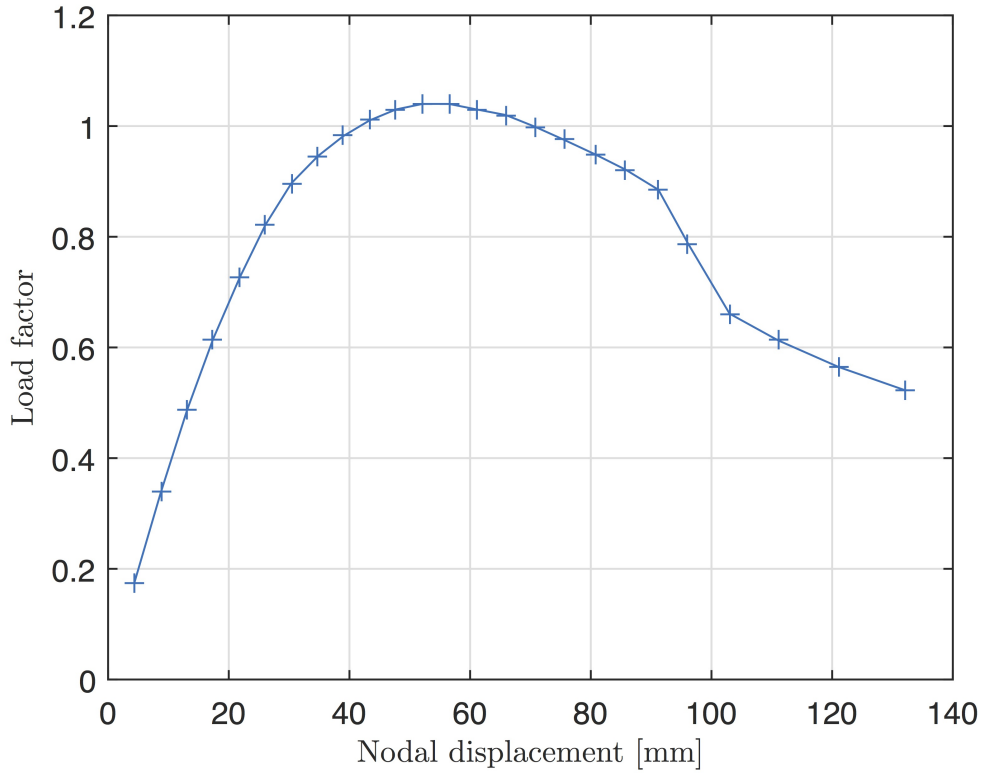


Figure 8.7: Load-displacement curve at the midspan in example 3, $\frac{R}{t} = 150$

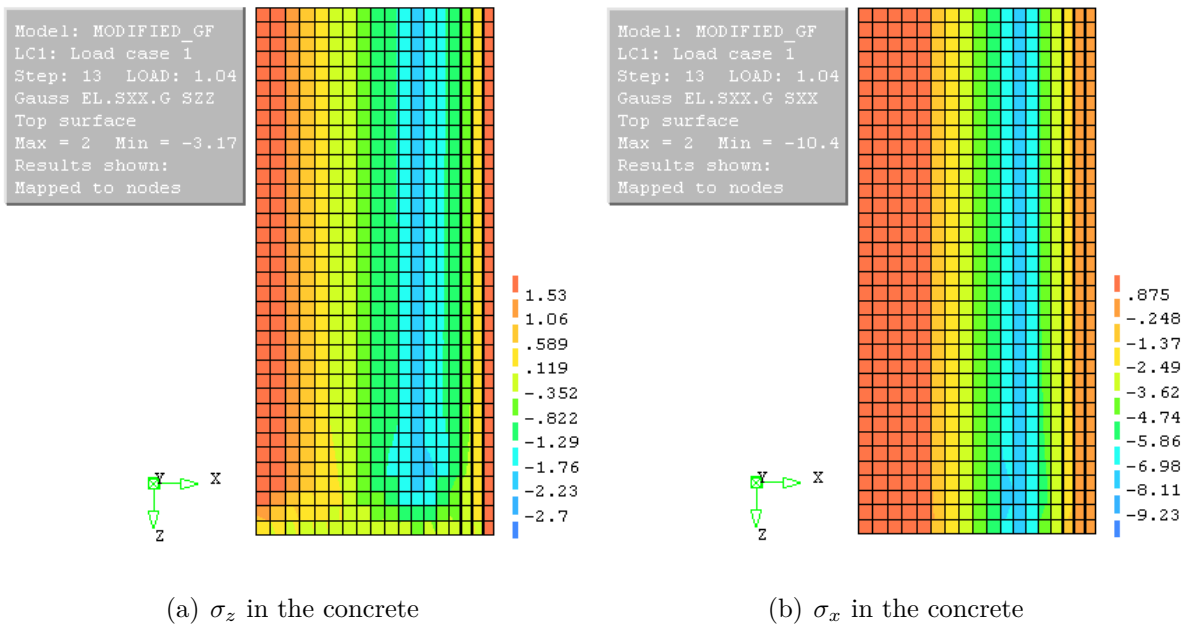


Figure 8.8: Stresses in the concrete at the maximum capacity

the fixed edge and the crown, and at the top surface in between. Post the limit value the load-deflection path goes downwards even when the stresses in the steel reinforcement starts to increase significantly. As there are large compression stresses in the circumferen-

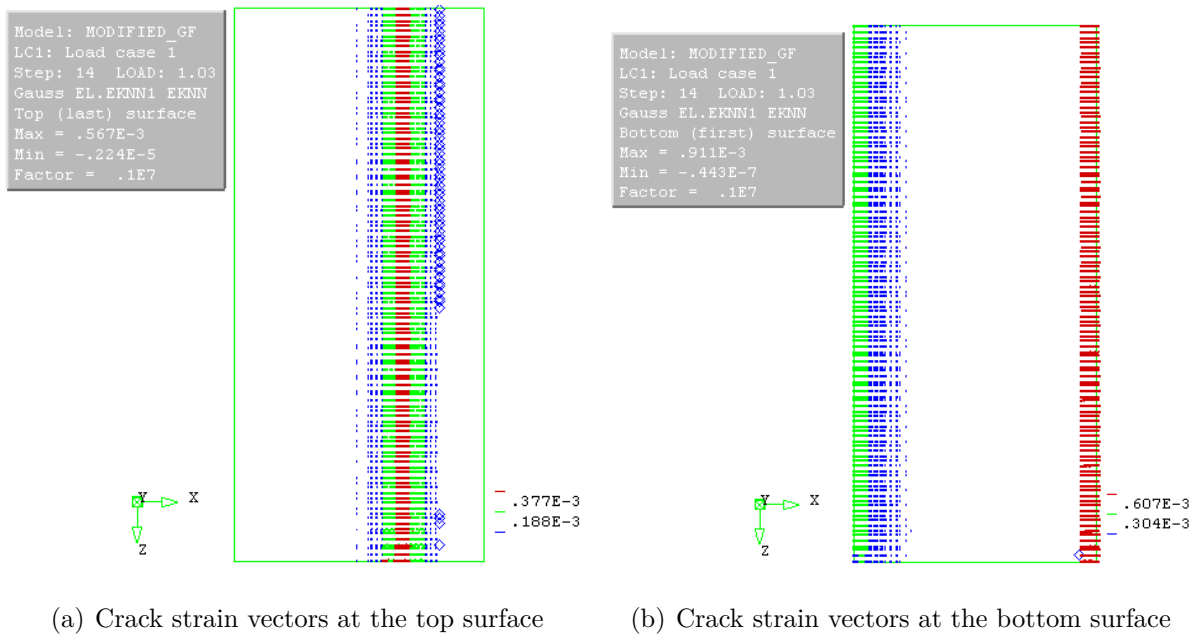


Figure 8.9: Crack strain vectors at load step 14

tial direction and the RC shell is relatively thin, buckling could be the failure mechanism. To investigate this further the analysis is again performed without taking in account the geometrical nonlinearity. This is because with the geometrically nonlinear analysis the stiffness matrix (relationship between force and displacement vectors) is updated between loading increments such that deformations which affect the structural behaviour could be incorporated. The load-deflection diagram from the new analysis is shown in Figure 8.10. Here it is clear that the load-deflection path continues upwards until either the compression strength limit in the concrete or tension strength of the steel reinforcements is reached. This is different to what is obtained in Figure 8.6 where both the geometric and material nonlinearity is considered.

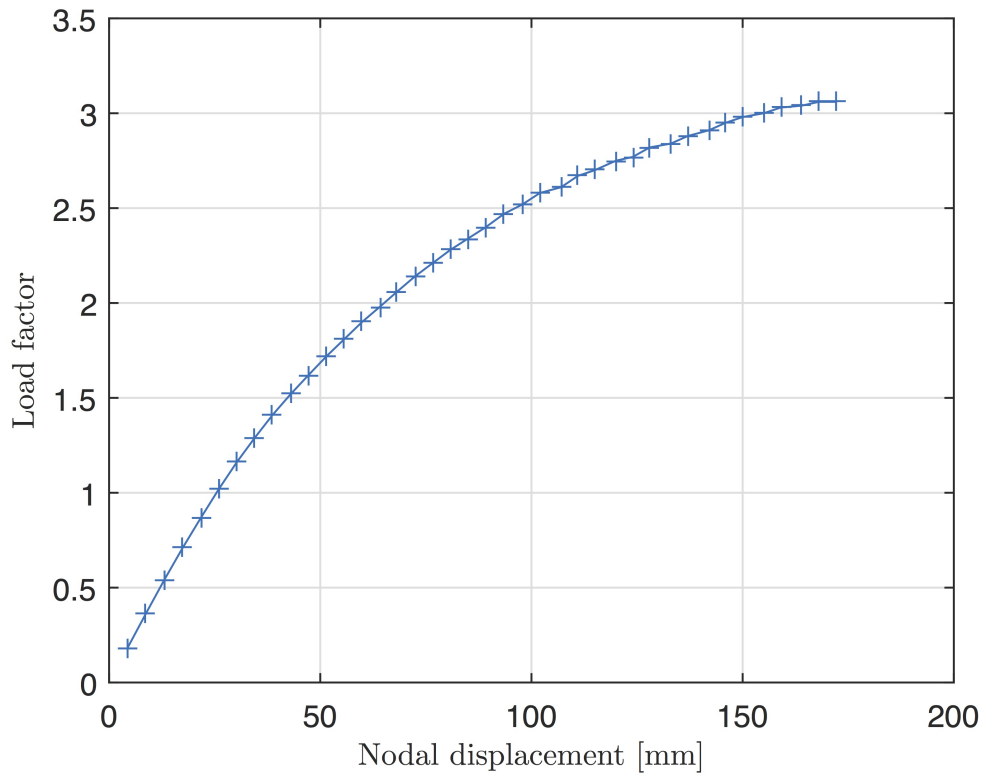


Figure 8.10: Load-deflection curve at midspan without geometrical nonlinearities, $\frac{R}{t} = 150$

8.3.5 Example 4: A simply supported circular cylindrical shell roof

Linear FEA

In this last example a simply supported cylindrical shell roof loaded with uniformly distributed external load is analysed. First a linear FEA of the structural model is performed. Afterwards the shell will be stiffened by using edge beams along its longitudinal edge, and analysed again. This is done to study the effect of the edge beam on the distribution of the stress resultants in the structure. Due to symmetry conditions, only the quarter of the shell will be modelled and analysed.

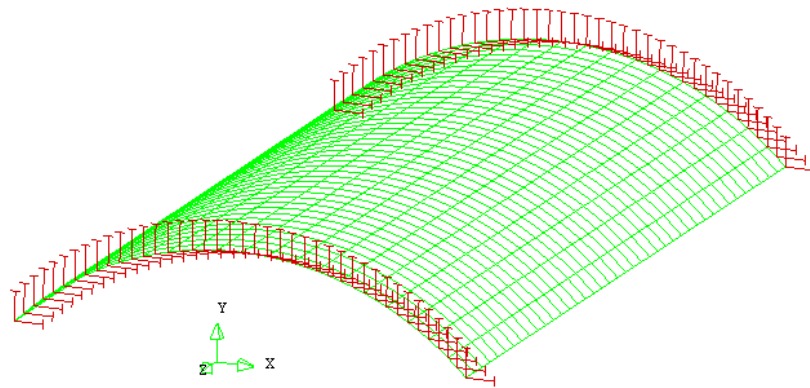
Table 8.4: Geometric properties of the RC shell

Description	Value
Length	20.27 m
Width	11.46 m
Shell thickness	76.20 mm
Beam width	304.80 mm
Beam height	685.80 mm
Radius	8.11 m
f_{ck}	$30 \frac{N}{mm^2}$
f_t	$2 \frac{N}{mm^2}$
E_{steel}	$2 \cdot 10^5 \frac{N}{mm^2}$
$E_{concrete}$	$3 \cdot 10^4 \frac{N}{mm^2}$
Total load	$3.83 \frac{kN}{m^2}$

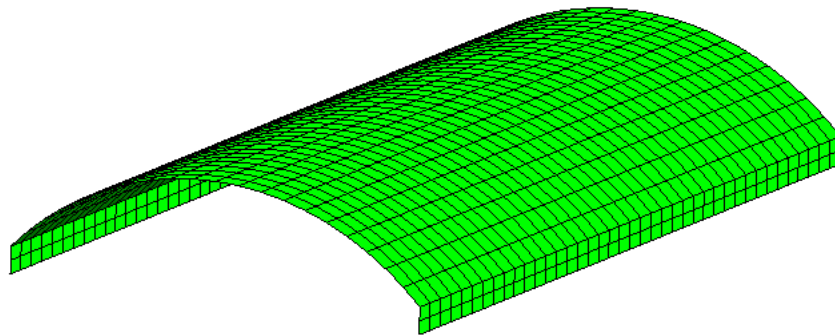
Analytical solution

This example is previously analytically calculated in the book called '*Thin concrete structures*' by Billington [1]. The structure is modelled in DIANA, as close as possible to what was assumed in the analytical calculations. The geometry and loading is the same as the analytical model. In Table 8.5 the results obtained from the FEA are compared with the solutions obtained from the analytical calculations. The results show that there are some deviations of varying magnitude between the analytical solutions and those from the FEA. The overall deviation varies along the φ direction. There are good agreements at certain locations while as there are significant deviations at others. In general some deviation between the analytical and FEA solutions is expected due to for instance:

- The assumptions made in the derivation of the analytical solution such as:



(a) Illustration of example 4



(b) Illustration of example 4 with edge beams

Figure 8.11: Illustrations of the structure in example 4

- The assumption of the external loading and boundary conditions only by the first term of the Fourier series, that is half of a sinus curve.
- The Shallow shell assumption
- The applied meshing in the finite element model is not fine enough
- Other possible deviations between what is considered in the analytically calculated example and the FEA model

To what extent the deviations are caused by the above reasons is difficult to conclude without looking closer into each and every one of them.

Then, edge beams are added along the longitudinal edges of the cylindrical shell roof, and the linear FEA is performed again. The results from this new FEA in comparison with the previous results are shown in Table 8.6. $\varphi = 0$ corresponds to the junction between the edge beam and the cylindrical shell roof. The edge beams are monolithically casted together with the RC shell surface. Their main purpose is to take up the large longitudinal tension stresses along the edge of the shell. This is well demonstrated in the fact that the force N_x along the edge $\varphi = 0^\circ$ drops from $1430 \frac{kN}{m}$ to $79 \frac{kN}{m}$. The edge

Table 8.5: Comparison between the FEA and analytical solutions of the structure in example 4

Loading		Angle φ (measured from edge)					
		45°	40°	30°	20°	10°	0°
$x = L/2, kN/m$							
N_x	Numerical	21.100	-11.131	-208.379	-346.091	26.826	1430.000
	Analytical	-4.918	-32.690	-208.945	-331.427	29,772	1445.234
$x = L/2, kN/m$							
N_φ	Numerical	-44.200	-44.055	-41.341	-30.262	-10.898	0.153
	Analytical	-52.100	-52.246	-50.641	-40.133	-16.491	0.000
$x = 0, kN/m$							
$N_{\varphi x}$	Numerical	0.025	2.761	-15.815	-88.294	-172.071	-5.520
	Analytical	0.000	-1.605	-26.269	-89.898	-136.599	0.000
$x = L/2, kNm/m$							
M_φ	Numerical	-11.900	-11.600	-9.427	-5.230	-0.918	0.004
	Analytical	-11.654	-11.432	-9.341	-5.204	-0.667	0.000

Table 8.6: Comparison between the results with and without edge beams

Loading		Angle φ (measured from edge)					
		45°	40°	30°	20°	10°	0°
$x = L/2, kN/m$							
N_x	With edge beam	-105.000	-107.446	-119.322	-114.214	-55.967	79.100
	Without edge beam	21.100	-11.131	-208.379	-346.091	26.826	1430.000
$x = L/2, kN/m$							
N_φ	With edge beam	-36.800	-36.188	-31.941	-24.053	-13.691	-2.900
	Without edge beam	-44.200	-44.055	-41.341	-30.262	-10.898	0.153
$x = 0, kN/m$							
$N_{\varphi x}$	With edge beam	0.004	-11.927	-39.196	-73.610	-105.817	-101.000
	Without edge beam	0.025	2.761	-15.815	-88.294	-172.071	-5.520
$x = L/2, kNm/m$							
M_φ	With edge beam	-1.750	-1.584	-0.452	1.080	1.602	-0.644
	Without edge beam	-11.900	-11.600	-9.427	-5.230	-0.918	0.004

beams has also some torsional stiffness which, as it can be seen in Table 8.6, contributes to reduce the moment M_φ .

Nonlinear FEA

The simply supported shell roof structure with edge beams is then analysed using non-linear FEA. The amount of steel reinforcement that is included in the structural model is as shown in Table 8.7. The thickness of the concrete shell in this example is small such that applying the minimum reinforcement cover according to Eurocode 2, together with an ordinary bar reinforcement is impossible. Therefore, the reinforcement layout is done on the basis of what is applied in the original numerical example [1]. The reinforcement calculations in the book are based on the principal tension forces, and the layout of the reinforcement is also done accordingly. Here, this is modified such that the orthogonal layout of the reinforcement is chosen and the amount of steel reinforcement is modified according to the material properties in Table 8.4. The solution procedure used is similar

Table 8.7: Amount of steel reinforcement [$\frac{mm^2}{m}$]

	Reinforcement	Grid	Bar
Edge beam	$A_{s,horizontal}$	226.19	490.87 × 3 mm^2 (3Ø25)
	$A_{s,vertical}$	166.77	-
Shell	$A_{s\varphi}$	146.73	
	A_{sx}	146.73	

to the previous example and is shown in Table 8.8. A quarter of the roof shell structure is meshed into a uniform quadratic mesh with a mesh size of 378.7 mm . The load-deflection diagram at a node in the midspan of the beam is shown in Figure 8.12. The diagram shows that the capacity of the structure surpasses a load factor of one, which again represents the applied loading. The load-deflection diagrams shows that the path reaches its first peak at load factor 1.24 before it drops back. The failure mechanism seems to be due to the accumulation of tension stresses at the midspan of the edge beams. At this limit point, both the tension stresses σ_{xx} and σ_{zz} has approached the tension strength of the concrete, see Figure 8.14. Following this limit value the stresses in the steel reinforcement dramatically changes from 221 $\frac{N}{mm^2}$ to 437 $\frac{N}{mm^2}$, see Figure 8.15. Thus, the strength of the steel reinforcement is reached. Post the peak value, it can be noticed that the analysis takes several number of iterations to find convergence.

The crack patterns before and after the peak point are as shown in Figure 8.13. The patterns are as expected concentrated at and around the midspan of the edge beam. Similarly, the stresses in the concrete and the reinforcement in the global z direction before and after the peak value are shown in Figures 8.14 and 8.15 respectively.

Table 8.8: Solution procedure for the nonlinear analysis

Variable	Chosen value/method
Nonlinearity	Physical and Geometrical
Load increment	0.1
Number of increments	50
Max. number of iterations	100
Iterative procedure	Regular Newton-Raphson with arc length control
Convergence criterion	Both force and displacement norm
Convergence Limit	0.01

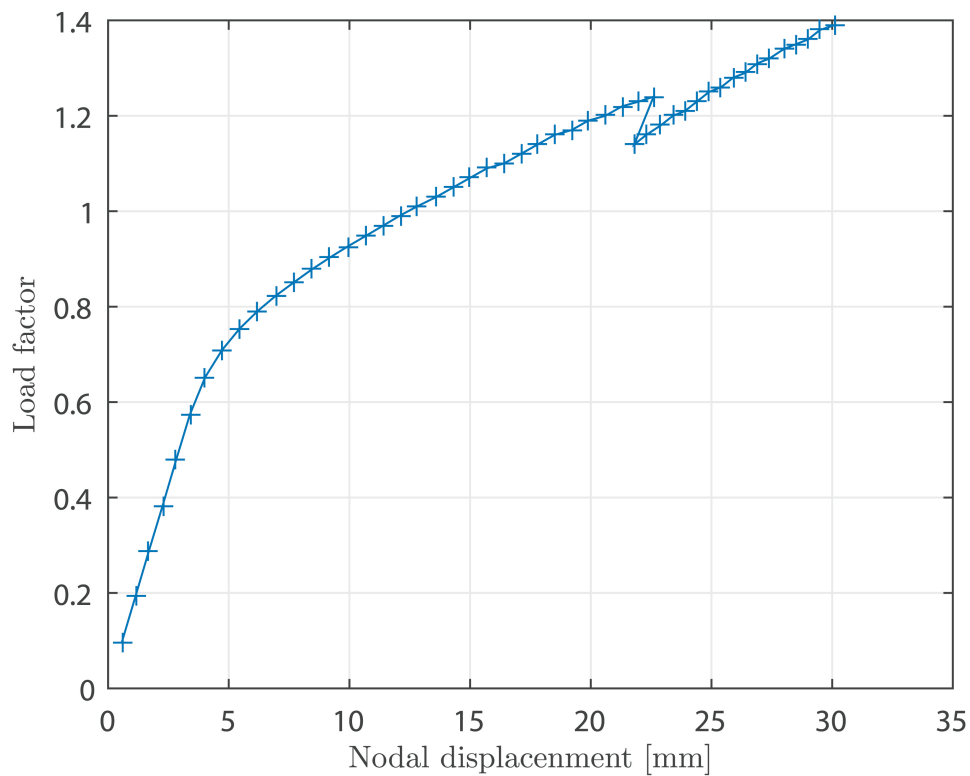
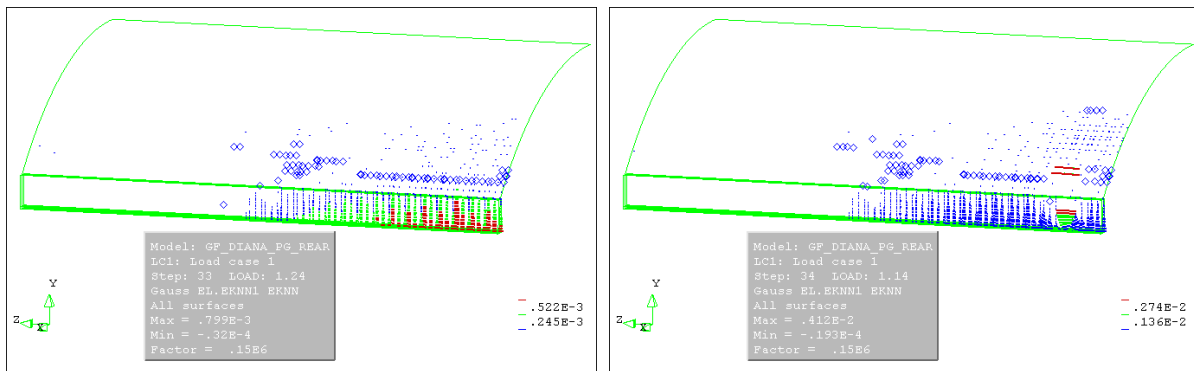


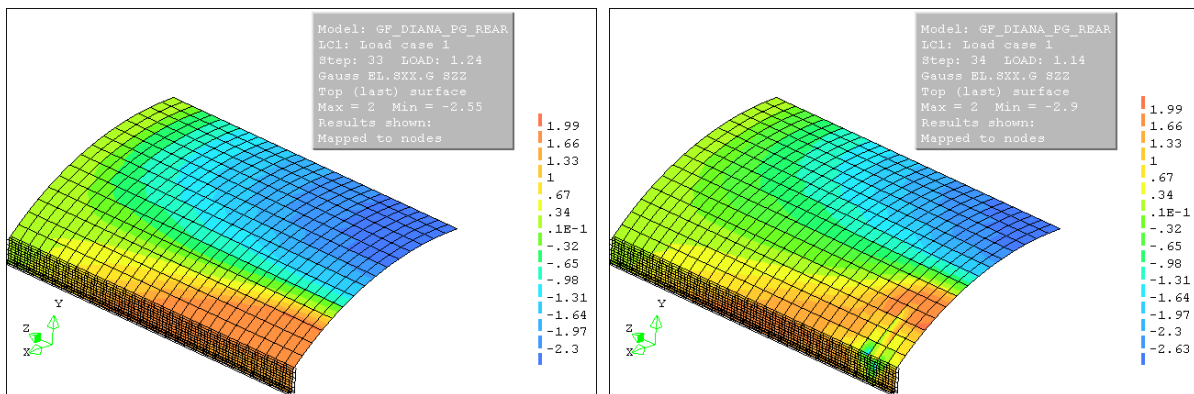
Figure 8.12: Load-displacement curve at the midspan of the edge beams



(a) Crack strain vectors at load step 33

(b) Crack strain vectors at load step 34

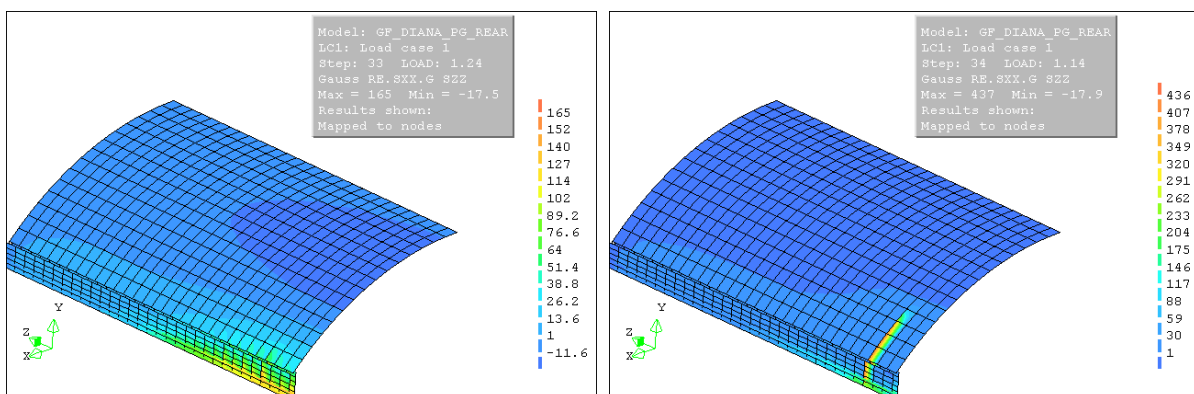
Figure 8.13: Crack patterns in the concrete before and after the peak point



(a) σ_{zz} at load step 33

(b) σ_{zz} at load step 34

Figure 8.14: Stresses in the concrete before and after the peak point



(a) σ_{zz} in the reinforcement at load step 33

(b) σ_{zz} in the reinforcement at load step 34

Figure 8.15: Stresses in the reinforcement before and after the peak point

8.4 Discussion

Generally, the analytical solution procedure of non axisymmetrical thin shells involve long computations. The circular cylindrical shell roof with symmetrical boundary conditions is one of such shells where there exists a complete analytical solution procedure for. However, the complete derivation of this doesn't fall within the scope of this thesis, and therefore is not included in here. The aim of the background theory presented in Section 8.2 is to show that how the analytical solution procedure relates to the general formulation of the theory of thin shells. The structural behaviour of such cylindrical shell roofs could be approximated by using beam and arch theories. Looking at the two numerical examples analysed in this chapter, one can draw some similarities.

In the first example the analytical solutions are obtained from the assumption that stress resultants vary only in φ direction, which is more like an arch type behaviour. The FEA however shows that there is some variation of the load effects along the longitudinal axis, and at there are some additional in-plane shear force and torsional moment present. When sampled further from the curved edge, the results of the linear FEA shows a good agreement with the analytical solutions except for N_x . Following the investigation in Appendix C, it has shown that adding horizontal constraint along the curved edge gives the same distribution of the N_x as in the analytical solution. The distribution of the other stress resultants remain the same. This confirms that the discontinuities at both ends of the shell are not accounted for in the analytical solution and are sources for deviation.

The structural behaviour of structure in example 4 is analogous to those of a beam with a hollow cross section. Similar to a simply supported beam the bending moment is highest at the midspan which results in a maximum tension stress at the bottom and a compression stress at the top of the cross-section. Hence, as it can be seen from Figure 8.14, at the midspan the tension stresses are concentrated around the edge beams and compression stresses are concentrated at the part of the shell around the crown. The analytical method is based on the theory of thin shells, with the assumption of shallow shells. The results of the analysis showed some deviation compared to the analytical solution. The sources of this deviation could be one or more of the reasons mentioned before. The best agreement is found for M_φ while as the membrane forces show deviation of varying magnitude. At certain locations however the results are very close to the analytical solutions. Therefore it is difficult to conclude specifically on what could cause the deviation that are shown.

From the results in example 3, one can conclude that the design method according to the two layered approach gives a good initial and conservative approximation for the required amount of steel reinforcement. However for relatively very thin concrete shells, it is difficult to design according to this method. Using ordinary bar reinforcement together with the required minimum reinforcement cover makes it challenging to divide the shell thickness into layers. In addition, casting such very thin RC shells with ordinary bar reinforcement at the construction site could prove to be difficult. Hence, a fibre based reinforcement could be a better suited alternative for very thin RC shells. However as this is not within the scope of this thesis it is not considered in here.

The nonlinear FEA are overall a little more demanding than the linear FEA. The choices of solution procedures and material models has a significant effect on the obtained results.

The analyst needs to be aware of the input parameters and expected outcome. Moreover a good knowledge of the FE program at hand and its capabilities is necessary. In the numerical examples, the material modelling and solution procedure that is chosen is just one way of performing the nonlinear analysis. It should be noted that there are different choices of material models and combinations of solution procedures that could be applied, and might be better suited to the problem at hand. Based on the stress concentrations and crack patterns that are obtained, the results are however as what could be expected on the basis of the linear FEA. The effect of including geometrical nonlinearities is also narrowly considered in Example 3. It has shown that there is a considerable difference in the results with and without taking into account geometrical nonlinearities. Hence, buckling analysis of thin shells should not be overlooked. However this is not within the scope of this thesis, and therefore will not be discussed any further.

The finite element mesh used in both the examples is a relatively coarse mesh. This is due to the limitations associated with the DIANA version used in this study. As the element size is used to estimate the crack bandwidth and is included in the calculations of the fracture energy, it has a direct effect on the material model. As the element size used in both the examples is larger than the limit size suggested by Kwak and Filippou [9] in their modified model, the new model should have been considered. However, as DIANA uses the model given by Eq. 7.9 as default to calculate the ultimate crack strain, we could not find any easy way to implement this model in DIANA. Therefore, this might give rise to some uncertainty on the accuracy of the results obtained from the nonlinear FEA. Moreover, specially in the last example, we have also noticed that the results of the nonlinear FEA are sensitive to the size of load increment that is chosen.

Chapter 9

Conclusion

The classical theory of thin shells which is briefly reviewed in this paper provides the general understanding behind the structural behaviour of shells. Loading on the surfaces of shells is mainly taken up by the membrane forces, however bending effects are eventually introduced for the compatibility of displacements and equilibrium of forces at the boundary. For axisymmetric shells, the general governing differential equations are significantly reduced. As it is demonstrated in this paper, for such structures it is fully possible to perform full analytical calculations. For shells of arbitrary geometry and loading however the analytical calculations become complicated or impossible without taking significant assumptions.

The first two examples in this paper illustrated the use of the analytical solution procedure in a practical setting. From the results obtained in both the examples one can observe that the moment and shear forces are highest at the edges and junctions as expected, and damp exponentially towards the intermediate parts of the shell structures. The cylindrical wall in example one is relatively short such that the boundary effects overlap before they damp out. Thus the solutions had to be obtained by considering the boundary effects from both edges simultaneously. This adds up to more computations, however based on the results obtained it can be said that it was successfully done. The membrane forces are almost solely dominated by the external loading, and they converge towards the membrane solution when moving further from the edges. This demonstrates that further from the boundary the membrane solution alone can give fairly accurate results.

The linear FEA analysis of the two examples in DIANA is performed by using both the L6AXI and CL9AX axisymmetric elements. As the mesh become refined the results obtained by using both elements converge close to the analytically obtained solutions. As the CL9AX element is a higher order element it converges quicker than the L6AXI. The comparison with the analytically obtained solutions is done with respect to the magnitude of the stress resultants at the edges. The largest deviation was found to be less than 7% compared to the analytical solutions. The general distribution of the stress resultant over the structure are also fairly close to those obtained from the analytical calculations. Following the linear FEA, the cylindrical wall with a circular plate on top in example 1 was designed in accordance with the Eurocodes. The accompanying nonlinear FEA showed that the structure has the necessary capacity to carry $1.02 \times$ the applied design

load. The failure mechanism is the accumulation of tension stresses at the junction with the circular slab.

Cylindrical shell roofs are the only non axisymmetric structures considered in this study. The linear and nonlinear FEA are performed by using the curved shell element CQ40S. In the third example a circular cylindrical shell roof with fixed edges along its longitudinal edge is considered. The results showed that a good agreement between the analytical and FEA results is obtained. The accompanying nonlinear analysis has shown that the structure is able to carry much more than the design load. This can indicate that the design method applied which is according to the two layered approach is conservative. When the thickness of the shell is reduced the ultimate capacity of the structure is reached long before the compression failure in the concrete or tension failure in the reinforcement is approached. Based on this and the arch like behaviour of the structure it has lead us to the conclusion that buckling might be the failure mechanism. Thus buckling of thin concrete shells is a significant structural behaviour that should not be overlooked.

In the fourth example a simply supported (along its curved edge) circular cylindrical shell roof is considered. When the FEA results are compared to the analytically obtained solutions a deviation of varying magnitude is observed. This deviation can be credited to possible low mesh density used in the FEA or/and inaccurate assumptions. It has also shown that the addition of edge beams considerably reduce the large tension stresses accumulated along the longitudinal edges. The accompanying nonlinear analysis has shown that the structure is able to carry $1.24 \times$ the applied load. The failure mechanism has shown to be the accumulation of stress at the bottom of the edge beams at the midspan. Considering the beam like behaviour of the structure this is more or less as what could be expected.

From this study it can be concluded that the analytical solution method is ,even for the trivial geometries considered in this study, quite lengthy and demanding. The long computations makes it highly exposed to calculation errors. Given the calculation are done error free, it however compares well with the results obtained from the FEA. For structural engineers dealing with such types of shells as considered in this study, it is highly advisable to have a type of script, spreadsheet or simple software which is based on the analytical solution method. The result from the analytical method can provide an independent way of verifying results from FEA. Moreover it provides the understanding and knowledge of the governing principles behind the structural behaviour of shells which is vital for the evaluation of FEA results involving shells of any geometry. The FEA is however still the most efficient and sometimes the only way of performing structural analysis of thin concrete shells.

9.1 Recommendation for future study

There are number of topics that are excluded from the scope of this paper. In addition there has also been some topics that we become aware of during the course of this thesis. Therefore we recommend the following topics to be the theme of future study papers.

- **Stability (Buckling) analysis of thin concrete shells**

Thin concrete shells are slender structural elements, therefore when exposed to compressive inplane forces there is high possibility for buckling failure. A study that will give an insight into the buckling behavior of thin concrete shells can be very beneficial for structural engineers.

- **Fiber-reinforced thin concrete shells**

Fiber based reinforcement in concrete shells is an ideal solution for constructing very thin concrete shells. It gives the possibility of easier casting process at the building site and less environment related requirements compared to ordinary bar reinforcement. Therefore the study of structural analysis involving fiber-reinforced concrete shells can add some enlightenment to this particular field of study.

- **Wind load on shells**

Wind load is one of the most common design loads. How to handle wind load on shell structures may not be a familiar knowledge to many structural engineers today. A study could for example be performed on how to calculate wind load on concrete shell structures according to the applicable codes and its corresponding load effects on the structures.

- **Creep and temperature effects on thin concrete shells**

These are two loads which are common in concrete structures. Thin concrete shells exposed to creep and temperature effects could be calculated analytically for some shell structures, and it could also be simulated in FEA. A practical application procedure of both methods could be an interesting topic to consider.

References

- [1] David P. Billington. *Thin shell concrete structures*. McGraw-Hill, New York, 1965.
- [2] C. R.. Calladine. *Theory of Shell Structures*. Cambridge University Press, 1983.
- [3] Srinivasan Chandrasekaran, SK Gupta, and Federico Carannante. Design aids for fixed support reinforced concrete cylindrical shells under uniformly distributed loads. *International Journal of Engineering, Science and Technology*, 1(1):148–171, 2009.
- [4] R.D. Cook. *Concepts and applications of finite element analysis*. Wiley, 2001.
- [5] TNO DIANA. *Diana - 9.4.4 User's Manual*, 2012. [Online; accessed April-2015].
- [6] M.P. do Carmo. *Differential Geometry of Curves and Surfaces*. Prentice-Hall, 1976.
- [7] E. Hines and D. Billington. Anton tedesko and the introduction of thin shell concrete roofs in the united states. *Journal of Structural Engineering*, 130(11):1639–1650, 2004.
- [8] F. Huijben, F. Van Herwijnen, and R. Nijse. Concrete shell structures revisited: Introducing a new 'low-tech' construction method using vacuumatics formwork. In *Structural Membranes 2011 - 5th International Conference on Textile Composites and Inflatable Structures*, pages 409–420. Export Date: 22 January 2015.
- [9] Hyo-Gyoung Kwak and Filip C Filippou. *Finite element analysis of reinforced concrete structures under monotonic loads*. Citeseer, 1990.
- [10] Per Kr Larsen. *Konstruksjonsteknikk: laster og bæresystemer*. Tapir akademisk forl., Trondheim, 2008. Nkr 280.00 2. utg.
- [11] A. E. H. Love. The small free vibrations and deformation of a thin elastic shell. *Philosophical Transactions of the Royal Society of London. A*, 179:491–546, 1888.
- [12] Kjell Magne Mathisen. Tkt4192 - finite element methods in strength analysis. NTNU, Detpartment of Structural Engineering, Autumn 2014. Lecture notes.
- [13] Svein I. Sørensen. *Betongkonstruksjoner: beregning og dimensjonering etter Eurocode 2*. Tapir akademisk forl., Trondheim, 2010. 2. oppl. med 290 s.
- [14] Svein Ivar Sørensen. Aksesymmetriske skall. NTNU, Institutt for konstruksjonsteknikk, 1999. Del II.
- [15] Norge Standard. *Eurokode 1:: Lastar på konstruksjoner. Del 1-3. Allmenne laster. Snølaster*. Standard Norge, Oslo, 2008. Norsk tekst.

- [16] Norge Standard. *Eurokode 2: Prosjektering av betongkonstruksjoner, Del 1-1, Allmenne regler og regler for bygninger*. Standard Norge, Lysaker, 2008. Engelsk tekst, NA på norsk.
 - [17] Norge Standard. *Eurokode: grunnlag for prosjektering av konstruksjoner*. Standard Norge, Lysaker, 2008. Norsk tekst.
 - [18] Chapter 2 fundamental theory of rotating shells of revolution. In K.Y. Lam Hua Li and T.Y. Ng, editors, *Rotating Shell Dynamics*, volume 50 of *Studies in Applied Mechanics*, pages 7 – 25. Elsevier, 2005.
 - [19] Stephen P. Timoshenko. *Theory of plates and shells*. McGraw-Hill, New York, 1940.
 - [20] Jan Arve Øveli og Svein Ivar Sørensen. Tkt4222 concrete structures 3. NTNU, Detpartment of Structural Engineering, Autumn 2014. Compendium.
 - [21] Eduard Ventsel and Theodor Krauthammer. *Thin plates and shells: theory, analysis, and applications*. Marcel Dekker, New York, 2001.
-

Appendix A

RC design according to Eurocode 2

A.1 Design of the cylindrical water reservoir in example 1

The design load effects for the cylindrical water tank calculated in example 1 are summarized in the following table.

	Cylindrical wall		Circular plate	
	Inner layer	Outer layer	Inner layer	Outer layer
M_x	14.61 $\frac{kNm}{m}$	42.02 $\frac{kNm}{m}$	-	-
M_r	-	-	31.42 $\frac{kNm}{m}$	42.02 $\frac{kNm}{m}$
M_t	-	-	31.42 $\frac{kNm}{m}$	5.16 $\frac{kNm}{m}$
Shear force	50.02 $\frac{kN}{m}$		30.6 $\frac{kN}{m}$	
Ring force	273.6 $\frac{kN}{m}$		-	

Table A.1: Design values of the load effects in example 1

Geometry:

$$h_c = 200 \text{ mm}$$

$$h_p = 200 \text{ mm}$$

$$b = 1000 \text{ mm}$$

Material:
Concrete

$$f_{ck} = 30 \frac{N}{mm^2}$$

$$\gamma_c = 1.5$$

$$\alpha_{cc} = 0.85$$

$$f_{cd} = \alpha_{cc} \frac{f_{ck}}{\gamma_c} = 0.85 \frac{35}{1.5} = 17 \frac{N}{mm^2}$$

$$f_{ctm} = 2.9 \frac{N}{mm^2}$$

Reinforcement

$$f_{yk} = 500 \frac{N}{mm^2}$$

$$\gamma_s = 1.15$$

$$f_{yd} = \frac{f_{yk}}{\gamma_s} = \frac{500}{1.15} = 434.78 \frac{N}{mm^2}$$

$$E = 2 \cdot 10^5 \frac{N}{mm^2}$$

Concrete cover

Following the guidelines in Eurocode 2 4.4.1.1(2) [13], the nominal concrete cover is defined as:

$$c_{nom} = c_{min} + \Delta c_{dev} = 25 + 10 = 35 \text{ mm}$$

Minimum reinforcement for concrete slabs is given in Eurocode 2 9.2.1.1(1)

$$A_{s,min} = \max\left(0.26 \left(\frac{f_{ctm}}{f_{yk}}\right) b_w d, 0.0013 b_w d\right) = \max(239.8, 206.7) = 239.8 \frac{mm^2}{m}$$

Minimum required spacing is given in Eurocode 2 9.3.1.1(3)

$$s_{max,slab} = \min(2h, 250) = 250 \text{ mm} \quad \text{in areas with maximum moment}$$

$$s_{max,slab} = \min(3h, 400) = 400 \text{ mm} \quad \text{in other areas}$$

A.1.1 Circular plate

Flexural reinforcement

Assuming a steel reinforcement with a diameter 12 mm $\rightarrow A_{\phi 12} = 113.1 \text{ mm}^2$, the effective thickness of the plate becomes:

$$d = h_p - \frac{\emptyset}{2} - c_{nom} = 200 - \frac{12}{2} - 35 = 159 \text{ mm}$$

The bending moment capacity of the concrete is given by:

$$M_{Rd} = K f_{cd} b d^2 = 0,275 \cdot 17 \cdot 1000 \cdot 159^2 \cdot 10^{-6} = 118.2 \frac{kNm}{m}$$

For more reading on the derivation of the above formula, the reader is recommended to read a book called 'Beregning og dimensjonering etter Eurocode 2' by professor Svein Ivar Sørensen [13].

Reinforcement at the edge:

In the radial direction

$$M_r = 42.02 \frac{kNm}{m}$$

$$M_{Rd} > M_r \longrightarrow \text{Partially utilized compression zone}$$

Then the internal moment arm becomes:

$$z = \left(1 - 0.17 \frac{M_r}{M_{Rd}}\right) d = \left(1 - 0.17 \cdot \frac{42.02}{118.2}\right) \cdot 159 = 149.39 \text{ mm}$$

but less than $0.95 \cdot d = 151.05 \text{ mm}$

Required reinforcement can then be calculated as:

$$A_s = \frac{M_r}{z f_{yd}} = \frac{42.02 \cdot 10^6}{149.39 \cdot 434.78} = 646.9 \frac{mm^2}{m}$$

With $\emptyset 12$ reinforcement, the required spacing becomes

$$s = \frac{A_{\emptyset 12}}{A_s} b = \frac{113.1}{646.9} \cdot 1000 = 174.8 \text{ mm}$$

If $s = 170 \text{ mm}$ is chosen, the final reinforcement is

$$\emptyset 12 s 170 \longrightarrow A_s = \mathbf{665.3} \frac{mm^2}{m}$$

In the tangential direction

$$M_t = 5.16 \frac{kNm}{m}$$

$$M_{Rd} > M_t \longrightarrow \text{Partially utilized compression zone}$$

Then the internal moment arm becomes:

$$z = \left(1 - 0.17 \cdot \frac{5.6}{118.2}\right) \cdot (159 - 12) = 146 \text{ mm}$$

Required reinforcement can then be calculated as:

$$A_s = \frac{5.16 \cdot 10^6}{146 \cdot 434.78} = 81.3 \frac{mm^2}{m}$$

$$A_s < A_{s,min} \longrightarrow A_s = A_{s,min} = 239.8 \frac{mm^2}{m}$$

With $\emptyset 12$ reinforcement, the required spacing becomes

$$s = \frac{113.1}{239.8} \cdot 1000 = 471.6 \text{ mm}$$

If $s = s_{max,slab} = 250 \text{ mm}$ is chosen, the final reinforcement is

$$\emptyset 12s250 \longrightarrow A_s = 452.4 \frac{mm^2}{m}$$

Reinforcement at the center:

In the radial and tangential directions

$$M_r = M_t = 31.42 \frac{kNm}{m}$$

$$M_{Rd} > M_r \longrightarrow \text{Partially utilized compression zone}$$

Then the internal moment arm becomes:

$$z = \left(1 - 0.17 \frac{M_r}{M_{Rd}}\right) d = \left(1 - 0.17 \cdot \frac{31.42}{137.7}\right) \cdot 159 = 152.83 \text{ mm} > 151.05 \text{ mm}$$

Required reinforcement can then be calculated as:

$$A_s = \frac{M_r}{z f_{yd}} = \frac{31.42 \cdot 10^6}{151.05 \cdot 434.78} = 478.4 \frac{mm^2}{m}$$

With $\emptyset 12$ reinforcement, the required spacing becomes

$$s = \frac{A_{\emptyset 12}}{A_s} b = \frac{113.1}{472.9} \cdot 1000 = 236.4 \text{ mm}$$

If $s = 235 \text{ mm}$ is chosen, the final reinforcement is

$$\emptyset 12s235 \longrightarrow A_s = 481.3 \frac{mm^2}{m}$$

Shear reinforcement

$$V_r = 30.6 \frac{kN}{m}$$

First, the requirement for shear reinforcement is checked using the formula in Eurocode

2 6.2.2(1)

$$V_{Rd,c} = \max([C_{Rd,c} k (100 \rho_1 f_{ck})^{\frac{1}{3}} + k_1 \sigma_{cp}] b_w d, (v_{min} + k_1 \sigma_{cp}) b_w d)$$

$$= \max(88.68, 48.39) = 88.68 \quad \frac{kN}{m}$$

$$k = \min(1 + \sqrt{\frac{200}{d}}, 2) = \min(2.12, 2) = 2$$

$$\rho_1 = \min\left(\frac{A_{sl}}{b_w d}, 0.02\right) = \min(0.0042, 0.02) = 0.0042$$

$$\sigma_{cp} = 0$$

$$C_{Rd,c} = \frac{k_2}{\gamma_c} = \frac{0.18}{1.5} = 0.12$$

$$v_{min} = 0.035 k^{\frac{2}{3}} f_{ck}^{\frac{1}{2}} = 0.304$$

$$V_r < V_{Rd,c} \longrightarrow \text{No need for shear reinforcement}$$

A.1.2 Cylindrical wall

Flexural reinforcement

Assuming a steel reinforcement with a diameter 12 mm $\longrightarrow A_{\phi 12} = 113.1 \text{ mm}^2$, the effective thickness of the shell becomes:

$$d = h_p - \frac{\emptyset}{2} - c_{nom} = 200 - \frac{12}{2} - 35 = 159 \text{ mm}$$

The bending moment capacity of the concrete is given by:

$$M_{Rd} = K f_{cd} b d^2 = 0,275 \cdot 19.83 \cdot 1000 \cdot 159^2 \cdot 10^{-6} = 118.2 \quad \frac{kNm}{m}$$

Outer layer

$$M_r = 42.02 \quad \frac{kNm}{m}$$

$$M_{Rd} > M_r \longrightarrow \text{Partially utilized compression zone}$$

Then the internal moment arm becomes:

$$z = \left(1 - 0.17 \frac{M_r}{M_{Rd}}\right) d = \left(1 - 0.17 \cdot \frac{42.02}{118.2}\right) \cdot 159 = 149.39 \text{ mm}$$

Required reinforcement can then be calculated as:

$$A_s = \frac{M_r}{z f_{yd}} = \frac{42.02 \cdot 10^6}{149.39 \cdot 434.78} = 646.9 \quad \frac{mm^2}{m}$$

With $\emptyset 12$ reinforcement, the required spacing becomes

$$s = \frac{A_{\phi 12}}{A_s} b = \frac{113.1}{646.9} \cdot 1000 = 174.8 \text{ mm}$$

If $s = 170 \text{ mm}$ is chosen, the final reinforcement is

$$\text{Ø}12s170 \longrightarrow A_s = \mathbf{665.3} \frac{\text{mm}^2}{\text{m}}$$

Inner layer

$$M_x = 14.61 \frac{\text{kNm}}{\text{m}}$$

$$M_{Rd} > M_r \longrightarrow \text{Partially utilized compression zone}$$

Then the internal moment arm becomes:

$$z = \left(1 - 0.17 \frac{M_r}{M_{Rd}}\right) d = \left(1 - 0.17 \cdot \frac{14.61}{118.2}\right) \cdot 159 = 155.66 \text{ mm} > 151.05 \text{ mm}$$

Required reinforcement can then be calculated as:

$$A_s = \frac{M_r}{z f_{yd}} = \frac{14.61 \cdot 10^6}{151.05 \cdot 434.78} = 222.46 \frac{\text{mm}^2}{\text{m}}$$

$$A_s < A_{s,min} \longrightarrow A_s = A_{s,min} = 239.8 \frac{\text{mm}^2}{\text{m}}$$

With Ø12 reinforcement, the required spacing becomes

$$s = \frac{113.1}{239.8} \cdot 1000 = 471.6 \text{ mm}$$

If $s = s_{max,slab} = 250 \text{ mm}$ is chosen, the final reinforcement is

$$\text{Ø}12s250 \longrightarrow A_s = \mathbf{452.4} \frac{\text{mm}^2}{\text{m}}$$

Shear reinforcement

$$V_r = 50.02 \frac{\text{kN}}{\text{m}}$$

First, the requirement for shear reinforcement is checked using the formula in Eurocode 2 6.2.2(1)

$$\begin{aligned} V_{Rd,c} &= \max\left([C_{Rd,c} k (100 \rho_1 f_{ck})^{\frac{1}{3}} + k_1 \sigma_{cp}] b_w d, (v_{min} + k_1 \sigma_{cp}) b_w d\right) \\ &= \max(77.99, 48.39) = 77.99 \frac{\text{kN}}{\text{m}} \end{aligned}$$

$$k = \min\left(1 + \sqrt{\frac{200}{d}}, 2\right) = \min(2.12, 2) = 2$$

$$\rho_1 = \min\left(\frac{A_{sl}}{b_w d}, 0.02\right) = \min(0.0028, 0.02) = 0.0028$$

$$\sigma_{cp} = 0$$

$$C_{Rd,c} = \frac{k_2}{\gamma_c} = \frac{0.18}{1.5} = 0.12$$

$$v_{min} = 0.035 k^{\frac{2}{3}} f_{ck}^{\frac{1}{2}} = 0.304$$

$$V_r < V_{Rd,c} \longrightarrow \text{No need for shear reinforcement}$$

Ring reinforcement

The circumferential force results in tension stresses through out the cylindrical shell. Therefore, it is assumed that stresses will be taken up by reinforcement.

$$N_\phi = 273.6 \frac{kN}{m}$$

$$A_{s\phi} = \frac{N_\phi}{f_{yd}} = \frac{273.6 \cdot 10^3}{434.78} = 629.28 \frac{mm^2}{m} \left(\frac{629.28}{2} = 314.64 \frac{mm^2}{m} \right)$$

To avoid cracking of the concrete surface, the reinforcement is divided and placed in the two layers. With $\emptyset 12$ reinforcement, the required spacing becomes

$$s = \frac{113.1 \cdot 2}{629.28} \cdot 1000 = 359.46 \text{ mm}$$

If $s = 250 \text{ mm}$ is chosen, the final reinforcement is

$$\emptyset 12s250 \longrightarrow A_s = 452.4 \frac{mm^2}{m}$$

Appendix B

Reinforcement design according to the two layered approach

B.1 Design of the cylindrical roof shell in example 3

The design loads for the cylindrical shell roof calculated in example 3 are summarized in the following table.

Design forces	Bottom layer ($\varphi = 0^\circ, x = 0$)	Top layer ($\varphi = 15^\circ, x = 0$)
N_φ	$-283 \frac{kN}{m}$	$-145 \frac{kN}{m}$
N_x	$-49.2 \frac{kN}{m}$	$0 \frac{kN}{m}$
$N_{x\varphi}$	$51.8 \frac{kN}{m}$	$0 \frac{kN}{m}$
M_φ	$21.4 \frac{kNm}{m}$	$-9.42 \frac{kNm}{m}$
M_x	$4.12 \frac{kNm}{m}$	$-0.179 \frac{kNm}{m}$
$M_{x\varphi}$	-0.635	$0 \frac{kNm}{m}$

Table B.1: Design values of the load effects in example 3

Geometry:

$$h_c = 176.78 \text{ mm}$$

$$b = 1000 \text{ mm}$$

Material:
Concrete

$$f_{ck} = 30 \frac{N}{mm^2}$$

$$\gamma_c = 1.5$$

$$\alpha_{cc} = 0.85$$

$$f_{cd} = \alpha_{cc} \frac{f_{ck}}{\gamma_c} = 0.85 \frac{30}{1.5} = 17 \frac{N}{mm^2}$$

$$f_{ctm} = 2.9 \frac{N}{mm^2}$$

Reinforcement

$$f_{yk} = 500 \frac{N}{mm^2}$$

$$\gamma_s = 1.15$$

$$f_{yd} = \frac{f_{yk}}{\gamma_s} = \frac{500}{1.15} = 434.78 \frac{N}{mm^2}$$

$$E = 2 \cdot 10^5 \frac{N}{mm^2}$$

Concrete cover

$$c_{nom} = 35 \text{ mm}$$

B.1.1 The two layered approach

This approach, which is based on dividing the forces into two membranes, is an easy way of doing first hand reinforcement calculation for shells. The method tends to underestimate the capacity of concrete shells and gives higher amount of reinforcement than necessary. However, using this approach for calculating the amount of steel reinforcement that can be applied as a first input into a FEA is efficient and less time consuming. The procedure for the following calculation is according to what is presented in the compendium for the class concrete structures 3 at NTNU [13].

Assuming uncracked membranes, we start with

$$t_1 = t_2 = 0.5h = 0.0884 \text{ m}$$

$$z = h - 0.5(t_1 + t_2) = 0.0884 \text{ m} \tag{B.1}$$

then,

$$k_1 = \frac{(h - t_2)}{(2h - t_1 - t_2)} = 0.5$$

$$k_2 = 1 - k_1 = 0.5 \tag{B.2}$$

Then the equivalent membrane forces become,

$$\begin{aligned}
 n_{x1} &= k_1 n_x + \frac{m_x}{z} = 0.5 \cdot -49.2 + \frac{4.12}{0.0884} = 22.01 \quad kN \\
 n_{\varphi 1} &= k_1 n_{\varphi} + \frac{m_{\varphi}}{z} = 0.5 \cdot -283 + \frac{21.4}{0.0884} = 100.61 \quad kN \\
 n_{x\varphi 1} &= k_1 n_{x\varphi} + \frac{m_{x\varphi}}{z} = 0.5 \cdot 51.8 + \frac{-0.635}{0.0884} = 18.72 \quad kN \\
 n_{x2} &= k_2 n_x + \frac{m_x}{z} = -71.21 \quad kN \\
 n_{\varphi 2} &= k_2 n_{\varphi} + \frac{m_{\varphi}}{z} = -383.6 \quad kN \\
 n_{x\varphi 2} &= k_2 n_{x\varphi} + \frac{m_{x\varphi}}{z} = 33.08 \quad kN
 \end{aligned} \tag{B.3}$$

The principal membrane forces are then calculated using

$$n_{11}^i = \frac{n_{xi} + n_{\varphi i}}{2} + \sqrt{\left(\frac{n_{xi} - n_{\varphi i}}{2}\right)^2 + n_{x\varphi i}^2} \tag{B.4}$$

which for the two membranes becomes

$$\begin{aligned}
 n_{11}^1 &= \frac{22.01 + 100.61}{2} + \sqrt{\left(\frac{22.01 - 100.61}{2}\right)^2 + (18.72)^2} = 104.84 \quad kN \\
 n_{11}^2 &= \frac{-71.21 - 383.6}{2} + \sqrt{\left(\frac{-71.21 - 383.6}{2}\right)^2 + (33.08)^2} = -67.75 \quad kN
 \end{aligned} \tag{B.5}$$

Based on this results, new set of membrane thicknesses are chosen and the the calculations are repeated.

$$\begin{aligned}
 n_{11}^1 > 0 &\longrightarrow t_1 = 2 \cdot c_{nom} = 0.070 \quad m(\text{cracked}) \\
 n_{11}^2 < 0 &\longrightarrow t_2 = 0.5h = 0.0884 \quad m(\text{uncracked})
 \end{aligned} \tag{B.6}$$

thus, the new set of membrane forces become

$$\begin{aligned}
 n_{x1} &= 19.94 \quad kN & n_{x2} &= -69.14 \quad kN \\
 n_{\varphi 1} &= 91.13 \quad kN & n_{\varphi 2} &= -374.13 \quad kN \\
 n_{x\varphi 1} &= 16.95 \quad kN & n_{x\varphi 2} &= 34.85 \quad kN
 \end{aligned} \tag{B.7}$$

The crack angle could be calculated based on yielding of the reinforcement

$$\tan^2 \phi + \left(\frac{n_x}{n_{x\varphi}} - \frac{n_{\varphi}}{n_{x\varphi}} \cdot \frac{A_{sx}}{A_{s\varphi}} \right) \tan \phi - \frac{A_{sx}}{A_{s\varphi}} = 0 \tag{B.8}$$

If $\frac{A_{sx}}{A_{s\varphi}} = 2$ is chosen, the crack angles in the two membranes is given by:

$$\begin{aligned}
 \tan^2 \phi + \left(\frac{19.94}{16.95} - \frac{91.13}{16.96} \cdot 2 \right) \tan \phi - 2 &= 0 \longrightarrow \phi_1 = 60.82^\circ \\
 \tan^2 \phi + \left(\frac{-69.14}{34.85} - \frac{-374.13}{34.85} \cdot 2 \right) \tan \phi - 2 &= 0 \longrightarrow \phi_2 = 8.07^\circ
 \end{aligned} \tag{B.9}$$

Then the internal forces in reinforcement and compression could be found as:

$$\begin{aligned} F_c &= \frac{n_{x\varphi}}{\sin \phi \cos \phi} \\ F_{sx} &= n_x + n_{x\varphi} \tan \phi \\ F_{s\varphi} &= n_\varphi + n_{x\varphi} \cot \phi \end{aligned} \quad (\text{B.10})$$

Inserting the calculated values yields

$$\begin{aligned} F_{c1} &= \frac{16.95}{\sin 60.82 \cos 60.82} = 39.82 \text{ kN} \\ F_{sx1} &= 19.94 + 16.95 \tan 60.82 = 50.3 \\ F_{s\varphi1} &= 91.13 + 16.95 \cot 60.82 = 100.59 \\ F_{c2} &= \frac{34.85}{\sin 8.07 \cos 8.07} = 250.7 \text{ kN} \\ F_{sx2} &= -69.14 + 34.85 \tan 8.07 = -64.2 \text{ kN} \\ F_{s\varphi2} &= -374.13 + 34.85 \cot 8.07 = -128.39 \text{ kN} \end{aligned} \quad (\text{B.11})$$

The required reinforcement for the cracked membrane:

$$\begin{aligned} A_{sx1} &= \frac{F_{sx}}{f_{yd}} = \frac{50.3 \cdot 10^3}{435} = 115.62 \frac{\text{mm}^2}{\text{m}} \\ A_{s\varphi1} &= \frac{100.59 \cdot 10^3}{435} = 231.25 \frac{\text{mm}^2}{\text{m}} \end{aligned} \quad (\text{B.12})$$

Control of concrete stress in compression

The concrete stresses in the compression field are given by:

$$\begin{aligned} V_{Rd,max} &= 0.6v'f_{cd} = 0.6 \left(1 - \frac{30}{250}\right) \cdot 17 = 8.98 \frac{\text{N}}{\text{mm}^2} \\ \sigma_{c1} &= \frac{F_{c1}}{t_1} = \frac{39.82 \cdot 10^3}{70 \cdot 1000} = 0.5689 \frac{\text{N}}{\text{mm}^2} < V_{Rd,max} \\ \sigma_{c2} &= \frac{F_{c2}}{t_2} = \frac{250.7 \cdot 10^3}{88.4 \cdot 1000} = 2.836 \frac{\text{N}}{\text{mm}^2} < V_{Rd,max} \end{aligned} \quad (\text{B.13})$$

This procedure is again used for different set of loads obtained from other locations on the shell surface. In this way the set of loads that result in the highest amount of required reinforcement are found. The nature of this procedure is better suited for a computational software, therefore we have scripted the procedure into Matlab. The above example is just to show the outline of the general procedure used. The script is attached in Appendix D.

Appendix C

Investigating the effect of the constraint along the curved edge in example 3

C.1 Additional constraint in Z direction

In this appendix, the previously mentioned deviation in the distribution of the force N_x which is shown in example 3 is to be investigated. Based on the assumptions that are made in the analytical calculation procedures, stress resultants vary only in φ -direction, thus no variation of load effects in the longitudinal direction. Since in the analytical method N_φ is obtained by scaling N_φ with Poisson's ratio ν i.e. N_x is cause solely by material compression/expansion in φ -direction. Thus the lack of restrain in both curved edges might be the cause of the deviation with the FEA results. To verify this, an additional translational constraint in x -direction (global z direction in DIANA) is introduced to this model as shown in figure C.1.

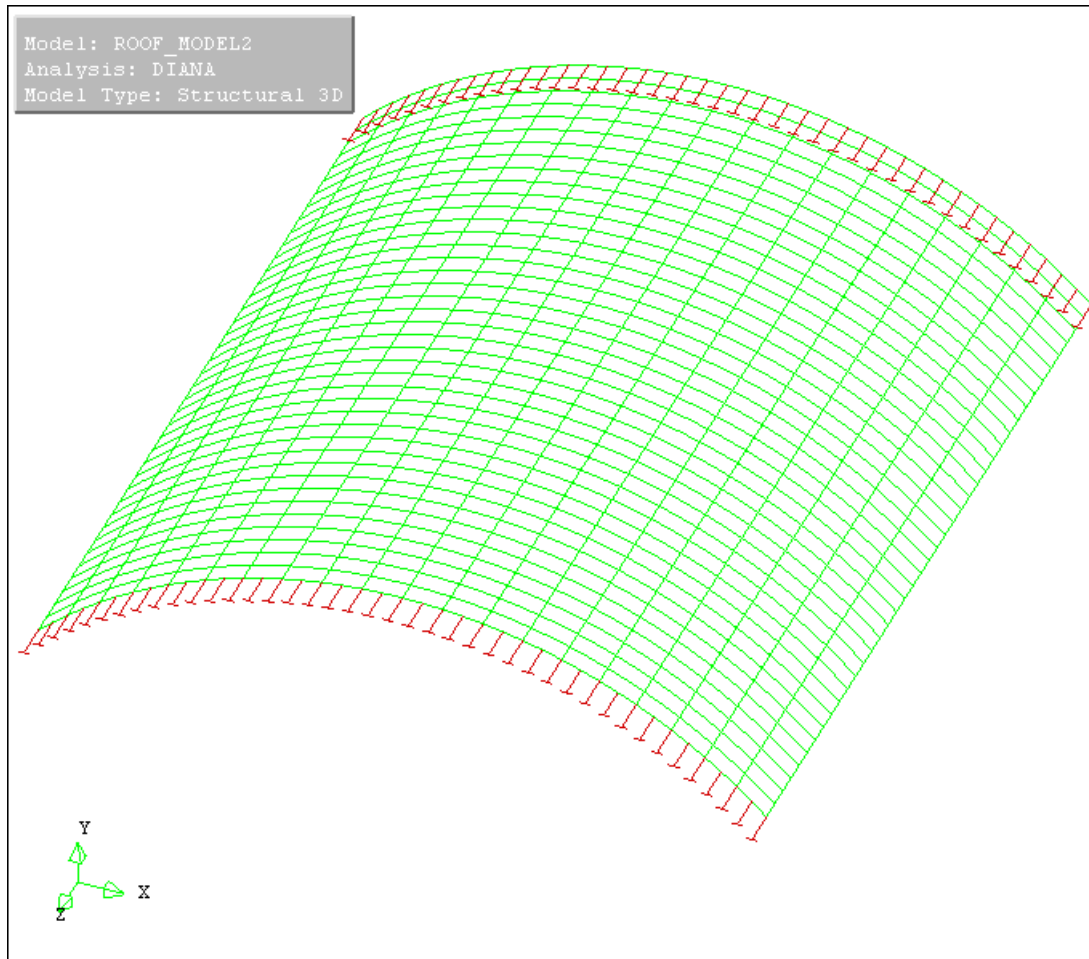
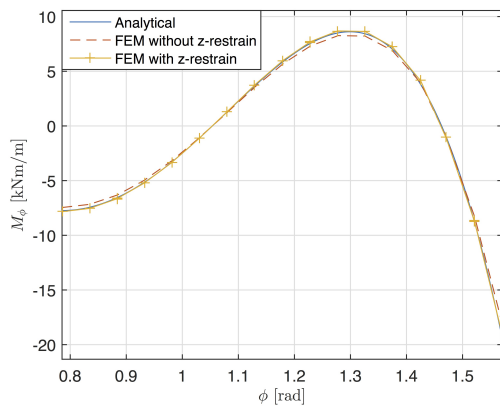
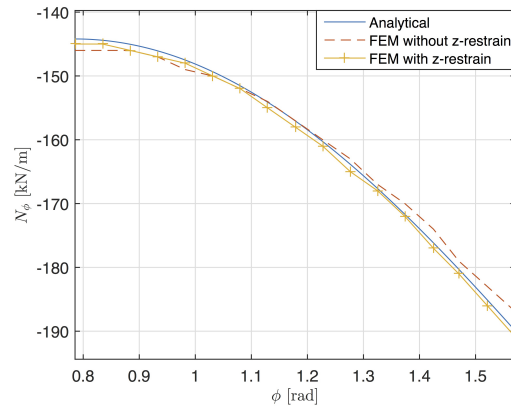


Figure C.1: New translational constraint in z-direction

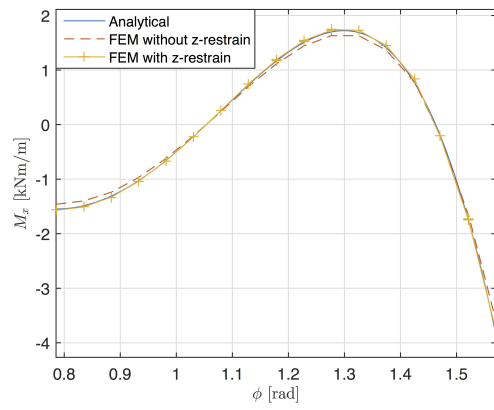
The results of the linear FEA of this modified model is compared to both the analytically obtained solutions, and the FEA results from the original model, see Figure C.2. The comparison shows that, after the additional constrain in Z direction along the curved edge is applied, all the stress resultants including N_φ agree well. This agreement is obtained because the model for the FEA is now closer to what is assumed in the analytical method. Similarly the variation of the stress resultants along the longitudinal axis is investigated. From Figure C.3, it is evident that there are some variations in the distribution of the stress resultants along the longitudinal direction, however drastic changes are located only near the curved edges. The effect of the restraint in Z direction is also presented in the figures, it has some contribution to the stability of the results along the longitudinal axis but the variation near the edge are still present.



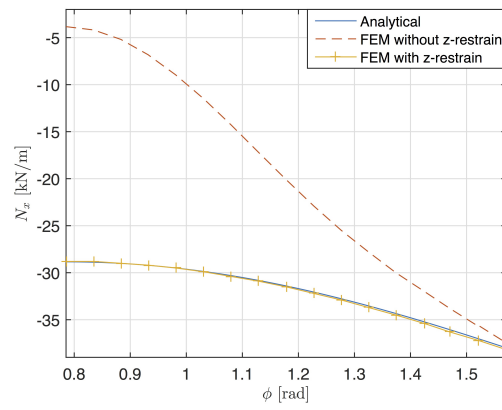
(a) Comparison of M_φ in φ -direction



(b) Comparison of N_φ in φ -direction

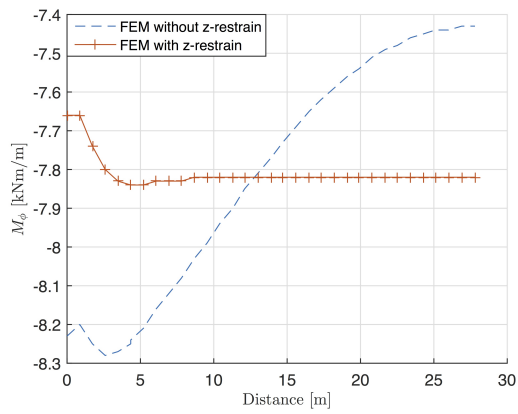


(c) Comparison of M_x in φ -direction

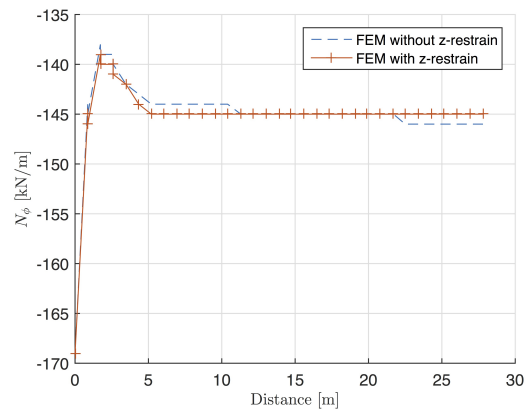


(d) Comparison of N_x in φ -direction

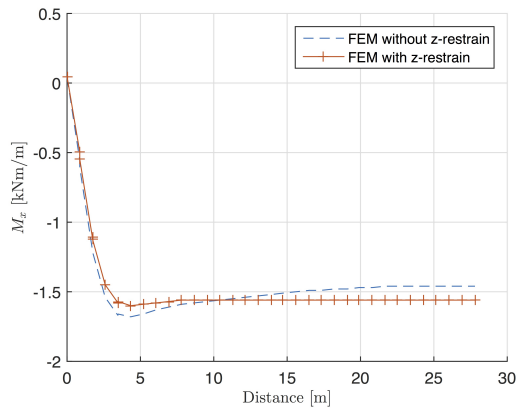
Figure C.2: Variation of the stress resultants in φ direction



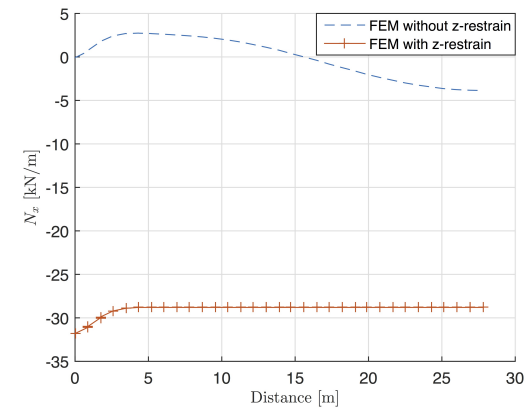
(a) Comparison of M_φ in longitudinal direction



(b) Comparison of N_φ in longitudinal direction



(c) Comparison of M_x in longitudinal direction



(d) Comparison of N_x in longitudinal direction

Figure C.3: Variation of the stress resultants in x direction

Appendix D

MatLab code


```

%% Reinforcement design of shells according to Two layer approach
clear all; close all;
syms phi

% Design load effects in kN and m
n_x = 0;
n_y = -145;
n_xy = 0;
m_x = -0.179;
m_y = -9.42;
m_xy = 0;

% Material properties
h = 0.117678;
c = 0.035;
f_yk = 500;
f_ctm = 2.9;
f_ck = 30;
f_cd = 0.85*f_ck/1.5;
f_yd = 435;

% Assumption; Concrete uncracked
t_1 = 0.5*h;
t_2 = 0.5*h;
z = h-0.5*(t_1+t_2)
k_1 = (h-t_2)/(2*h-t_1-t_2)
k_2 = 1-k_1;

% Design membrane forces
n_x1 = k_1*n_x+m_x/z
n_y1 = k_1*n_y+m_y/z
n_xy1 = k_1*n_xy+m_xy/z % bottom layer
n_x2 = k_2*n_x-m_x/z
n_y2 = k_2*n_y-m_y/z
n_xy2 = k_2*n_xy-m_xy/z % top layer

% Principal membrane force
n_11=(n_x1+n_y1)/2+(((n_x1-n_y1)/2)^2+n_xy1^2)^0.5
n_12=(n_x2+n_y2)/2+(((n_x2-n_y2)/2)^2+n_xy2^2)^0.5

%%
% Cracked >0 or uncracked <0 % A_sx/Asy
p = 0.5;

% Crack angle
A_1 = vpa(solve((tan(phi))^2+(n_x1/n_xy1-(n_y1/n_xy1)*p)*tan(phi)-
p==0));
A_2= vpa(solve((tan(phi))^2+(n_x2/n_xy2-(n_y2/n_xy2)*p)*tan(phi)-
p==0));
if (n_xy>0) ;phi_1=A_1(A_1>0) ;elseif (n_xy<0) ;phi_1=A_1(A_1<0) ;end
if (n_xy>0) ;phi_2=A_2(A_2>0) ;elseif (n_xy<0) ;phi_2=A_2(A_2<0) ;end
a_1 = vpa(phi_1*180/pi)
a_2 = vpa(phi_2*180/pi)

% Forces for reinforcement
F_c1 = n_xy1/(sin(phi_1)*cos(phi_1));
F_sx1 = n_x1+n_xy1*tan(phi_1)

```

% Analytical solution in closed form for cylindrical shell roofs fixed along longitudinal edges and uniformly distributed loading. Taken from the paper by Srinivasan Chandrasekaran1, S.K.Gupta, Federico Carannante.

clear all; close all; clc;

syms phi

f = pi/4 *% Angle in circumferential direction measured from the edge*

L = 55.54; *% Length of the RC shell roof in longitudinal direction*

R = 17.6; *% Circumferential radius*

t = 0.176; *% Thickness of the RC shell roof*

p = 9; *% Uniform distributed load*

E = 30*10^6; *% Young's modulus*

v = 0.2; *% Poisson's ratio*

B = (p*R^2*(1-v^2))/(16*E*t^3*(2*t^2*f^2+24*R^2*(f^2-1)+24*R^4*cos(2*f)+(12*R^2+t^2)*f*sin(2*f)));

C_9 = (48*B*t^2*R^2*((t^2*(8*f^2-3)+12*R^2*(8*f^2-1))*cos(f)+3*(4*R^2+t^2)*(cos(3*f)-4*f*sin(f)))/(12*R^2+t^2);

C_12 = 4*B*((12*R^2+t^2)^2*f*((1+4*f^2)*cos(f)-cos(3*f))+4*sin(f)*((12*R^2+t^2)^2*f^2+6*R^2*(36*R^2+5*t^2)*cos(2*f)-6*(36*R^4+5*R^2*t^2)));

C_14 = 8*B*f*sin(f)*(12*R^2+t^2)^2*((12*R^2*(2*f^2-5)+t^2*(2*f^2-1))/(12*R^2+t^2)-cos(2*f))+96*R^2*B*(36*R^2+5*t^2)*sin(2*f)*sin(f);

w = 1/(2*R*(12*R^2+t^2)*(v^2-1));

% Stress functions

N_f = 4*w*E*t^3*(C_14*cos(phi)-C_12*sin(phi))+p*w*R^2*(v^2-1)*(cos(f)*((12*R^2-t^2)*cos(phi)-2*(12*R^2-t^2)*phi*sin(phi))+2*(12*R^2+t^2)*phi*cos(phi)+(12*R^2-t^2)*sin(phi))*sin(f);

M_f = (w*E*t)/(6*R)*(C_9*(12*R^2+t^2)^2+24*R^2*t^2*(C_14*cos(phi)-C_12*sin(phi)))+p*w*R^3*(v^2-1)*(sin(f)*(2*(12*R^2+t^2)*phi*cos(phi)-3*(4*R^2+t^2)*sin(phi))-cos(f)*(3*(4*R^2+t^2)*cos(phi)+2*(12*R^2+t^2)*phi*sin(phi)));

N_x = v*N_f;

M_x = v*M_f